Dissertation

New aspects of STIM1 signaling: Stimulus-specific contribution of mitochondrial Ca^{2+} uptake to STIM1 activation and SOCE

submitted by

Dr. med.

András Tamás Deák

for the Academic Degree of

Doctor of Philosophy

(PhD)

at the

Medical University of Graz

Institute of Molecular Biology and Biochemistry

under the supervision of

Assoc.-Prof. Dr. Roland MALLI

2014

DECLARATION

I hereby declare that this dissertation is my own original work and that I have fully acknowledged by name all of those individuals and organizations that have contributed to the research for this dissertation. Due acknowledgement has been made in the text to all other material used. Throughout this dissertation and in all related publications I followed the guidelines of “Good Scientific Practice”.

Graz, 14th of August 2014

.

ACKNOWLEDGEMENTS

I would like to express my most sincere gratitude to all those people who supported me during my medical- and PhD-studies, in particular my parents, my family, my girlfriend, my friends and all former and present colleagues of mine.

I thank to Prof. Dr. László Hunyady, chair of the Institute of Physiology, Semmelweis University, who recruited me in 2007 as a "research student" in his laboratory, where I could start my scientific work under the supervision and guidance of Dr. Péter Várnai to whom I would also like to express my gratitude.

I would like to acknowledge my former colleagues in the Hunyady/Várnai Laboratory and my present colleagues in Graz, namely Markus Waldeck-Weiermair, Alexander Bondarenko, Rene Rost, Sonja Barth, Claire Jean-Quartier, Neelanjan Vishnu, Muhammad Rizwan Alam, Muhammad Jadoon Khan, Sandra Blass, Corina Madreiter, Nicole Hofmann, Christiane Klec, Therese Macher, Warisara Parichatikanond, Lukas Groschner and Felix Karsten for their support and excellent technical assistance.

I would also like to thank to Dr. Michael Poteser and Prof. Dr. Klaus Groschner from the Institute of Biophysics, Medical University of Graz, for their useful suggestions and critical evaluation of my work.

And last but not least, special thanks to my Principle Investigator Assoz.-Prof. Dr. Roland Malli for his continuous support and patience. He was always ready to help and assist me, discuss and solve problems, whenever it was needed. I would also like to express my greatest gratitude to Prof. Dr. Wolfgang Graier, who - together with Roland - provided me the opportunity to join a great research team in the Medical University of Graz, and was always fair, enthusiastic, encouraging and critical enough to fuel my motivation to perform high-quality research.

TABLE OF CONTENTS

LIST OF ABBREVIATIONS

ATP	Adenosine triphosphate
AUC	Area under the curve
BAPTA	1,2-bis(o-aminophenoxy)ethane-N,N,N',N'-tetraacetic acid)
BHQ	2,5-Di-t-butyl-1,4-benzohydroquinone
$[Ca^{2+}]_{cyto}$	Cytosolic free calcium concentration
$[Ca^{2+}]_{ER}$	Endoplasmic reticulum free calcium concentration
$[Ca^{2+}]_{mito}$	Mitochondrial free calcium concentration
CaM	Calmodulin
CCE	Capacitative calcium entry
CFP/YFP/OFP/RFP	Cyan/Yellow/Orange/Red fluorescent protein
CNS	Central nervous system
CRAC channel	Calcium release activated calcium channel
DMEM	Dulbecco's modified eagle medium
EGTA	Ethylene glycol tetraacetic acid
EMRE	Essential MCU regulator element
ER/SR	Endoplasmic/Sarcoplasmic reticulum
FP	Fluorescent protein
FRET	Förster resonance energy transfer
FURA-2AM	Fura-2 acetoxymethyl ester
GECI	Genetically encoded calcium indicator
GPCR	G-protein-coupled receptor
His	Histamine
IMM/OMM	Inner/Outer mitochondrial membrane
IP_3	Inositol 1,4,5-trisphosphate
IP_3R	Inositol 1,4,5-trisphosphate receptor
KO/KD	Knockout/Knockdown
Letm1	Leucine zipper-EF-hand containing transmembrane protein 1
MCU	Mitochondrial calcium uniporter
MCUR1	Mitochondrial calcium uniporter regulator 1
MFN-2	Mitofusin 2
MICU1	Mitochondrial calcium uptake 1
mPTP	Mitochondrial permeability transition pore
NCLX	Sodium calcium lithium exchanger
NFAT	Nuclear factor of activated T-cells

PLCß	Phospholipase C beta
PM	Plasma membrane
PMCA	Plasma membrane Ca^{2+} ATPase
RBL	Rat basophilic leukemia cell line
Rhod-2	Rhodamine-2
SERCA	Sarco/endoplasmic reticulum Ca^{2+} ATPase
SOCE	Store-operated calcium entry
STIM1	Stromal interacting molecule 1
TG	Thapsigargin
TRPC	Transient receptor potential cation channel
UCP2/3	Uncoupling protein 2 and 3
VDAC	Voltage-dependent anion channel

SUMMARY

Store-operated Ca^{2+} entry (SOCE) is a ubiquitous Ca^{2+} influx pathway in mammalian cells activated following depletion of the endoplasmic reticulum (ER) Ca^{2+} stores. The essential physiological role of SOCE is the replenishment of depleted Ca^{2+} pools and the generation of sustained cytosolic Ca^{2+} signals required for fundamental cellular functions such as the secretion of vesicle contents, cytoskeleton remodeling or gene transcription. It is now recognized that deficiencies in SOCE may also associated with pathomechanisms of certain diseases including immunodeficiency, cardiac hypertrophy or Alzheimer´s disease.

The molecular mechanism of SOCE activation is virtually based on the complex interaction of the ER-spanning stromal interacting molecule (STIM) 1 protein and plasma membrane (PM) Ca^{2+} channels such as Orai or transient receptor potential cation channels (TRPC). STIM1 serves as the central multifunctional "relay" in the activation mechanism of SOCE. It acts as a "detector" by sensing ER Ca^{2+} content through its luminal Ca^{2+} binding domain. STIM1 functions also as a "courier" by migrating across the ER to subplasmalemmal areas and delivers the message to the PM that the Ca^{2+} stores are empty. Moreover, STIM1 is an "operator" of SOCE, as it directly binds to and activates store-operated Ca^{2+} channels. Although the activation mechanism and the components of the SOCE machinery are well described, the regulation of SOCE is still under extensive research.

One part of this research focuses on the understanding how mitochondria control SOCE. Even though, it has been established long ago that mitochondrial Ca^{2+} uptake contributes to SOCE regulation, the exact mechanisms, how this is accomplished, are still insufficiently clarified. The unclear results partly originate from the fact that proteins mediating mitochondrial Ca^{2+} uptake [*i.e.* mitochondrial Ca^{2+} uniporter (MCU), mitochondrial calcium uptake 1 (MICU1), uncoupling protein 2/3 (UCP2/3), leucine zipper-EF-hand containing transmembrane protein 1 (Letm1)] have been identified only recently. Thus, the contribution of mitochondrial Ca^{2+} uptake to SOCE has been investigated indirectly until now.

This work was designed to elucidate the molecular mechanisms underlying the mitochondrial control of SOCE. For this purpose a new technique was established, which enabled the simultaneous recording of mitochondrial and cytosolic Ca^{2+} signals in the same individual cell with fluorescent microscopy. With a series of organelle-associated Ca^{2+}

measurements using a newly constructed mitochondrial Ca^{2+} probe (4mtD1GO), evidence was found for distinct modes of mitochondrial Ca^{2+} uptake depending on sarco/endoplasmic reticulum Ca^{2+} ATPase (SERCA) activity. Taking advantage of these findings, the direct involvement of mitochondrial Ca^{2+} buffering in SOCE was also investigated. These experiments were performed in HeLa cells stably depleted of either MCU or UCP2. The lack of either of these two proteins results in decelerated STIM1 activation and impaired SOCE following cell stimulation with an IP_3-generating agonist. Upon artificially augmented cytosolic Ca^{2+}-buffering or ER Ca^{2+} depletion by SERCA inhibitors, STIM1 activation did not rely on intact mitochondrial Ca^{2+} uptake. However, MCU-dependent mitochondrial sequestration of Ca^{2+} entering through the SOCE pathway was essential to prevent slow deactivation of SOCE.

In summary, the findings herein support the existence of distinct mitochondrial Ca^{2+} uptake routes and highlight a special and tight regulation of STIM1 activation and SOCE by mitochondria. Considering the central role of STIM1, the identification of any molecular mechanisms that regulate this protein under physiological conditions of cell stimulation will help to improve our understanding of other STIM1-dependent cell signaling events as well.

ZUSAMMENFASSUNG

Der speicherregulierte Kalziumeinstrom (SOCE) sorgt in vielen Zellen für Kalziumnachschub von außen. Aktiviert wird SOCE durch eine Entleerung des wichtigsten intrazellulären Kalziumspeichers, dem Endoplasmatischen Retikulum (ER). Strömen Kalziumionen (Ca^{2+}) in Zellen, werden Kalziumspeicher wieder aufgefüllt und Kalziumsignale erzeugt. Diese Kalziumerhöhungen lösen spezifische Reaktionen aus. Dabei können unterschiedliche Zellfunktionen moduliert werden. SOCE steuert zum Beispiel die Entleerung zellulärer Vesikel, die Architektur des Zellskeletts und die Expression bestimmter Gene. Störungen im SOCE können zur Entwicklung von Erkrankungen wie Immunschwäche, Herzleiden und Alzheimer beitragen.

Der molekulare Mechanismus der SOCE Aktivierung besteht in einer Wechselwirkung zwischen den in der ER-Membran lokalisierten STIM1-Proteinen und Kalziumionenkanälen der Plasmamembran (PM). Zu diesen bekannten Ionenkanälen zählen die Orai und TRPC Eiweißmoleküle. STIM1 Proteine funktionieren dabei wie Schalter, welche die Kalziumkonzentration im Inneren des ERs messen und bei einer Kalziumentleerung des Organells in Richtung PM wandern. Dort binden sie an entsprechende Kalziumkanäle der PM und aktivieren SOCE. Obwohl dieser Mechanismus der SOCE-Aktivierung gut aufgeklärt ist, wird die Regulation dieses Kalziumeinstromweges ausgiebig erforscht.

Ein Teil dieser Forschung beschäftigt sich mit der Untersuchung der Rolle von Mitochondrien in der Regulation des SOCEs. Wenngleich schon lange bekannt ist, dass Mitochondrien einen Einfluss auf diesen Kalziumeinstromweg haben, ist der genaue Mechanismus dafür nicht geklärt. Unklarheiten darüber wie Mitochondrien SOCE beeinflussen ergaben sich vor allem dadurch, dass jene Moleküle, welche Ca^{2+} in das Innere von Mitochondrien leiten sehr lange unbekannt waren. Heute kennt man aber wichtige Proteine für die Aufnahme von Ca^{2+} in die Mitochondrien. Zu diesen Eiweißmolekülen zählen MCU (mitochondrial Ca^{2+} uniporter), MICU1 (mitochondrial calcium uptake 1), Letm1 (leucine zipper-EF-hand containing transmembrane protein 1) und das UCP2/3 (uncoupling protein 2/3).

In dieser Arbeit wurden Mechanismen, über welche Mitochondrien SOCE beeinflussen, untersucht. Dafür wurde ein neuer fluoreszierender Sensor zur simultanen Messung von Kalziumsignalen in Mitochondrien und dem Zytosol entwickelt. Mit Hilfe dieses

Kalziumsensors konnte gezeigt werden, dass in Abhängig der SERCA, eine Kalziumpumpe des ERs, unterschiedliche Kalziumaufnahmewege an den Mitochondrien aktiviert werden. Durch den Einsatz von shRNA zur spezifischen Unterdrückung der Expression von Eiweißmolekülen, welche an der Kalziumaufnahme von Mitochondrien beteiligt sind, wurde die Existenz unterschiedlich zusammengesetzter Kalziumaufnahmestellen an Mitochondrien untermauert. Diese Ergebnisse dienten als Basis für Untersuchungen über die Rolle der Kalziumaufnahme- und Pufferung von Mitochondrien am SOCE. Dafür wurden HeLa Zellen mit einer spezifischen Unterdrückung der Expression von einerseits UCP2 und andererseits MCU verwendet. In beiden Zellklonen war die Kalziumaufnahme in Mitochondrien stark reduziert und die IP_3-induzierte STIM1 Aktivierung verringert. Wenn aber die zytosolische Kalziumpufferkapazität künstlich erhöht war oder Kalzium aus dem ER durch Hemmung der SERCA mobilisiert wurde, dann erfolgte die STIM1 Aktivierung unabhängig von Mitochondrien. Die MCU abhängige Aufnahme von einströmenden Kalziumionen in Mitochondrien war allerdings notwendig, um eine langsame Hemmung von SOCE durch Ca^{2+} selbst aufzuheben.

Zusammenfassend untermauern diese Ergebnisse die Existenz unterschiedlicher Kalziumaufnahmewege in Mitochondrien und zeigen, wie eng und spezifisch Mitochondrien die Aktivierung von STIM1 und SOCE regulieren. Bedenkt man die zentrale Rolle der STIM1 Aktivierung in der Zellphysiologie, so haben diese Erkenntnisse auch Bedeutung für das Verständnis anderer STIM1-abhängiger Prozesse der zellulären Signalverarbeitung.

1. INTRODUCTION

1.1 Origin of store-operated Ca^{2+} entry (SOCE)

Ca^{2+} is a versatile and universal second messenger regulating a wide range of cellular functions. Rapid changes of cytosolic Ca^{2+} control a variety of spatially and temporally distinct cellular responses including neurotransmitter release, immune cell response, muscle contraction, cell proliferation or apoptosis (1). Cytosolic Ca^{2+} elevations result either from Ca^{2+} mobilization from the largest intracellular Ca^{2+} storage organelle, the endoplasmic reticulum (ER), or from Ca^{2+} influx across plasma membrane Ca^{2+} channels. By the mid-1980s it was established that stimulation of certain cell surface receptors, typically G protein-coupled receptors (GPCRs), with Ca^{2+}-mobilizing hormones or neurotransmitters induces the hydrolysis of plasma membrane phosphoinositides by phospholipase C (PLC) enzymes. This yields the diffusible messenger inositol-1,4,5-trisphosphate (IP_3), which binds to the IP_3 receptor (IP_3R) on the ER membrane evoking a robust Ca^{2+} release from the lumen of the ER into the cytosol (2). The initial Ca^{2+} release from the ER causing a transient increase in cytosolic Ca^{2+} is followed by a stimulated Ca^{2+} entry from the extracellular area. This results in a sustained elevation of cytosolic Ca^{2+}, which persists as long as the ER stores are empty. This phenomenon was first described by James W. Putney in 1986, who introduced the concept of capacitative Ca^{2+} entry (CCE), which was later renamed as store-operated Ca^{2+} entry (3,4). The term SOCE refers to the mechanism that Ca^{2+} store depletion directly activates Ca^{2+} influx into the cytosol through Ca^{2+} channels of the plasma membrane (5). The essential physiological role of this process is the replenishment of depleted ER stores and the generation of sustained cytosolic Ca^{2+} signals required for Ca^{2+}-dependent cellular functions.

A few years later in 1992 electrophysiological studies in mast cells and lymphocytes identified the inward rectifying Ca^{2+} current that mediates SOCE (6). Hoth and Penner used a whole-cell patch clamp configuration in mast cells to record an inward rectifying, highly selective Ca^{2+}-current activated in response to Ca^{2+} store depletion, which they named Ca^{2+} release activated Ca^{2+} current (I_{CRAC}) (6). Similar inward rectifying Ca^{2+} currents activated upon Ca^{2+} mobilization by IP_3 were shown in Jurkat T-cells as well (7). Additional studies revealed, that this current is not exclusively under the control of ER Ca^{2+} store content, but intact respiring mitochondria has a strong influence on it and, thus, on SOCE (8,9).

After these landmark discoveries the integration of SOCE into well-established models of Ca^{2+} homeostasis was delayed for more than a decade, as the molecular components of this complex machinery were unknown. The breakthrough came in the mid 2000's with the identification of the Ca^{2+}-sensor stromal interacting molecule (STIM) 1 and STIM2 (10,11), followed shortly thereafter by the discovery of the Orai proteins, the pore-forming subunits of the store-operated Ca^{2+} channel (12,13). These key findings opened a new era of SOCE research. Current studies aim to establish the whole set of molecules/mediators that control SOCE machinery, and completely unveil regulatory mechanisms underlying SOCE. Many of these works are dedicated to characterize the relationship between SOCE and other Ca^{2+} signaling mechanisms (e.g.: mitochondrial Ca^{2+} handling). Furthermore, by now a large number of evidence highlight that SOCE and its constituents play a critical role in health and disease (*see chapter 1.7*).

1.2 Origin of STIM

The STIM proteins, "the multifunctional Ca^{2+} sensors of SOCE", came to light outside the Ca^{2+} signaling field. STIM proteins (previously known as SIM or GOK) were originally described as cell surface molecules mediating the survival and/or proliferation of pre-B lymphocytes (15). Moreover they have been shown to suppress growth of rhabdomyosarcomas and rhabdoid tumors (16,17). To date, two members of the human (h) STIM protein family, hSTIM1, hSTIM2 and a splice-variant (STIM1L) have been described (22). In addition to that, a non-mammalian homologue was found in *Drosophila* (dStim1) (14).

The fundamental role of STIM1 and 2 in SOCE was recognized in 2005, when two independent studies using RNAi screening demonstrated that STIM is the ER Ca^{2+} sensor, that links Ca^{2+} store depletion to Ca^{2+} influx (10,11). In their experimental setups both groups used thapsigargin (Tg), an irreversible sarco/endoplasmic reticulum Ca^{2+}-ATPase (SERCA) blocker compound. Added to cells, Tg prevents the reuptake of Ca^{2+} from the cytosol to the ER lumen and, thus, leads to a passive depletion of the ER Ca^{2+} store. The decline in luminal Ca^{2+} store content causes STIM1 redistribution to subplasmalemmal area and effectively triggers Ca^{2+} influx through CRAC channels. The loss of STIM1 by an RNAi-mediated knockdown attenuated the Tg-triggered Ca^{2+}-entry. The essential role of STIM1 in the SOCE phenomenon was proven by a series of cytosolic Ca^{2+}-measurements, patch-clamp recordings and Mn^{2+} quench assays in the respective studies. It soon became

clear that most mammalian cell types rely primarily on STIM1 for SOCE and CRAC channel activation (10,11,18), whereas STIM2 was found to be responsible for regulating basal cytosolic and ER Ca^{2+} levels (19). By contrast, in cells of the central nervous system (CNS) STIM2, but not STIM1 was shown to be the key mediator of SOCE (20,21).

1.3 Ca^{2+} sensing function of STIM1

Human STIM1 is type I membrane protein containing several structural domains within its polypeptide sequence and it shares a high structural similarity with STIM2 (22,23). (**Figure 1.1**).

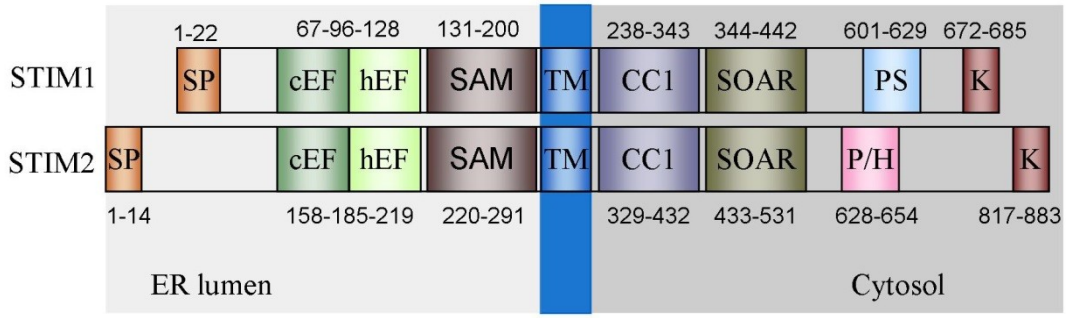

Figure 1.1 Structural features of STIM1 and STIM2 proteins *[modified and adopted from* (22)]

Both proteins include a signal peptide (SP), an EF-hand-SAM Ca^{2+} binding and interacting site, a transmembrane, domain (TM), a coiled-coil domain (CC1), a STIM-Orai activation region (SOAR) and a lysine-rich domain (K). STIM2 has a distinct upstream and a longer flexible tail containing a proline/histidine-rich domain (PH), but lacks the proline/serine rich domain (PS) seen in STIM1.

The N-terminus of STIM1 is located in the ER lumen, which is connected by a single transmembrane domain (TM) to its C-terminus, which faces the cytosol. The luminal part of the protein includes a canonical EF-hand domain (cEF), a non-Ca^{2+} binding hidden EF-hand domain (hEF), and a sterile alpha motif domain (SAM) with two glycosylation sites. Although Ca^{2+} binds only to the cEF domain, the stability of the whole EF-hand-SAM domain is important for its Ca^{2+} sensing role (24).

In quiescent cells ER Ca^{2+} stores are filled and the EF-hand domain is in a Ca^{2+} bound state. Ca^{2+} mobilization from the ER leads to the decrease of $[Ca^{2+}]_{ER}$ and consequently Ca^{2+} dissociates from the EF-hand domain. This results in the exposure of hydrophobic residues in the EF-hand-SAM complex, thereby initiating STIM1 oligomerization (**Figure 1.2**) (25). Mutation of acidic residues in the cEF-hand domain causes STIM1 oligomerization independently of ER Ca^{2+} content (24). Expression of STIM1 with such

cEF-hand domain mutations results in constantly activated STIM1 (which localized almost entirely in the subplasmalemmal area) and constitutively active CRAC channel. The Ca^{2+} affinity of the EF-hand domain has also been assessed. The luminal EF-hand–SAM domain of STIM1 binds Ca^{2+} with a dissociation constant (Kd) of ~200 μM , whereas that of STIM2 was found to be 2-fold higher (Kd ~400 μM) (19,24). Hence, STIM2 is more sensitive to small changes in luminal Ca^{2+} in comparison to STIM1; moreover it is a weaker activator of Orai channels (26). Therefore STIM2 is rather considered to be a feed-back regulator of basal ER luminal and cytosolic Ca^{2+} levels, whereas STIM1 is the ubiquitous transducer and activator of CRAC channels in most cell types except for the brain (20) and dendritic cells (27), where STIM2 is the key mediator of SOCE activation.

1.4 Oligomerization and translocation of STIM1

In resting conditions STIM1 is distributed homogenously on the ER membrane in a dimeric state (25,28) maintained through interactions mediated by the coiled-coil 1 (CC1) and SOAR domains (28). Following store depletion, the STIM1 dimers undergo rapid oligomerization, in which both N-terminal [between EF-hand SAM domains (24)] and C-terminal intermolecular interactions [between CC1 domains, in particular amino acids 249–390 (29)] were shown to play a role. Subsequently the STIM1 multimers redistribute to ER-PM junctions within few seconds to form higher aggregates referred to as „STIM1 puncta" (11,30). Oligomerization of STIM1 was found to be the necessary and sufficient molecular event that precedes the migration of STIM1 throughout the ER. This was experimentally proved by Luik and colleagues (31), who used a truncated STIM1 construct fused to protein domains having inducible heterodimerization ability. The luminal Ca^{2+}-sensing domain of STIM1 was replaced with FKBP12, a rapamycin-binding protein, or the FKBP-rapamycin binding (FRB) domain of the mammalian target of rapamycin (mTOR). Addition of a rapamycin analogue compound oligomerized the fusion proteins and caused them to accumulate at ER-PM junctions and activate CRAC channels without previous Ca^{2+} depletion from the ER. These artificially created STIM1 oligomers localized to the same sites in the ER-PM junctional area where the wild-type STIM1 did following ER Ca^{2+} depletion (31).

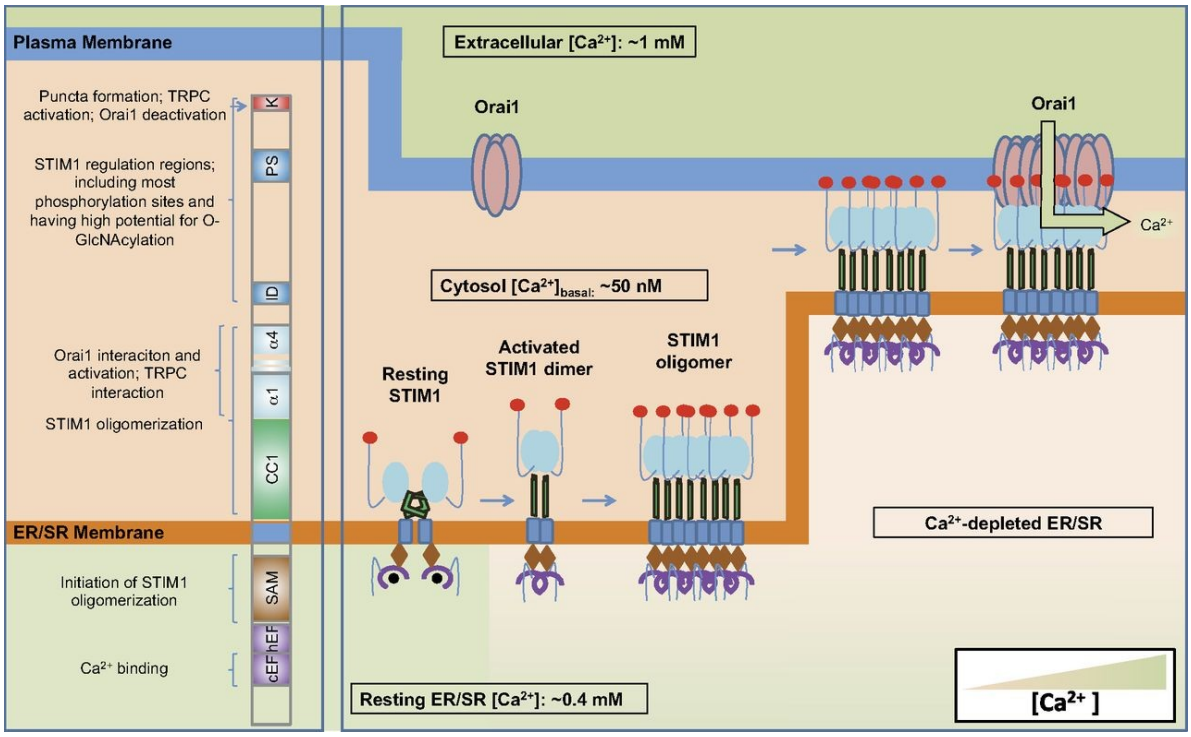

Figure 1.2 Molecular mechanism of STIM1 activation and SOCE [modified and adopted from (22)]

STIM1 is type 1 membrane protein. Its canonical Ca^{2+} binding EF-hand motif (cEF), the hidden EF-hand (hEF), and the sterile alpha motif (SAM) domain resides in the ER/SR lumen. The cytosolic region of STIM1 consists of 3 coiled coil domains [CC1 and STIM1-Orai activating region (SOAR); for stabilizing STIM1 oligomerization, Orai1 interaction and activation, and transient receptor potential proteins (TRPC) interaction], an inhibitory domain [ID; for fast Ca^{2+}-dependent store-operated Ca^{2+} channels (SOC) inactivation], a proline/serine-rich domain (PS), and a lysine-rich domain (K; for STIM1 oligomer translocation, Orai1 inactivation, and TRPC activation).

Under resting conditions, when ER/SR Ca^{2+} stores are filled ($[Ca^{2+}]$ ~ 0.4 mM), Ca^{2+} binds to the cEF-hand of STIM1, and STIM1 forms a dimer through intermolecular interaction between coiled coil domains. Upon ER Ca^{2+} depletion, Ca^{2+} dissociates from STIM1, resulting in a conformational change initiated by the SAM domain, followed by extension of the CC1 cytosolic domain, initiating STIM1 oligomerization. The STIM1 oligomers then translocate to the ER -PM junctions, where they interact with and activates Orai1 leading to SOC entry (SOCE). Under resting conditions Orai1 consists of either a homodimer or homotetramer, whereas upon activation it forms a hexamer.

1.5 Coupling of STIM1 to store-operated Ca^{2+} channels

Although STIM1 possesses an ER Ca^{2+}-sensing and a signal transducer function, it is ultimately the interaction between STIM1 and store-operated plasma membrane Ca^{2+} channels that triggers Ca^{2+} influx into the cell. Two types of SOC pore-forming subunits have been described so far: the Orai channels (12,13,23,32) and TRPCs (33,34). One year after the identification of STIM1, Orai1 was described as the store-operated Ca^{2+} pore accomplishing capacitative Ca^{2+} influx (12,35). Orai1 has two highly conserved homologues, Orai2 and Orai3, but the physiological roles of the latter two is less well

defined compared with Orai1 (22). Orai1 was predicted to have four transmembrane domains (36,37) and it is still slightly unclear whether it forms homodimers (38) or tetramers (39) under resting conditions, but according to a recent study describing the crystal structure of Orai1, it seems feasible that upon activation it is organized into a hexameric structure (36).

STIM1 clusters at the ER-PM junction were shown to co-localize with Orai (40,41), suggesting direct interaction between the proteins yielding I_{CRAC} activation. Results of FRET measurements (42,43) and co-immunoprecipitation assays also supported this theory (44). Direct physical interaction and the interacting sites within STIM1 and Orai1 molecules have been demonstrated by Park et al. using GST pulldown assay (45). They identified two functional domains of STIM1 involved in the formation of active STIM1-Orai1 complexes. The C-terminal polybasic domain of STIM1 is required for STIM1 targeting to ER-PM junctions in the nominal absence of Orai1. In addition, a 107 residue CRAC activation domain (CAD) in STIM1 binds directly to the N and C termini of Orai1 (45). Similar activation domains (with nearly overlapping sequences) of STIM1 named STIM-Orai activating region (SOAR) (46) and a shorter Orai1-activating small fragment (OASF) (47) were also described by two additional independent studies, confirming the initial assumptions of a direct STIM1-Orai1 coupling. Furthermore, McNally and colleagues recognized that binding of STIM1 to Orai1 does not only control channel gating, but determines the ion selectivity of the store-operated Ca^{2+} pore as well (48).

Although Orai channels are the most established targets of STIM, TRPCs were also shown to be closely associated with STIM (33,34,49). TRPCs belong to a non-selective ion channel family consisting of seven members (TRPC1-7), which mediate the influx of mono- and divalent cations including Na^{+}, Ca^{2+}, Ba^{2+}, or Sr^{2+}. They exhibit various properties, regulation mechanisms and physiological functions and most of them are store-operated. [For detailed characterization of TRPCs see (34,49)]. Long before the role of STIM1 and Orai1 in SOCE was recognized, TRPC1 had already been described as a potential mediator of this Ca^{2+} influx pathway in Chinese hamster ovary (CHO) cells (50). This initial observation was subsequently confirmed in other cell types as well (51,52). Ever since, the role of TRPCs in SOCE have been extensively investigated (34,53,54), yet, their direct involvement in the machinery is still often debated (55,56). It is currently assumed that, Orai1 and TRPC1 cell-type specifically form the Ca^{2+} pore in a

heterogeneous complex, generating distinct patterns of Ca^{2+} signals in cells that are decoded for the regulation of specific cellular functions (22,34).

1.6 Regulation of STIM1-Orai1 dependent SOCE machinery

Although the participants of the SOCE machinery are sufficiently described, the underlying regulatory mechanisms which control or finely tune SOCE are not entirely clarified. One remarkable feature of STIM1 activation is its structural rearrangement once Ca^{2+} dissociates from its EF-hand domain. According to the model of Korzienowsky et al. electrostatic interactions between basic residues in the CAD/SOAR domain and acidic residues within STIM1-CC1 mask the CAD/SOAR domain, thereby preventing its coupling to Orai1 under resting conditions (57). Dissociation of Ca^{2+} from the luminal end of STIM1 causes conformational change in both N- and C-terminal side of the molecule. This action "frees" the CAD/SOAR domain and induces the oligomerization of STIM1 (57). Activated STIM1 oligomers subsequently migrate to PM proximity and anchor to negatively charged phospholidpids of the PM through their elongated C-terminal polybasic domain. The activated oligomeric STIM1 can then tether and trap Orai1 channels diffusing in the PM. At the same time, an electrostatic interaction between the exposed acidic domains in CAD/SOAR and basic domains in the C terminus of Orai1 results in formation of the activated channel complex, thereby allowing Ca^{2+} entry. This conformational rearrangement of STIM1 upon activation was referred to as an "intermolecular switch" that enables a direct coupling with Orai1 (57,58). Furthermore, a recent study revealed that the active SOAR domain has a dual function. On one hand, SOAR directly binds to Orai1, triggering its activation, as shown originally by Yuan et al. (46). On the other hand, the study of Covington et al. indicates that SOAR is also involved in mediating STIM1 oligomerization (28). This observation further supports the concept of "an intermolecular switching", which is a necessary event leading to the activation of Orai1 by STIM1.

Apart from the "intermolecular switching" phenomenon, STIM1 activation and coupling to Orai1 is influenced by other factors as well, such as the stoichiometry of STIM1 and Orai1 molecules (23,59). While other observations propose that these proteins work in a large macromolecular complex to mediate the Ca^{2+} influx (41). STIM1 activation is also controlled by certain kinases [e.g.: SGK-1 or AMPK (60); ERK1/2 (61);]. Numerous phosphorylation sites of STIM1, which predominantly localize between its ID and K domains on the C-terminus (see **Figure 1.2**), have been described (61,62). Phosphorylation

of these amino acids by AMPK for instance may prevent a too excessive SOCE activation, when energy reserves are low (60), whereas phosphorylation by ERK1/2 regulates STIM1-Orai1 coupling (61). However, the exact physiological role of many phosphorylation sites is still elusive.

In one of our earlier works, we also investigated STIM1-Orai1 coupling and introduced a novel aspect of this interaction (63). In this study the impact of endocannabinoids on SOCE was tested. We found that N-arachydonoylglicine (NAGly), a derivate of the well-known endocannabinoid N-arachidonoylethanolamid, (also referred to as anandamide), reversibly hinders the coupling of STIM1 to Orai1, thereby attenuates SOCE. In the study it was postulated that NAGly might trigger a cellular signaling cascade, which involves the activation of certain kinases (e.g.: ERK1/2), leading to the suppression SOCE. We found however no experimental evidence for such action of NAGly, thus, this assumption still awaits clarification.

The activation and deactivation of STIM–Orai coupling is a steady-state event that is controlled by the influx of Ca^{2+} itself. Several intriguing regulatory mechanisms – including Ca^{2+}-dependent fast and slow inactivation of CRAC channels (*see also chapter 1.8*) - have been described (56,64-66), On one hand, entering Ca^{2+} is pumped back to the ER by SERCA and the increase of $[Ca^{2+}]_{ER}$ terminates STIM1 activation, disaggregates STIM1 clusters and turns off SOCE (56). On the other hand, sophisticated manipulation of cytosolic and ER Ca^{2+} levels revealed that global and localized cytoplasmic Ca^{2+} elevations have a negative feedback effect on STIM1 clustering/SOCE independently of ER Ca^{2+} content (64,65). The fact that cytosolic Ca^{2+} *per se* feeds back on SOCE activation/deactivation proposes an intrinsic cellular mechanism, which prevents over-activation of SOCE and avoids Ca^{2+} overloading of the cell.

Through their ability to take up cytoplasmic Ca^{2+}, mitochondria regulate both activation and inactivation of CRAC channels and in turn SOCE. The various sites of action of mitochondria on SOCE are summarized in *chapter 1.8.*

1.7 Role of SOCE in physiology and pathology

The ultimate coordinated function of ER Ca^{2+} release and subsequent SOCE is essential in generating cytosolic Ca^{2+} oscillations, which control a variety of cellular functions including Ca^{2+} mediated gene expression. As shown in **Figure 1.3**, the cellular signaling

events downstream of STIM/Orai-dependent SOCE are predominantly accomplished through the calmodulin-calcineurin-NFAT (nuclear factor of activated T-cells) signaling axis (22,67,68). It is now well established, that many different cell types and tissues rely on a SOCE-driven Ca^{2+} signaling cascade to maintain their normal intracellular Ca^{2+} homeostasis (68). Although only a few documented disease states could be specifically attributed to a failure of SOCE approximately ten years ago (49), by now numerous "STIMophaties" (23), "CRAC channelopathies" (69) and disorders related to a defect of this signaling pathway have been described (68).

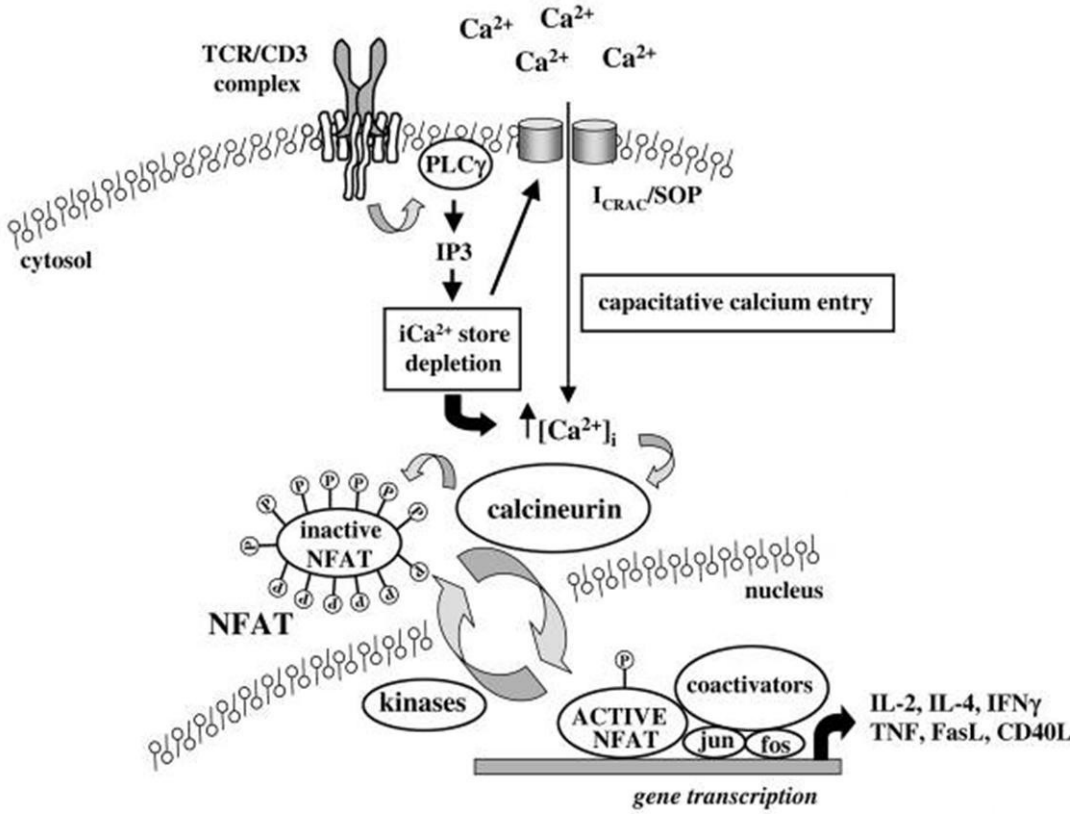

Figure 1.3 Schematic diagram of NFAT translocation and activation in T-cells [modified and adopted from (70)]

The illustration summarizes the downstream effects of cytosolic Ca^{2+} signals generated by SOCE. After TCR ligation and PLCγ1 activation, newly generated IP_3 binds to its receptor on the ER surface inducing the release of Ca^{2+} from internal stores. Store depletion triggers the opening of store-operated channels (SOC) in the plasma membrane that allows the influx of Ca^{2+} (I_{CRAC}). This leads ultimately to activation of the serine-phosphatase calcineurin, which removes the phosphate groups of NFAT. Dephosphorylated NFAT translocates from the cytosol to the nucleus, where it participates in mediating calcium-inducible gene expression of different cytokines (e.g: IL-2, IL-4, TNF, IFNγ) or cell surface proteins (CD40L, FasL) in co-ordination with other transcription factors (jun/fos). Abbreviations: iCa^{2+} - intracellular calcium; $I_{CRAC/SOP}$ - calcium-release-activated calcium current; PLCγ - phospholipase Cγ; TCR - T-cell receptor, NFAT –nuclear factor of activated T-cells, IL – interleukine, TNF – tumor necrosis factor) IFN – interferon)

Initially, SOCE/CCE (I_{CRAC}) was described in immune cells (6,7). Moreover, immunological studies led to the discovery of the store-operated Ca^{2+} channel subunit Orai (12). SOCE is of particular importance in immune cell function, as these cells have small internal Ca^{2+} stores, therefore, they strongly rely on extracellular Ca^{2+} influx through SOCE (67,71). Any kind of failure of SOCE in immune cells (lymphocytes, NKs; macrophages; mast cells) leads to their insufficient activation and proliferation, deficient cytokine production and secretion (67). In fact, the defect of the Ca^{2+} influx results in a weak immune response to antigen stimuli. Phenotypically, the malfunction of SOCE may yield auto-immunity, decreased anti-tumor immune response, or even severe combined immunodeficiency (SCID) (67). In $STIM1^{KO}$ or $Orai1^{KO}$ animal models an immunodeficiency of varying severity is present in most cases, however the defects of STIM/Orai signaling may cause non-immunological disorders as well. These disorders may affect the cardiovascular system [e.g.: cardiac hypertrophy (22)], skeletal muscle differentiation and function (72), platelet function (73) or the nervous system (74). False SOCE signaling may also promote tumor growth by increasing oncogenic activity (75) or by reducing anti-tumor immune response (76). The list of cells, tissues and organs, where malfunctioning SOCE can cause disorders, is far from complete. Currently ongoing research aims to unveil more physiological and pathophysiological conditions, where SOCE plays a major role.

1.8 Mitochondrial regulation of CRAC channels and SOCE

As introduced earlier, SOCE in under the strong control of mitochondria. Long before the identification of the molecular components, a close functional relationship between SOCE, I_{CRAC} and mitochondrial Ca^{2+} uptake was revealed in immune cells [reviewed in (49,77)]. Initially Hoth and colleagues reported that a chemically induced mitochondrial depolarization suppresses SOCE in T-lymphocytes. This was the first evidence of a functional coupling between mitochondria and SOCE (8). In the early 2000´s Parekh and colleagues performed a series of electrophysiological studies in mast cell (78,79), which confirmed the initial findings of Hoth et al., and further extended their conclusions (8). In their studies they described that intact respiring mitochondria are essential for store-operated Ca^{2+} current. Moreover, they also reported that stimulation of cell-surface receptors with an IP_3-generating agonist activates detectable I_{CRAC} only, if mitochondria are

maintained in an energized state by an "energizing-cocktail", which was added to the cells prior to experiments. [The exact composition of the cocktail is described in (78)]

Mitochondrial Ca^{2+} buffering has also been shown to contribute to both to the activation and maintenance of SOCE. Ca^{2+} released from the ER by IP_3 is rapidly taken up by mitochondria. This, on one hand can induce a more pronounced Ca^{2+} release (80,81), on the other hand, reduces the amount of Ca^{2+}, which can be pumped be to the ER lumen by SERCA. This leads again to a more extensive Ca^{2+} influx through CRAC channels (80,82). As mentioned earlier (*see chapter 1.6*) the Ca^{2+} that enters through CRAC channels feeds back to induce slow or fast inactivation of the channel (66,83). Fast inactivation appears within milliseconds, and it has been shown to be related to a local feedback effect of Ca^{2+} and calmodulin (CaM) activation (83,84). On the contrary, Ca^{2+}-dependent slow inactivation requires a bulk rise in cytoplasmic Ca^{2+} and it develops in tens of seconds. Through their ability to buffer incoming Ca^{2+}, mitochondria can reduce the rate of development as well as the overall extent of slow inactivation (77,78).

As indicated by the study of Singaravelu et al., STIM1 migration is another molecular event, where mitochondria were shown to interfere with SOCE (85). Strong mitochondrial depolarisation evoked by chemical uncoupling agents (e.g.: FCCP), apart from their detrimental effect on mitochondrial Ca^{2+} uptake, reduced STIM1 puncta-formation without harming STIM1 oligomerization. Interestingly, this phenomenon was highly dependent on the presence of mitofusin 2 (MFN2), a mitochondrial fusion protein that tethers the organelle to the ER (86). If MFN2 level was reduced in the cells by specific siRNAs, SOCE has become insensitive to mitochondrial depolarization. The authors concluded that "mitofusin 2 acts as a brake, attenuating Ca^{2+} influx after mitochondrial depolarisation. Depolarised mitochondria are unable to buffer cytoplasmic Ca^{2+} and, thus, Ca^{2+} overload leads to cell death. Termination of Ca^{2+} entry under these conditions by mitofusin 2 might therefore serve as a protective mechanism to prevent excessive Ca^{2+} rise" (85).

Likewise in many other studies (8,9,78,79), in the aforementioned work of Singaravelu et al. mitochondrial Ca^{2+} uptake was typically diminished by chemical uncouplers such as carbonyl cyanide-4-(trifluoromethoxy)-phenylhydrazone (FCCP) or antimycin A, an inhibitor of complex III of the respiratory chain. Addition of such compounds causes a strong mitochondrial depolarization, which eliminates the driving force for Ca^{2+} to enter the mitochondria thereby abrogating Ca^{2+} accumulation of the organelle. The observation

that such toxins also attenuate SOCE was first made by Hoth and colleagues (8). Subsequently this approach has been widely used to study the SOCE-mitochondria relationship. These toxins however do not solely diminish mitochondrial Ca^{2+} uptake, but may also have many other unspecific effects on the mitochondrial homeostasis such as the depletion of the ATP pool or matrix acidification. Hence, the utilization of such toxins is eventually an indirect approach to investigate the mitochondria-SOCE relationship. Notably, at that time, when most of these landmark observations describing the mitochondrial regulation of SOCE were made, the identity of the mitochondrial Ca^{2+} transporter proteins were unknown. Very intensive research of the recent years led to the identification of numerous proteins that mediate mitochondrial Ca^{2+} uptake *(see chapter 1.10)*.

1.9 Principles of mitochondrial Ca^{2+} handling

Mitochondria beside its well-established central role in cellular bioenergetics can accumulate and release Ca^{2+}. The transfer of Ca^{2+} into mitochondria is linked to several vital cellular functions including energy homeostasis regulation, ROS production or cell survival (87). Moreover, it has a strong regulatory feed-back effect on cellular Ca^{2+} signaling events, which involve the regulation of SOCE as well (49,77). Ca^{2+} from the cytoplasm enters the mitochondrial matrix through the outer and inner mitochondrial membrane (OMM and IMM respectively) and it is buffered within the organelle. The outer mitochondrial membrane (OMM) is relatively permeable to Ca^{2+} ions due to the presence of the voltage-dependent anion channel (VDAC), which allows the diffusion of ions and smaller molecules. Ca^{2+} however, cannot penetrate the IMM, but is transported by a complex and not yet fully understood mechanism into the matrix (see below). This Ca^{2+} transport uses the driving force provided by mitochondrial membrane potential ($\Delta\Psi_m$=~−180 mV) itself, which is generated upon proton pumping by respiratory chain components (reviewed in (87-89).

As for the mitochondrial Ca^{2+} extrusion, it is mostly accepted that the mitochondrial Na^+/Ca^{2+} exchanger (NCLX) activity is determinant in excitable cells (90), and NCLX inhibition or silencing does not completely abolishes Ca^{2+} efflux (91). This indicates that other mechanisms are involved in this process, from which, one proposed mechanism is mediated by the H^+/Ca^{2+} antiporter (92). Some evidence suggest that under certain

physiological or pathological conditions, the mitochondrial permeability transition pore (mPTP) is also involved in the efflux, but its participation is not entirely clarified (88,93).

1.10 Components of the mitochondrial Ca^{2+} uptake machinery

As mentioned above, the uptake of Ca^{2+} into the mitochondrial matrix involves complex mechanisms, which have been in the focus of very intensive research for decades. The search for the molecular constituents of mitochondrial Ca^{2+} uptake started about 50 years ago, but only the discoveries of the last couple of years has brought the long-awaited breakthrough on this field. Due to the development of new screening techniques (particularly the high-throughput RNAi screening), there has been a recent "burst" in the number of studies identifying molecular components of the uptake machinery, or as it is currently referred to as the mitochondrial calcium uniporter complex (MCUC) (89,94).

1.10.1 Mitochondrial Ca^{2+} uniporter (MCU)

Initially a short report more than 20 years proposed that MCU was most likely a gated channel (95). The molecular identity of MCU remained however unknown until recently. Although an electrophysiological study in 2004 by Clapham et al. confirmed the original idea that MCU forms a Ca^{2+} specific ion channel (96), the molecular nature of this long searched protein was first unraveled simultaneously by two independent studies in 2011 (97,98). MCU (or also referred to as CCDC190A) is located in the IMM, possesses two putative transmembrane helixes, its down-regulation inhibits and overexpression increases Ca^{2+} sequestration by mitochondria. Recently, employing structural bioinformatics techniques it has been shown that the putative pore region of MCU is defined by eight helices (99). In the original study of De Stefani et al. it was also shown that a point mutation in the predicted pore forming domain of MCU abolishes the current of wild-type MCU (97). Moreover, the same group very recently described a homolog of MCU named MCUb, which acts as a dominant-negative regulator of the MCU complex (99). Although MCU is considered to be the core component of the ubiquitous mitochondrial Ca^{2+} channel, surprisingly the loss of the protein does not yield strong phenotypical changes in the knockout mouse model (100).

1.10.2 Mitochondrial Ca^{2+} Unipoter Regulator 1 (MCUR1)

MCUR1 (or previously named CCDC90A) was identified by siRNA screening in HEK293T (101). It is a 40-kDa protein with two transmembrane domains and one coiled-coil region. The N- and C-terminus face the intermembrane space, while the major part of the protein is located in the matrix. Cells depleted of MCUR1 exhibit a block of mitochondrial Ca^{2+} uptake and several bioenergetics defects such as increased autophagy and reduced sensitivity to apoptosis, without any impact on mitochondrial membrane potential (101). Co-immunoprecipitation experiments suggest that MCUR1 interacts with MCU, but not with MICU1, and its overexpression results in an increase of mitochondrial Ca^{2+} uptake, but only when MCU is present (94,101). MCUR1 appears also to regulate the expression of MCU, as downregulation of MCUR1 results in a significant increase of both the mRNA and the protein levels of MCU. The authors concluded that MCUR1 is not a specific regulator of MCUC, but has additional important functions (yet unknown), which are independent from the regulation of mitochondrial Ca^{2+} uptake (101).

1.10.3 Mitochondrial Ca^{2+} uptake (MICU)

MICU1 was identified approximately one year before MCU as a promising candidate to mediate mitochondrial Ca^{2+} uptake (102). KO of MICU1 in HEK293 cells abolished mitochondrial Ca^{2+} uptake, though its overexpression did not have a severe impact on the rate and extent of Ca^{2+} uptake by the organelle (102). MICU1 was also shown to be essential for the Ca^{2+} homeostasis of pancreatic ß-cells and its contribution to metabolism-secretion coupling was highlighted (103). MICU1 is a 54-kDa membrane protein, possessing two classical EF-hand Ca^{2+}binding domains (102), but it was predicted to have only one very short membrane-spanning domain, thus it is unlikely to form a channel. A subsequent publication assigned MICU1 as a "gatekeeper" for MCU-mediated mitochondrial Ca^{2+} sequestration: accordingly MICU1 inhibits the MCU-driven mitochondrial Ca^{2+} uptake under resting conditions and sets a cytoplasmic Ca^{2+} concentration threshold for mitochondrial Ca^{2+} uptake (104). In the absence of MICU1 mitochondria is overloaded by Ca^{2+}, which triggers excessive reactive oxygen species generation and sensitivity to apoptotic stress. The "gatekeeper" function of MICU1 was further specified by the findings of Csordas et al (105). According to that study, MICU1 faces the intermembrane space to sense cytoplasmic Ca^{2+} and it regulates not only the Ca^{2+} threshold of the uptake, but contributes to the cooperative activation of MCU. To make the

"MCU/MICU1-assembly" even more complex, Plovanich and colleagues described MICU2 and MICU3 (106), two paralogues of MICU1 that have considerable impact on the mitochondrial Ca^{2+} transfer under certain circumstances (e.g. in response to large cytosolic Ca^{2+} pulses). A most recent study even proposes a functional crosstalk between the MICU paralogues by formation of dimers, which finely tune MCU-mediated mitochondrial Ca^{2+} uptake (107).

1.10.4 Uncoupling protein 2 and 3 (UCP2/3)

The uncoupling proteins belong to a family of proton channels/transporters. Their prototype UCP1 is located in the IMM and was originally shown to be a "physiological uncoupler" of electron transport and oxidative phosphorylation, and mediator of thermogenic proton leak in brown adipose tissue (108,109). Their fundamental role in mitochondrial Ca^{2+} uptake was first described by our group in 2007 (110). We found that downregulation of UCP2 and UCP3 by specific RNAi leads to a substantial decrease in mitochondrial Ca^{2+} uptake, whereas the overexpression of UCP2 and UCP3 increased the efficacy of mitochondrial Ca^{2+} accumulation. As conclusion it was drawn that UCP2 and UCP3 are elementary units of mitochondrial Ca^{2+} uptake machineries, but they do not form the channel pore itself (110). Although contribution of UCPs to mitochondrial Ca^{2+} sequestration was challenged by some studies (111,112), many functional data (94,113,115) including present work (116,117) provides evidence that UCP2/3 is a major determinant of the mitochondrial Ca^{2+} uptake machinery under certain conditions of cell stimulations. Moreover, our latest findings indicate that MCU- and UCP2-dependent mitochondrial Ca^{2+} uptake regulates STIM1 activation and SOCE in the same manner *(see chapter 3.3)*.

1.10.5 Leucine zipper EF hand-containing transmembrane protein 1 (Letm1)

In 2009 a high-throughput RNAi screening assay revealed Letm1 as a mediator of a Ruthenium Red insensitive electrogenic Ca^{2+}/H^{+} antiport (118), which is distinct from the MCU-mediated Ca^{2+} accumulation of mitochondria (115,118). Downregulation of Letm1 resulted in inhibition of Ca^{2+} uptake, but its overexpression hardly affected the process (118). Interestingly Letm1 is present in yeast, named Yol027/Mdm38, [this was not the case in UCP2 and 3 (110)] and its KO phenotype can be rescued by the expression of mammalian Letm1 (119). Their discoverers maintain that Letm1 is a Ca^{2+}/H^{+} antiport that

insures energy dependent mitochondrial Ca^{2+} uptake at low cytosolic Ca^{2+}concentrations (120,121).

1.10.6 Essential MCU regulator element (EMRE)

EMRE, the newest member of the mitochondrial Ca^{2+} uptake complex (122), was identified by quantitative mass spectrometry and a series of co-immunoprecipitation assays. EMRE is a ~10-kD protein with a predicted mitochondrial targeting sequence, a predicted transmembrane domain and a highly conserved acidic C-terminus. In the isolated complex, MCUs and MICUs were found together with EMRE, while MCUR1 was not associated with the other proteins (122). EMRE was shown to interact with MCU at the IMM and with MICU1 in the intermembrane space, thus it is proposed that EMRE may act as a bridge between MCU and MICUs, but not with MCUR1 (122).

As seen above, the intensive experimental work of the last 5-7 years have brought an enormous breakthrough on the field of mitochondrial Ca^{2+} uptake research, since numerous members of the MCUC were successfully identified and characterized. However, the molecular nature of these proteins, their function and interactions are still insufficiently characterized. For instance, it is not yet understood, whether all these components work together in a huge macromolecular complex or they are activated in a cascade-like manner. Is their functioning cell-specific or only a part of them are active depending on the mode of cell stimulation? Hence, future research should aim to describe and elaborate the functional interrelation of these newly identified proteins that mediate mitochondrial Ca^{2+} sequestration. Moreover, it also seems feasible that “newer players would join the already complex game of mitochondrial Ca^{2+} uptake”.

1.11 Aims of the study

As introduced in the previous chapters, both mitochondrial Ca^{2+} uptake and SOCE are intensively explored, hot topics of cellular Ca^{2+} signaling. The molecular constituents of SOCE and the components of the mitochondrial Ca^{2+} uptake machinery have been identified recently. However, the underlying regulatory mechanisms, especially the functional interrelation between the mechanisms are not yet fully understood. In view of recent findings and the existing knowledge on the field of SOCE- and mitochondrial Ca^{2+} uptake-research, current work was designed to achieve the following goals:

(i) To establish new methods and expand the palette of techniques, which allow assessment and quantification of mitochondrial Ca^{2+} handling

(ii) To characterize distinct mitochondrial Ca^{2+} uptake routes, in particular, the functional composition of mitochondrial Ca^{2+} transporters upon different modes of cell stimulation

(iii) To investigate the role of mitochondrial Ca^{2+} handling in SOCE activation by employing a novel approach. Instead of using chemical uncoupling compounds (e.g FCCP), the goal is the specific suppression of mitochondrial Ca^{2+} uptake by siRNAs and the examination of its impact on SOCE.

2. METHODS AND MATERIALS

This chapter is based on the "Methods and Materials" sections of the following studies (116,117,123).

2.1 Chemicals

Table 1 summarizes the chemicals used for the experimental work.

Table 1: List of compounds			
Name	**Source (Company)**	**Conc. of working solution**	**Short description**
Histamine	Sigma	100 µM	Endogenous H_1 and H_2 receptor agonist; mobilizes Ca^{2+} from internal stores (124)
BHQ	Sigma	15 µM	Selective, reversible inhibitor of SERCA (125)
ATP	Sigma	100 µM	P_2 purinergic receptor agonist; mobilizes Ca^{2+} from internal stores (126)
Thapsigargin	Abcam	1 µM	Selective, irreversible inhibitor of SERCA (127)
Oligomycin	Sigma	2 µM	Inhibitor of F_1F_0 ATP synthase (128)
FCCP	Sigma	2 µM	Chemical uncoupler of electron transport and oxidative phosphorylation; permeabilizes the IMM to protons (129)
Fura-2AM	TefLabs	2 µM	Chemical Ca^{2+} indicator. When added to cells, the compound accumulates in the cytosol and allows ratiometric imaging of changes in $[Ca^{2+}]_{cyto}$ (130)
BAPTA-AM	Abcam	10 µM	Cell-permeant chelator, highly selective for divalent cations (131)
EGTA	Sigma	1 mM	Chelator with high specificity for Ca^{2+} ions (132)

2.2 Cell culture

Experiments were performed in the human umbilical vein endothelial cell line EA.hy926 and in HeLa cells. For certain experiment *(see chapter 3.3)*, the HeLa SilenciX® knockdown cells (Tebu-bio, Le-Perray-en-Yvelines, France) stably expressing scrambled siRNA (Control), or siRNA against the mitochondrial calcium uniporter (MCU^{KD}) or the uncoupling protein 2 ($UCP2^{KD}$) were used. Both cell types (EA.hy926 and HeLa cells) were cultured in a humidified incubator at 37 °C and 5% CO_2 and were kept in Dulbecco's Modified Eagle Medium (DMEM) containing 10% fetal calf serum (FCS), 100 U/ml penicillin, 100 mg/ml streptomycin. The culture medium of EA.hy926 cells were

additionally supplemented with 1% HAT (5 mM hypoxanthin, 20 mM aminopterin and 0.8 mM thymidine).

2.3 Transfection of cells

Fluorescent protein (FP)-tagged constructs alone or together with SiRNAs were incorporated into cells by (lipo)transfection. Transfection protocols are described in details below.

2.3.1 Transfection of plasmid DNA

Cells were seeded on glass cover slips (Ø=30 mm) 24 hours prior to transfection. At 60–80% confluence, cells were transfected with 1.5-2 µg (per 30-mm well) of plasmid DNA encoding the respective FP-tagged construct using 4µg per well TransFastTM transfection reagent (Promega, Madison, WI) in 1 ml of serum- and antibiotic-free DMEM medium. Cells were kept in a humidified incubator (37 °C, 5% CO_2) for 4–5 hours before changing back to complete medium. All experiments were performed either 24 or 48 hours after transfection.

2.3.2 Transfection of plasmid DNA together with siRNA

When cells were transfected with plasmid DNA together with SiRNA a slightly different protocol was applied. Cells on glass cover slips (at 60-80 % confluence) were incubated for 1 hour in a transfection medium composed of 1-2 µg plasmid DNA, 4µg TransFastTM reagent, 100 nM SiRNA and 0.5 ml DMEM (without serum and antibiotics). Following 1 hour incubation period, 0.5 ml incomplete DMEM was given additionally to the cells and they were kept in a humified incubator (37 °C, 5% CO_2) for overnight. After overnight incubation the transfection medium was replaced with the full DMEM medium and experiments were performed either 48 or 72 hours after transfection.

2.4 SiRNAs and approval of their respective knockdown efficiencies

2.4.1 SiRNAs against various mitochondrial proteins

The siRNAs against human (h) MCU, UCP2/3 and Letm1 were obtained from Microsynth (Balgach, Switzerland) and their nucleotide sequences (5´-3´) were as follows:

si1-hMCU: GCCAGAGACAGACAAUACUtt

si2-hMCU: GGAAAGGGAGCUUAUUGAAt

si1-hLetm1: UCCACAUUUGAGACUCAGUtt

si2-hLetm1: AUGUUCCAUUUGGCUGCUGtt;

si-hUCP2: GCACCGUCAAUGCCUACAAtt;

si-hUCP3: GGAACUUUGCCCAACAUCAtt.

For controls, a scrambled siRNA was used: UUCUCCGAACGUGUCACGUtt.

2.4.2 RNA isolation and cDNA synthesis

Total cellular RNA from control and target siRNA-treated HeLa cells was isolated using an RNA isolation kit provided by PEQLAB Biotechnologie GmbH (Erlangen, Germany). We followed the isolation protocol provided by the manufacturer. Cells grown in 6-well plates to 100 % confluence were washed twice with PBS. After washing, a cell lysis buffer was added to the cells. The lysate was transferred to a DNA removing column and was centrifuged at 12,000 g for 1 minute. Equal volume of 70 % ethanol was added to the flow-through of the DNA removing column. The solution was mixed well and the complete lysate was applied onto a PerfectBind RNA Column, which was followed by a centrifugation step at 10,000 g for 1 minute. The flow-through was discarded; the column was reinserted into a fresh collection tube and it was washed twice with 500 µl and 600 µl of wash buffer 1 and wash buffer 2 respectively at a centrifugation speed of 10,000 g for 1 minute. After the second washing the empty column was centrifuged at 10,000 g for another 2 minutes. RNA was eluted in 50-100 µl of nuclease-free water and centrifuged at 5000 g for 1 minute.

For reverse transcription, the concentration of the isolated RNA was assessed on a spectrophotometer (UviLine 9400, SCHOTT Instruments, Mainz, Germany). Reverse transcription of 2 µg of RNA was carried out using a cDNA synthesis kit from Applied Biosystems (USA) on a thermal cycler (PEQLAB). The reverse transcription master mix was composed of:

10x RT buffer	*2.0 µl*
100 mM dNTP mix	*0.8 µl*
10x RT Random Primers	*2.0 µl*
Reverse Transcriptase	*1.0 µl*
RNase Inhibitor	*1.0 µl*

Nuclease-free H_2O	*3.2 µl*
Total per reaction	***10 µl***

The thermal cycler protocol was as follows:

Step 1 (25 ºC)	*10 minutes*
Step 2 (37 ºC)	*120 minutes*
Step 3 (85 ºC)	*5 minutes*
Step 4 (4 ºC)	*∞ minutes*

2.4.3 Real-Time PCR

The knockdown efficiency of respective siRNAs was validated by performing Real-time PCR with the QuantiFast SYBR Green RT-PCR kit (Qiagen, Hilden, Germany) using 96-well plates on LightCycler 480 (Roche Diagnostics, Vienna, Austria). RNA polymerase II (RPOL2) was used as housekeeping control. Primers for RPOL2, UCP2, UCP3, MCU and LETM1 were obtained from Invitrogen® and their sequences (5' – 3') are as follows:

RPOL2 for: CATTGACTTGCGTTTCCACC,
RPOL2 rev: ACATTTTGTGCAGAGTTGGC,
UCP2 for: TCCTGAAAGCCAACCTCATG,
UCP2 rev: GGCAGAGTTCATGTATCTCGTC,
UCP3 for: AGAAAATACAGCGGGACTATGG,
UCP3 rev: CTTGAGGATGTCGTAGGTCAC,
MCU for: TTCCTGGCAGAATTTGGGAG,
MCU rev: AGAGATAGGCTTGAGTGTGAAC,
Letm1 for: TGTTCTTCAAGGCCATCTCC,
Letm1 rev: TGTTGCTGTGAAGCTCTTCC.

The real-time PCR master mix consisted of:

cDNA (10-50x dilution)	*1-3 µl*
SYBR Green PCR Master Mix,	*2 µl*
Forward Primer (10 µM)	*1 µl*
Reverse Primer (10 µM)	*1 µl*
Nuclease free H_2O	*variable*
Total per reaction	*10 µl*

The thermal cycler protocol was as follows:

Initial heat activation (95 ºC)	*50 minutes*
Two-step cycling (repeated 40x)	
Denaturation (95 ºC)	*10 seconds*
Annealing and extension (60 ºC)	*30 seconds*

Data was analyzed by ΔΔCt method, as described previously (103). Knock-down efficiency was in the same range as previously reported for endothelial cells (115).

2.4.4 Validation of MCU- and UCP2-knockdown in SilenceX HeLa cells

RNA isolation from SilenceX Control, MCU^{KD}, and $UCP2^{KD}$ HeLa cells, cDNA synthesis and suqsequent real-time PCR were performed as described in the previous chapter. RPOL2 was used as a housekeeping control. Primers for RPOL2 and MCU sequences are shown in the previous chapter. For human UCP2 the QuantiTect® Primer Assays (Qiagen, Cat.No. QT00014140) were used.

2.5 Measurement of mitochondrial membrane potential

HeLa cells were loaded with 1 μM of the ratiometric dye JC-1 (Invitrogen) in culture medium at 37 °C for 40 min, washed with PBS, dissociated by trypsinization, centrifuged at 1250 rpm for 5 min and re-suspended in a Ca^{2+}-containing buffer described in chapter 2.8. JC-1 fluorescence was detected using a fluorescence spectrophotometer (Hitachi F-4500, Hitachi, Inula, Austria). JC-1 was excited at 490 nm and 540 nm and emission was collected at 540 nm and 590 nm, respectively. The basal fluorescence ratio was normalized to the ratio after dissipation of mitochondrial membrane by 10 μM FCCP**.**

2.6 Measurement of oxygen consumption rate (OCR)

Cells were plated in XF96 polystyrene cell culture microplates (Seahorse Bioscience) at a density of 30000 cells per well. After an overnight incubation, cells were washed and preincubated for 30 min in unbuffered XF assay medium (Seahorse Bioscience) supplemented with 5.5 mM D-glucose and 1 mM sodium pyruvate at 37°C in a non-CO_2 environment. Oxygen consumption rates were subsequently measured using an XF96 extracellular flux analyzer.

2.7 Measurement of cellular ATP content

Separation of adeninenucleotides was performed on a Hypersil ODS column (5 µm, 250 x 4 mm ID), using a L2200 autosampler, two L-2130 HTA pumps, and a L2450 diode array detector (all from VWR Hitachi) as described in (133). The wavelength for detection of adenine nucleotides was set at 254 nm. EZchrom Elite (VWR) was used for data acquisition and analysis. After trypsinisation and mild centrifugation (supernatant discarded) cellular proteins of HeLa cells were precipitated with 250 µL of perchloric acid (0.4 mol/L). After centrifugation (12,000 x g), 100 µL of the supernatant were neutralized with 10-12 µL of potassium carbonate (2 mol/L, 4°C). The supernatant obtained after centrifugation was used for HPLC analysis (injection volume: 40 µL). The pellets of the acid extract were dissolved in 0.5 mL of sodium hydroxide (0.1mol/L) and used for protein determination (BCA Assay; Pierce).

2.8 Buffer solutions for Ca^{2+} imaging experiments

Prior to experiments cells were washed and maintained for 20 minutes in a HEPES buffered solution (EH-buffer) containing (in mM): 138 NaCl, 5 KCl, 2 $CaCl_2$, 1 $MgCl_2$, 1 HEPES, 2.6 $NaHCO_3$, 0.44 KH_2PO_4, 0.34 Na_2HPO_4, 10 D-glucose, 0.1 % vitamins, 0.2 % essential amino acids and 1% penicillin/streptomycin; pH adjusted to 7.4 with NaOH. During the experiments cells were perfused with a Ca^{2+} containing experimental buffer (EB), which consisted of (in mM): 145 NaCl, 5 KCl, 2 $CaCl_2$, 1 $MgCl_2$, 10 D-glucose and 10 HEPES; pH adjusted to 7.4 with NaOH. In experiments, where a Ca^{2+} free solution was applied to the cells, the $CaCl_2$ was replaced by 1 mM EGTA.

2.9 Cytosolic Ca^{2+} measurements

2.9.1 Fura-2 technique

Rapid changes of cytosolic [Ca^{2+}] were monitored with fluorescent microscope using the chemical Ca^{2+} indicator Fura-2-acetoxymethyl ester (Fura-2AM). When added to cells, Fura-2AM enters through the plasma membrane and once inside the cell, the acetoxymethyl groups are cleaved by cellular esterases. This traps the dye within the cell, and leads to its accumulation predominantly in the cytosol (130). Fura-2 is a dual excitation indicator and allows a ratiometric imaging of cytosolic Ca^{2+}. Its peak absorbance shifts from 340 nm in the Ca^{2+} bound state to 380 nm in the Ca^{2+}-free state. Therefore,

elevated $[Ca^{2+}]_{cyto}$ leads to an increase of fluorescent signal at 340 nm; while fluorescence decreases at 380 nm excitation. Fluorescence occurs at a peak wavelength of 505 ± 5 nm for excitation at either UV wavelength.

2.9.2 Experimental setup

Prior to experiments, cells were kept in the EH-buffer supplemented with 2 μM Fura-2AM (TEFLabs, Austin, TX, USA) at room temperature for 45 minutes. Following incubation, cells were washed twice with EB to remove extracellular Fura-2AM. Cytosolic Ca^{2+} measurements were performed on a Zeiss Axiovert 200M microscope (Zeiss Microsystems, Jena, Germany) equipped with a motorized filter wheel (Ludl, Electronic Products, Hawthorne, NY, USA) and a 40× objective (Plan NeoFluar 40x/1.3 Oil DIC; Zeiss Microsystems, Jena, Germany). Fura-2/AM-loaded cells were alternately illuminated at 340 and 380 nm (340HTI15 and 380HTI15 excitation filters; Omega Optical Brattleboro, VT, USA) using an XBO lamp (Visitron Systems) as light source. Emission was collected at 510 nm (510WB40 emission filter; Omega Optical Brattleboro, VT, USA) with a cooled charge-coupled device (CCD) camera (Photometrics, Tucson, USA).

2.9.3 Mn^{2+} quench assay

Fura-2/am loaded HeLa cells were perfused with the Ca^{2+}-containing EB supplemented with 100 μM $MnCl_2$. Mn^{2+} quench of cytosolic fura-2 fluorescence upon 100 μM histamine addition was measured with the Ca^{2+} imaging system described above at 360 nm excitation wavelength.

2.10 Intra- and intermolecular Förster Resonance Energy Transfer (FRET) measurements

2.10.1 STIM1 oligomerization

Oligomerization of STIM1 was monitored by measuring intermolecular FRET between CFP-STIM1 and YFP-STIM1 as shown recently (42,63). HeLa cells were transiently transfected with the respective FP-tagged STIM1 constructs. Regions of interest, where FRET was measured, covered whole individual cells. (*We thank to C. Romanin, Linz, Austria for providing us the FP-labeled STIM1 constructs.*)

2.10.2 Assessment of mitochondrial Ca^{2+} uptake with genetically encoded Ca^{2+} indicators (GECIs)

Initially, the Ca^{2+} sensing bioluminescent protein aequorin was successfully targeted to mitochondria and was primarily used to visualize changes of the free mitochondrial Ca^{2+} concentration ($[Ca^{2+}]_{mito}$) (134). However this probe exhibits weak bioluminescent signals from the biochemical reaction, thus the aequorin-based probes can hardly be used to monitor $[Ca^{2+}]_{mito}$ on the single cell level. This limitation does not persist for the genetically encoded fluorescent mitochondrial Ca^{2+} reporters.

Genetically encoded mitochondrial Ca^{2+} probes are protein-based fluorescent indicators targeted into mitochondrial matrix (MM) via a specific mitochondrial signal sequence (134), and they are typically incorporated into cells by gene transfer techniques. These probes are usually divided in two classes: the single fluorescent protein (FP)- and the Förster resonance energy transfer (FRET)-based Ca^{2+} sensors. Single FP sensors including the pericams (135), the GCamPs (136) and the recently developed GECOs (137) consist of a circularly permuted FP (cpFP) flanked by a genetically modified Ca^{2+} binding domain, the calmodulin (CaM) and its interacting peptide (M13) from the myosine light chain kinase. A common feature of these sensors is the ability of their integrated cpFPs to modulate their spectral properties in response to changes of Ca^{2+} concentration.

The other large group of fluorescent Ca^{2+} reporters is the FRET-based cameleons, which consist of two different fluorescent proteins possessing overlapping spectral properties. The "prototype" of such sensors contains the previously mentioned CaM and M13 domains, which were inserted in tandem between the cyan and the yellow fluorescent proteins (CFP/YFP) (138). Cameleons in a Ca^{2+}-bound state undergo a conformational change, whereupon the donor CFP gets in close proximity to the acceptor YFP yielding an enhanced energy transfer between the two fluorophores. Cameleons are, thus, ratiometric indicators: increase of FRET is coupled with the decrease of CFP fluorescence. This can be quantified by calculating the ratio of fluorescent emissions measured at 535 nm and 480 nm excitation (FRET Ratio). Since the introduction of the first cameleon in 1997, several derivates of this Ca^{2+} sensor with improved Ca^{2+} sensitivities (139), higher FRET-efficiencies, increased pH stability and appropriate mitochondrial targeting have been developed (140,141). In this current study the 4mtD3cpv cameleon (*kindly provided by R.Y.Tsien, San Diego, USA*) and its red-shifted variant the 4mtD1GO were used to assess

mitochondrial Ca^{2+} uptake. 4mtD3cpv encompasses a CFP and a circularly permuted Venus (cpv) as FRET donor/acceptor fluorophore pair and contains a tandem duplicated targeting sequence of cytochrome C oxidase (COX) VIII, which ensures an adequate mitochondrial targeting of the probe in HeLa cells (140). 4mtD1GO is described in details in *chapter 3.11*.

2.10.3 Assessment of ER Ca^{2+} dynamics

Dynamic changes of $[Ca^{2+}]_{ER}$ were visualized in cells expressing the FRET-based, ER-targeted cameleon D1ER (*kindly provided by R.Y. Tsien, San Diego, USA*) (142). This probe similarly to the aforementioned Ca^{2+} reporters contains a mutated calcium binding site (CaM) together with an interacting domain (M13), which is referred to as Ca^{2+} sensitive design 1 (D1). D1 is cloned in between the FRET donor/acceptor fluorophores enhanced CFP and citrine fluorescent proteins. To ensure appropriate ER-targeting, the calreticulin signal sequence MLLPVLLLGLLGAAAD was added 5′ to CFP, and an ER retention sequence, KDEL, was added to the 3′ end of citrine (142).

2.10.4 Imaging setup for FRET experiments

CFP/YFP-based FRET measurements were performed on an inverted microscope (Axio Observer.A1, Zeiss) equipped with a polychromator illumination system (VisiChrome, Visitron Systems) and a thermoelectric-cooled CCD camera (Photometrics CoolSNAP HQ, Visitron Systems). Cells were imaged with a 40x oil immersion objective (Plan Fluor 40 x, Nikon). Excitation of the fluorophores was at 440 ± 10 nm (440AF21, Omega Optical) and emission was recorded at 480 and 535 nm using emission filters (480AF30 and 535AF26, Omega Optical) mounted on a motorized filter-wheel (MAC 6000/5000, Ludl Electronic Products, Hawthorne, NY, USA). Results of FRET measurements are shown as the ratio of $F_{535}/F_{480}/R_0$ (where R_0 is the basal ratio) to correct for photobleaching and/or photochromism as described in (123).

2.11 Simultaneous mitochondrial and cytosolic Ca^{2+} measurements

2.11.1 Design and construction of 4mtD1GO-Cam

The Ca^{2+} sensitive calmodulin/M13 sequence (D1) from the D1ER probe was amplified via PCR and the internal ClaI restriction site was deleted by silent mutation using the

primers as follows: 5′-GGATCGATATGCATGACCAACTGACAGAA-3′,5′-GGCCATCACCGTCAATATCT-3′, 5′-GGAAGCAGATATTGACGGTG-3′ and 5′-AAGAATTCCATGAGCTCCAGTGCCCCG-3′ (123). D1 was then subcloned between the ClaI and EcoRI restricition sites into the newly developed red-shifted mitochondrial ATP sensor (4mtGO-ATeam)(133) after removing the ATP sensing ε-subunit of the bacterial F_oF_1-ATP synthase sequence. Accordingly, exchanging the ATP sensing ε-subunit to D1 resulted in a new plasmid coding for the mitochondrial targeted Ca^{2+} sensitive probe 4mtD1GO-Cam, respectively.

2.11.2 Imaging setup for simultaneous Ca^{2+} measurements

Co-imaging of fura-2 and the red-shifted cameleon 4mtD1GO was performed on a digital wide field imaging system, the Till iMIC (Till Photonics Graefelfing, Germany) using a 40x objective (alpha Plan Fluar 406, Zeiss, Göttingen, Germany). For illumination of fura-2 and the cameleons an ultrafast switching monochromator, the Polychrome V (Till Photonics) was used. Fura-2 was excited alternatively at 340 nm and 380 nm and the red-shifted cameleons were excited at 477 nm, respectively. To avoid optical bleed-through an excitation filter (E500spuv, Chroma Technology Corp, Rockingham Vermont, USA) and a dichroic filter (495dcxru) were installed. Emission light was simultaneously collected at 510 nm (fura-2 and GFP of GOCams) and at 560 nm (FRET-channel of GO-Cams) using a single beam splitter design (Dichrotome, Till Photonics) that was equipped with a dual band emission filter (59004m ET Fitc/Tritc Dual Emitter, Chroma Technology Corp) and a second dichroic filter (560dcxr, Chroma Technology Corp). The light path and the optical properties of the filters used for the co-imaging experiments are illustrated in **Figure 2.1**. Images were recorded with a charged coupled device (CCD) camera (AVT Stringray F145B, Allied Vision Technologies, Stadtroda, Germany). For the data acquisition and the control of the digital fluorescence microscope the live acquisition software version 2.0.0.12 (Till Photonics) was used. Results of FRET measurements are shown as the ratio of $F_{560}/F_{510}/R_0$ (where R_0 is the basal ratio) to correct for photobleaching and/or photochromism as described in (123).

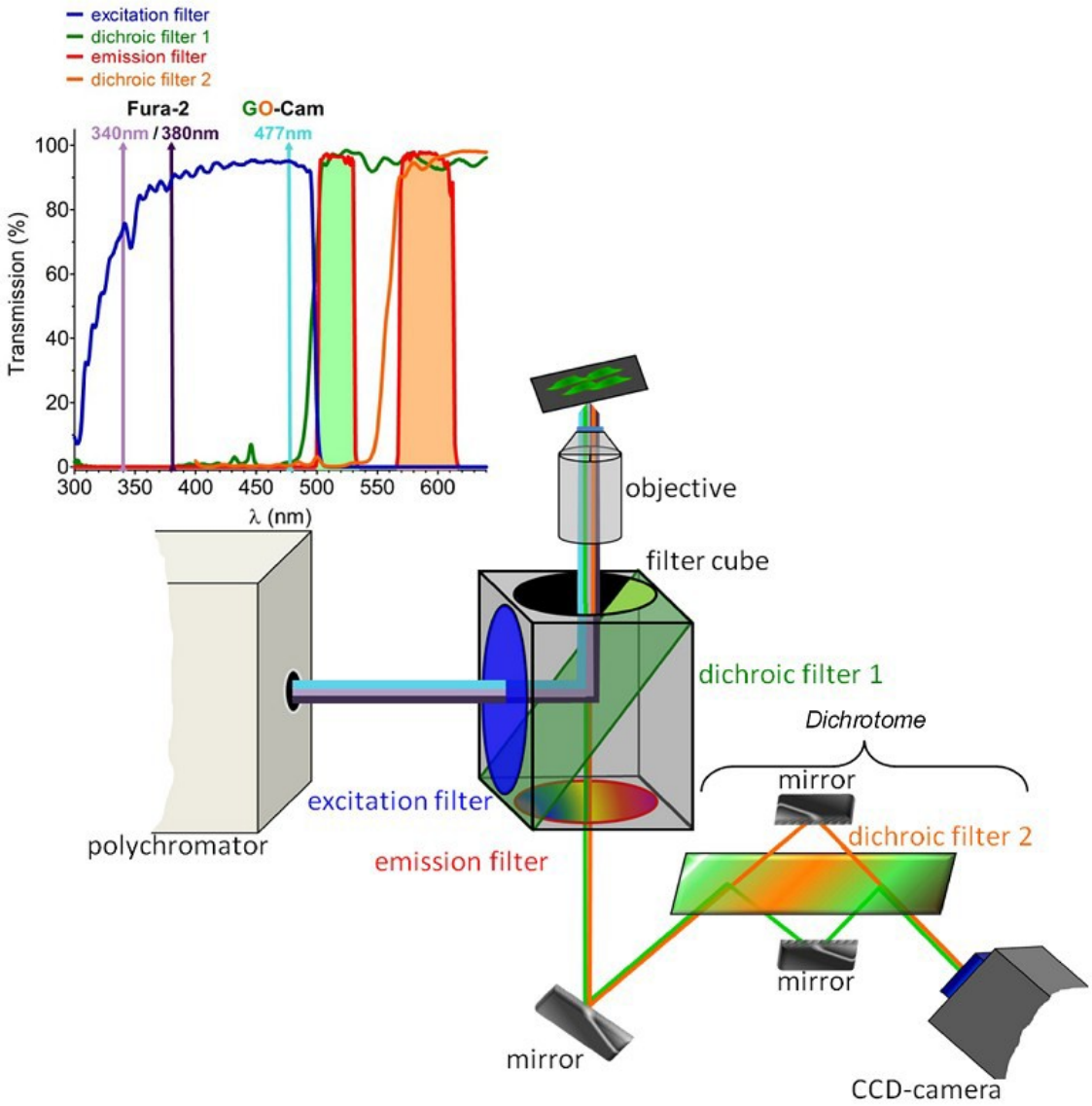

Figure 2.1 Imaging setup for the simultaneous recording of fura-2 and the red-shifted cameleon 4mtD1GO-Cam ***[modified and adopted from (123)]***.

Schematic representation of the imaging system with light paths of the excitation (violet=340 nm, dark blue=380 nm, and light blue=477 nm) and emission light (green=510 nM and orange=560 nM) and the optical filters used to simultaneously image fura-2 and the red-shifted cameleon..

2.12 Confocal analysis and 3D rendering

High resolution morphological analysis of subcellular structures was performed with array confocal laser scanning microscopy (ACLSM). The ACLSM was built on an inverse, fully automatic microscope (Axio Observer.Z1, Zeiss, Göttingen, Germany) that was equipped with a 100x objective (Plan-Fluor 100x/1.45 Oil, Zeiss), a Nipkow-based confocal scanner unit (CSU-X1, Yokogawa Electric Cooperation, Tokyo, Japan), a motorized filter wheel (CSUX1FW, Yokogawa Electric Cooperation). Fluorophores were illuminated with laser

light at 405 nm; 488 nm and 515 nm. Emitted light was acquired with a CCD camera (CoolSNAP-HQ, Photometrics,) using the emission filters ET480/40m ET535/30m and E570LPv2 (Chroma Technology Corp.) mounted on a computer-controlled fast filter wheel (Ludl Electronic Products). All devices were controlled by VisiView Premier Acquisition software (Visitron Systems). The ER and mitochondria z-stacks (Z-scan step size 0.2 μm) were deconvoluted using the iterative quick maximum likelihood estimation algorithm (QMLE) of Huygens 2.4.1p3 (SVI, Hilversum, Netherlands). Subsequently combined 3D rendering of the organelles were performed with Imaris 3.3 software (Bitplane AG, Zurich, Switzerland). Quantitative mitochondrial shape analysis and co-localization computations were performed with the integrated morphometric analysis plug-in of MetaMorph 7.7.0.0 software (Visitron). The intensity threshold values of shape analysis and co-localization computations did not significantly differ within all the samples analyzed and were determined over a range that completely eliminated background fluorescence, but preserved organelle structures, as described in (110,116).

3. RESULTS

3.1 Spatiotemporal correlations between cytosolic and mitochondrial Ca^{2+} signals using a novel red-shifted mitochondrial targeted cameleon

Current chapter follows the study of Waldeck-Weiermair et al. 2012 (123).

3.1.1 Design and concept of 4mtD1GO-Cam

We first aimed to establish a technique, which allows a parallel and real-time characterization of cytosolic and mitochondrial Ca^{2+} signals in the same individual cells. Circularly-permutated FP based sensors (e.g. mtRP) or the CFP/YFP-based Ca^{2+} probe 4mtD3CPV are reliable tools to visualize changes in $[Ca^{2+}]_{mito}$. However, they cannot be used together with fura-2AM, because of the overlapping spectral properties of the different fluorescent reporters. In order to overcome this problem, a novel mitochondrial targeted FRET-based sensor was designed and constructed *(see chapter 2.11.1)*, which can be used simultaneously with fura-2 without the occurrence of any optical bleed-through. This novel cameleon named D1GO-Cam contains a circularly permutated monomeric enhanced GFP (cp173-mEGFP) as FRET donor and the monomeric Kusabira-Orange 2 (mKO_2) as FRET acceptor **(Figure 3.1 A).** Accordingly, using the Ca^{2+} sensitive design 1 (D1) (139) flanked by these FPs shifts the excitation and emission wavelengths of the -+dprobe towards the red hue, where the fluorescence of the cytosolic fura2 indicator does not interfere anymore **(Figure 3.1 B).** In analogy to the CFP/YFP-based cameleons [21,28], the COX VIII signal sequence was fused four times in tandem at the 5´-end of the D1GO-Cam, in order to ensure a successful targeting of the red-shifted cameleon (4mtD1GO) into the mitochondrial matrix of different mammalian cells **(Figure 3.1 C).**

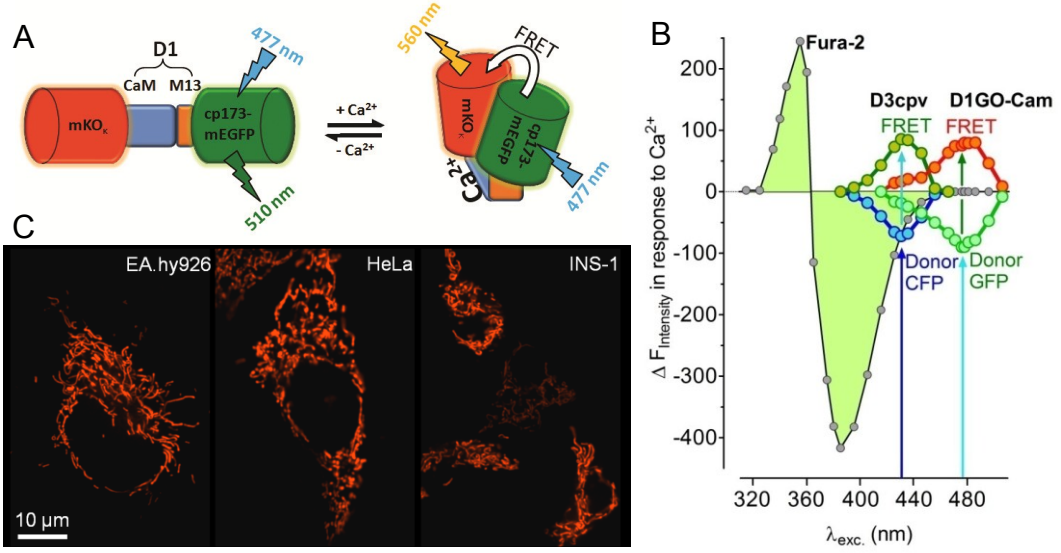

Figure 3.1 Schematic representation of D1GO-Cam, its optical properties and mitochondrial targeting *[modified and adopted from* (123)*]*

(**A**) D1GO consists of a Ca^{2+}-bindig site (CaM) and its interacting peptide (M13). The two interacting sites were named D1 domain. D1 is flanked by a modified red fluorescent protein (mKO_k) and a circularly permutated enhanced green fluorescent protein (cp173-mEGFP). Ca^{2+} binding of the probe yields enhanced FRET between donor (mEGFP) and acceptor (mKO_k) fluorophores. Flash symbols indicate excitation/emission wavelengths

(**B**) Spectral overlap between Fura-2 and CFP/Venus-based D3cpv or mEGFP/mKOk-based D1GO-Cam cameleons respectively. Spectral scans were performed in Ea.hy926 cells with a digital wide-field fluorescence microscope. Exposure time was 100 ms at each wavelength. Cells were either loaded with Fura-2 or transiently transfected with the respective probes. During the scans cells were stimulated with 10 mM ionomycin in the presence of 2 mM Ca^{2+}

(**C**) Mitochondrial expression of the red-shifted cameleon in endothelial (EA.hy926), HeLa and pancreatic ß cells (INS-1). Appropriate mitochondrial targeting of the probe was achieved by the N-terminal mitochondrial target sequence COX VIII (4mtD1GO)

3.1.2 Co-imaging of the mitochondrial targeted 4mtD1GO-Cam with Fura-2 in mammalian cells

After validating the appropriate mitochondrial targeting of 4mtD1GO, the suitability of simultaneous recordings of cytosolic and mitochondrial Ca^{2+} signals in mammalian cells was tested. Experiments were performed in endothelial (EA.hy926) and in tumor cells (HeLa) in the presence of extracellular Ca^{2+}. Ca^{2+} signals were evoked by the admission of the IP_3-generating agonist histamine, which mobilizes Ca^{2+} from the internal Ca^{2+} stores (**Figure 3.2**). In EAhy926 cells a fast increase of free [Ca^{2+}] was observed in both subcellular compartments in response to histamine, however the mitochondrial Ca^{2+} signal was clearly delayed and increased with a slower kinetic compared to cytosolic Ca^{2+} elevation (**Figure 3.2 A**). Notably, mitochondrial Ca^{2+} elevation upon histamine admission started only, when the cytosolic Ca^{2+} signal had already reached 80% of its maximum. Moreover, within approximately 2 minutes following histamine washout, free Ca^{2+} was removed from the cytosol by the Ca^{2+}-extrusion mechanisms and $[Ca^{2+}]_{cyto}$ decreased to basal level. Likewise in the endothelial cells, histamine-induced rise of $[Ca^{2+}]_{mito}$ lagged clearly behind the cytosolic Ca^{2+} signal in HeLa cells (**Figure 3.2 B**). In order to exclude that the differences in the kinetics between $[Ca^{2+}]_{mito}$ and $[Ca^{2+}]_{cyto}$ arise from differences in the Ca^{2+} affinities and/or the on and off kinetics of the two Ca^{2+} sensors used (i.e. fura-2 and 4mtD1GO-Cam), similar experiments were performed using the non-targeted (i.e. cytosolic) D1GO-Cam simultaneously with fura-2. As shown in **Figure 3.2 C**, the curve obtained with D1GO-Cam was virtually identical with the respective fura-2 signal. These

results highlight the reliability and accuracy of this newly established technique that allows the detailed investigation of the association between cytosolic and mitochondrial Ca^{2+} signals within the same individual cell with a high temporal resolution.

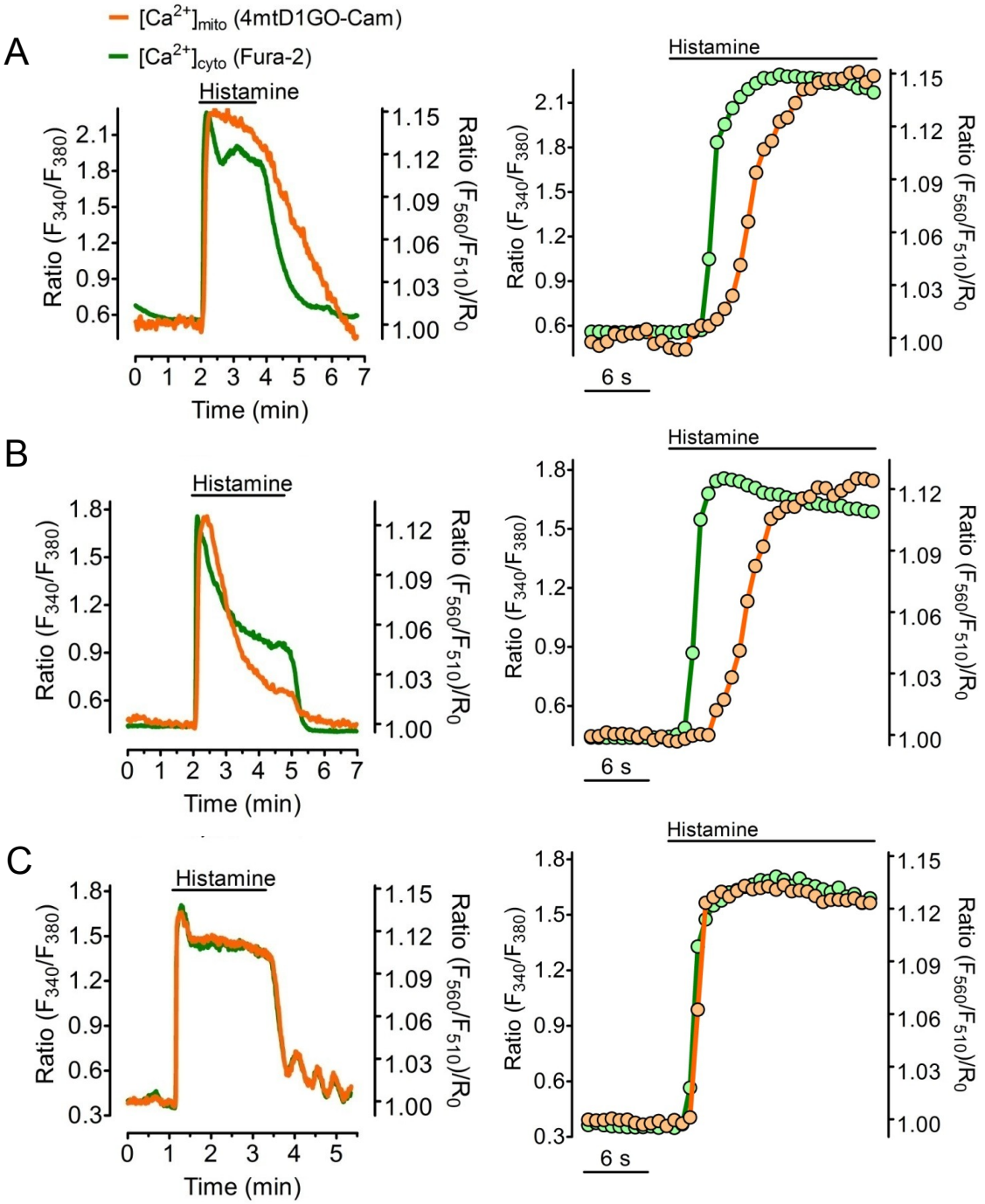

Figure 3.2 Coupling of $[Ca^{2+}]_{cyto}$ and $[Ca^{2+}]_{mito}$ in different mammalian cells *[modified and adopted from* (123)*]*

Fura-2/am-loaded cells expressing the respective red-shifted Ca^{2+} probe were stimulated with 100 µM histamine in the presence of extracellular Ca^{2+}. *Left panels:* Representative traces of cytosolic (green; left y-axis) and mitochondrial

(orange; right y-axis) Ca^{2+} signals from the same individual cells over time. *Right panels:* Respective zooms into the onset of Ca^{2+} signals

(**A**) Temporal correlation of $[Ca^{2+}]_{cyto}$ and $[Ca^{2+}]_{mito}$ in EA.hy926 cells

(**B**) Temporal correlation of $[Ca^{2+}]_{cyto}$ and $[Ca^{2+}]_{mito}$ in HeLa cells

(**C**) Time-course changes of cytosolic Ca^{2+} signals measured simultaneously with Fura-2 and D1GO-Cam

3.2 Molecularly distinct routes of mitochondrial Ca^{2+} uptake are activated depending on SERCA activity

Current chapter is based on the study of Waldeck-Weiermair M.; Deak A. et al. 2013 (117).

3.2.1 SERCA inhibition decelerates the IP_3-mediated mitochondrial Ca^{2+} uptake

As described in the previous chapter, simultaneous organelle-associated Ca^{2+} measurements with Fura-2 and the newly developed mitochondrial Ca^{2+} probe 4mtD1GO-Cam revealed a significant lag between increase of $[Ca^{2+}]_{cyto}$ and $[Ca^{2+}]_{mito}$. This approach was used to further examine the coupling of cytosolic and mitochondrial Ca^{2+} signals in HeLa cells **(Figure 3.3)**. Moreover, we aimed to investigate, how this coupling is influenced by SERCA inhibition, or by an siRNA-mediated transient knockdown of different mitochondrial proteins (UCP2/3, MCU, Letm1), which were shown to be mediators of mitochondrial Ca^{2+} uptake (*see chapter 1.10*).

As first step, similar experiments as shown in **Figure 3.2** were performed. HeLa cells expressing 4mtD1GO were loaded with fura-2 (**Figure 3.3 A**) and were stimulated with an IP_3-generating agonist in the absence of extracellular Ca^{2+}. In accordance with previous findings (**Figure 3.2**), the admission of histamine induced a fast increase of both cytosolic and mitochondrial Ca^{2+} levels also in the absence of extracellular Ca^{2+} (**Figure 3.3 B**), indicating an efficient transfer of Ca^{2+} from the ER into mitochondria. The cytosolic Ca^{2+} signal occurred slightly earlier than the respective mitochondrial Ca^{2+} elevation within the same single individual cell. Pretreatment of the cells with the SERCA inhibitor thapsigargin 40 seconds prior to histamine addition, enhanced the cytosolic Ca^{2+} elevation. Notably, in the presence of thapsigargin, $[Ca^{2+}]_{cyto}$ has already started to increase slowly, indicating the passive leaking of Ca^{2+} from the ER. This weak thapsigargin-induced cytosolic Ca^{2+} signal was not accompanied by a significant elevation in $[Ca^{2+}]_{mito}$.

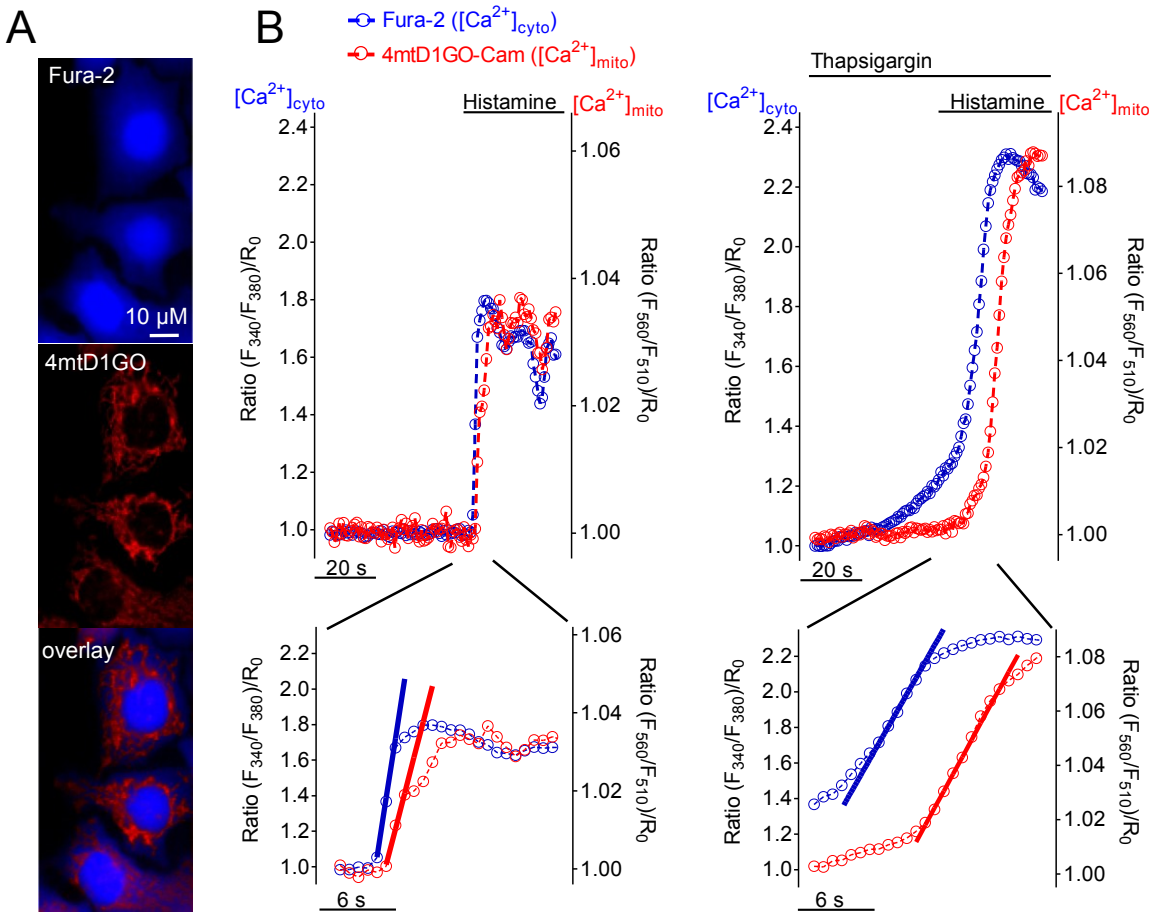

Figure 3.3 SERCA inhibition prior to IP_3-mediated Ca^{2+} release modifies the kinetics of Ca^{2+} signals and coupling between $[Ca^{2+}]_{cyto}$ and $[Ca^{2+}]_{mito}$ *[modified and adopted from* (117)*]*

(**A**) Fura-2/AM-loaded HeLa cells (blue) were transiently transfected with the mitochondrial Ca^{2+} sensor 4mtD1GO-Cam (red). Images were acquired with a fully automated wide-field fluorescence microscope

(**B**) *Upper panels:* representative traces of cytosolic (blue curves) and mitochondrial (red curves) Ca^{2+} signals in HeLa cells upon stimulation with 100 µM histamine in the absence of Ca^{2+} (upper-left panel). SERCA inhibition was achieved by the admission of 1 µM thapsigargin 40 s prior to cell treatment with histamine (upper-right panel). Data are expressed as normalized ratios: $(F_{340}/F_{380})/R_0$ for $[Ca^{2+}]_{cyto}$ and $(F_{560}/F_{510})/R_0$ for $[Ca^{2+}]_{mito}$. R_0 was calculated from basal ratio values for each individual cell respectively. *Lower panels*: zoom-in of upper panels showing which part was used for calculating the slope of Ca^{2+} increase. Following onset, each curve was fitted using linear regression to assess maximal slope of $[Ca^{2+}]$ elevations.

Subsequent addition of histamine evoked a more pronounced rise of both $[Ca^{2+}]_{cyto}$ and $[Ca^{2+}]_{mito}$ (**Figures 3.3 and 3.4**). However, these signals increased with a slower kinetics compared with respective Ca^{2+} elevations in the absence of the SERCA inhibitor (**Figures 3.3 and 3.4**). In addition, the time gap between the appearance of histamine induced cytosolic and respective mitochondrial Ca^{2+} rise was considerably augmented in the presence of thapsigargin (**Figure 3.4 C**). This indicates that SERCA inhibition decelerates the transfer of Ca^{2+} into mitochondria upon IP_3-mediated Ca^{2+} release. A correlation

between changes of $[Ca^{2+}]_{cyto}$ and respective mitochondrial Ca^{2+} signals revealed that cytosolic Ca^{2+} was almost twice as much elevated in the presence of thapsigargin, until mitochondrial Ca^{2+} uptake was activated (**Figure 3.4 D**). These experimental protocols, illustrating the distinct kinetics of the compartmental Ca^{2+} rises and coupling between $[Ca^{2+}]_{cyto}$ and $[Ca^{2+}]_{mito}$, were subsequently used to investigate role of the individual proteins, (*i.e.* UCP3, Letm1, and MCU).

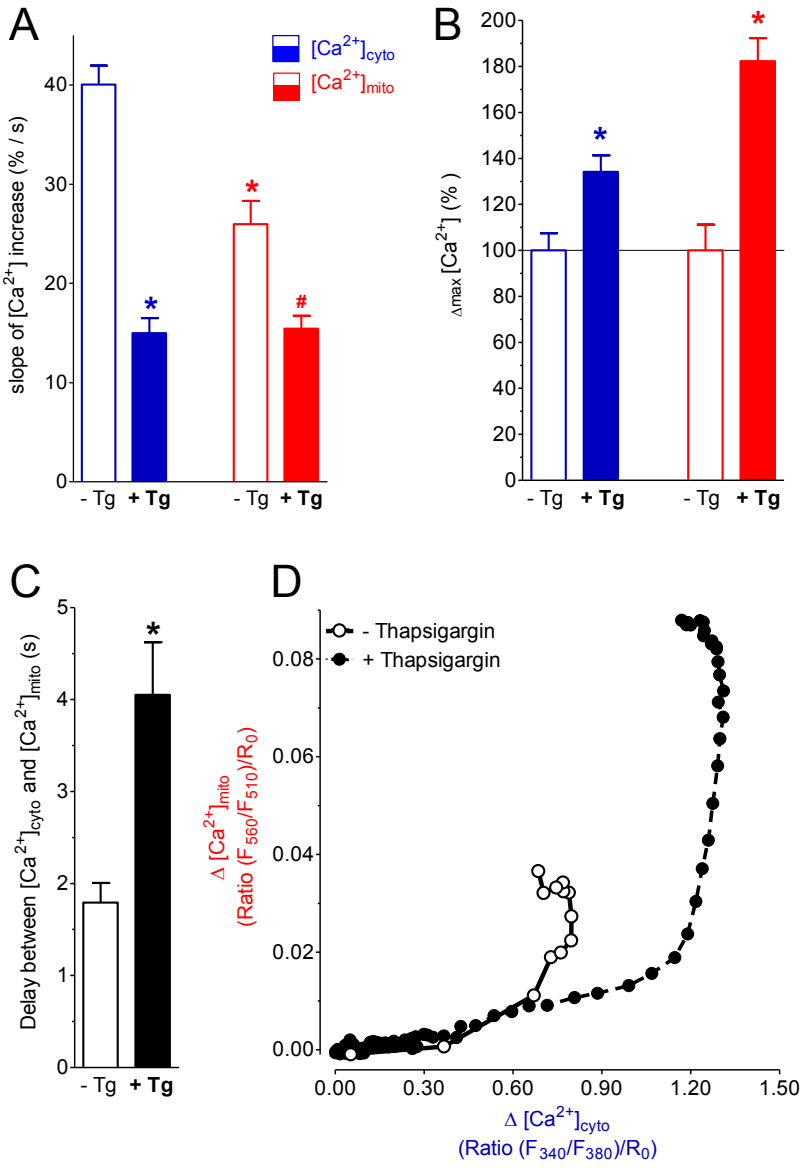

Figure 3.4 Temporal correlations of histamine-evoked cytosolic and mitochondrial Ca^{2+} signals upon SERCA blockade (Statistical analyses of the simultaneous recordings shown in Figure 3.3) ***[modified and adopted from* (117)*]***

(**A**) Bar charts represent the maximal slopes of $[Ca^{2+}]_{cyto}$ (blue columns) and $[Ca^{2+}]_{mito}$ (red columns) increases upon histamine stimulation in the absence (-Tg, n=18) or presence of thapsigargin pre-treatment (+Tg, n=15). Data show mean±s.e.m. *P < 0.05 versus $[Ca^{2+}]_{cyto}$ in the absence of thapsigargin (-Tg); #*P* < 0.05 versus $[Ca^{2+}]_{mito}$ in the absence of thapsigargin (-Tg)

(**B**) Bar charts represent the max delta ratios in the absence (-Tg) or presence (+Tg) of thapsigargin pre-incubation. Cytosolic and mitochondrial $[Ca^{2+}]$ elevations in response to cell treatment with 100 µM histamine were defined as 100%. Data show mean±s.e.m. *P<0.05 versus $[Ca^{2+}]_{cyto}$ in the absence of thapsigargin (-Tg); #P < 0.05 versus $[Ca^{2+}]_{mito}$ in the absence of thapsigargin (-Tg)

(**C**) Lag times in seconds between cytosolic and respective mitochondrial Ca^{2+} rises in the absence (n=18) or presence (n=15) of Tg pretreatment. Data show mean±s.e.m. *P<0.05 versus in the absence of thapsigargin (-Tg);

(**D**) Representative temporal correlations between histamine-induced changes of $[Ca^{2+}]_{cyto}$ (x-axis) and $[Ca^{2+}]_{mito}$ (y-axis) in the absence (open circles) or upon pretreatment with thapsigargin (filled circles*)*

3.2.2 SERCA inhibition switches mitochondrial Ca^{2+} uptake from a UCP3-dependent to a Letm1-dependent mode

We speculated that the SERCA-dependent differences in the kinetics of mitochondrial Ca^{2+} signals probably reflect the involvement of distinct mitochondrial Ca^{2+} uptake routes. To investigate this assumption, additional experiments were performed, in which the level of various mitochondrial proteins (i.e. UCP2/3, Letm1 and MCU) was reduced by a transient transfection of specific siRNAs against the respective proteins. Knockdown efficiency of the respective siRNAs was validated by qPCR in one of our earlier works (115). In line with previous studies, a (110,113,143) transient knockdown of UCP3 significantly suppressed the histamine-induced mitochondrial Ca^{2+} signal, while the respective cytosolic Ca^{2+} elevation was only minimally affected (**Figure 3.5 A & B**). This is in line with a recent finding showing that, SERCA blockade with thapsigargin added shortly before histamine, abolishes the inhibitory effect of UCP3-knockdown on mitochondrial Ca^{2+} uptake (143).

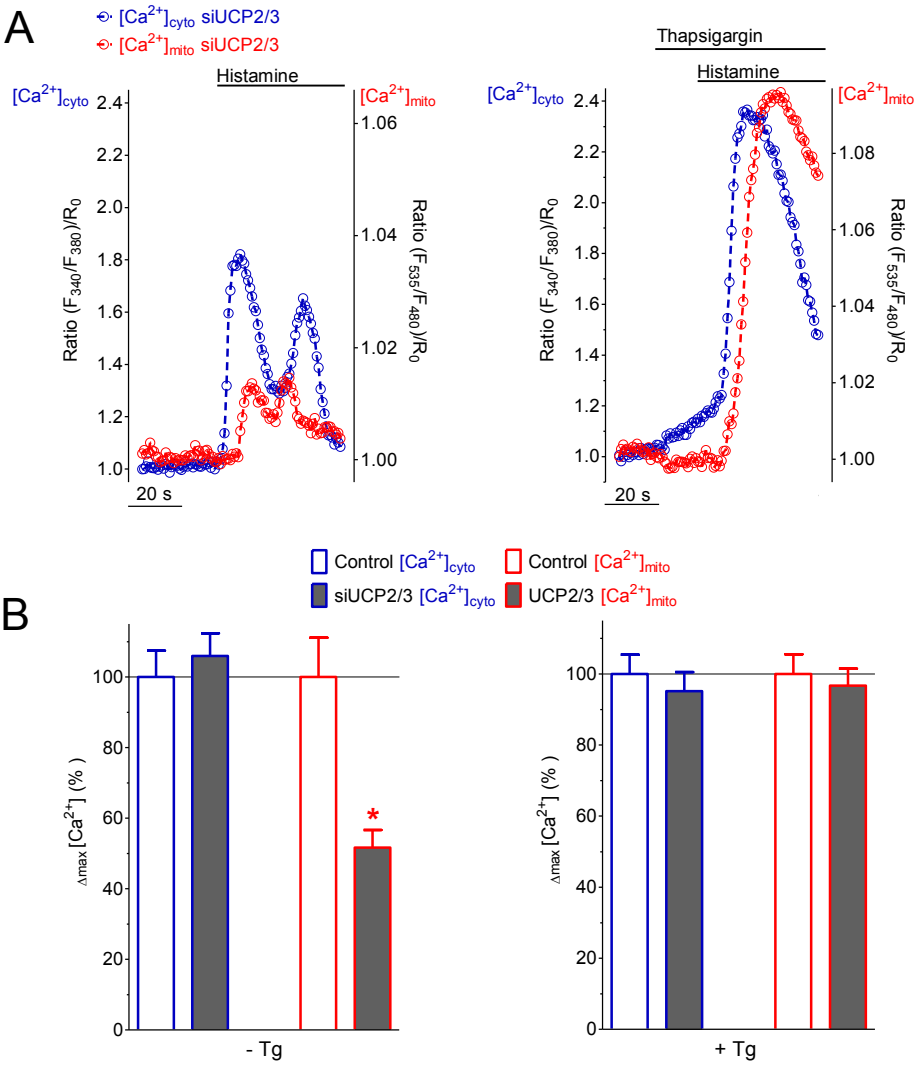

Figure 3.5 UCP2/3 contributes to mitochondrial Ca^{2+} uptake, if SERCA is active *[modified and adopted from (117)]*

(**A**) Representative recordings of $[Ca^{2+}]_{cyto}$ (blue) and $[Ca^{2+}]_{mito}$ (red) in single individual HeLa cells transfected with siRNAs against UCP2/3. Cells were treated with 100 µM histamine alone (left panel) or were pre-incubated with 1 µM thapsigargin (right panel) prior to histamine admission.

(**B**) Statistical evaluation of histamine-evoked cytosolic and mitochondrial Ca^{2+} signals in HeLa cells transfected either with scrambled siRNA (control, open columns) or with siRNA against UCP2/3 (siUCP2/3, full columns). Experiments were performed in the absence (-Tg; n=18 for control and n=19 for siUCP2/3) or in the presence of thapsigargin pretreatment (+Tg; n=15 for control and n=17 for siUCP2/3). The delta maximums of cytosolic and mitochondrial Ca^{2+} signals under control conditions were defined as 100%. Data show mean±s.e.m.*P<0.05 versus Control $[Ca^{2+}]_{mito}$

Analogous experiments were performed in HeLa cells, in which not UCP2/3, but Letm1 was transiently silenced. In this setup mitochondrial Ca^{2+} sequestration upon IP_3-mediated Ca^{2+} mobilization in the absence of thapsigargin was not affected (**Figure 3.6 left panels**). On the contrary, if SERCA activity prior to agonist admission was blocked, the

mitochondrial Ca^{2+} signals were strongly attenuated in cells diminished of Letm1 (**Figure 3.6 right panels**).

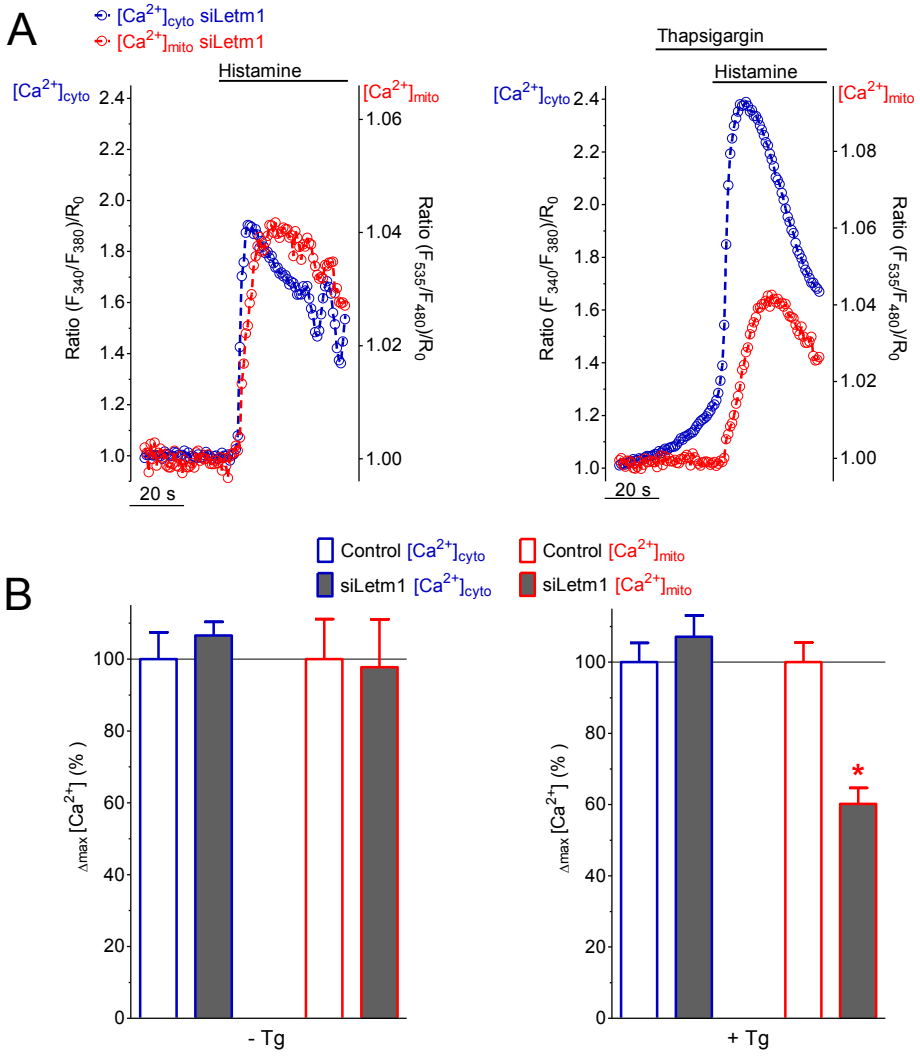

Figure 3.6 Letm1 mediates mitochondrial Ca^{2+} uptake, if SERCA is inactive *[modified and adopted from* (117)*]*

(**A**) Representative recordings of $[Ca^{2+}]_{cyto}$ (blue) and $[Ca^{2+}]_{mito}$ (red) in single individual HeLa cells transfected with siRNAs against Letm1. Cells were treated with 100 µM histamine alone (left panel) or were pre-incubated with 1 µM thapsigargin (right panel) prior to histamine admission.

(**B**) Statistical evaluation of histamine-evoked cytosolic and mitochondrial Ca^{2+} signals in HeLa cells transfected with siRNA against Letm1 (siLetm1, full columns). Experiments were performed in the absence (-Tg; n=19 for siLetm1) or in the presence of thapsigargin pretreatment (+Tg; n=17 for siLetm1). Open columns (control) are identical with those shown in Figure 3.5. Data show mean±s.e.m. *P < 0.05 versus Control $[Ca^{2+}]_{mito}$

3.2.3 MCU contributes to mitochondrial Ca^{2+} uptake independently from SERCA activity

As next step, the impact of transient MCU depletion on the coupling of cytosolic and mitochondrial Ca^{2+} signals was investigated. The peak cytosolic Ca^{2+} elevation was minimally altered in response to IP_3-mediated Ca^{2+} mobilization (**Figure 3.7**). However, respective mitochondrial Ca^{2+} signals were strongly diminished in cells reduced of MCU (**Fig. 3, A & B**). Notably, down-regulation of MCU suppressed mitochondrial Ca^{2+} accumulation both in the absence and presence of thapsigargin pre-stimulation (**Figure 3.7**). This indicates that MCU facilitates mitochondrial Ca^{2+} uptake independently of SERCA activity and, thus regardless the mode of Ca^{2+} mobilization.

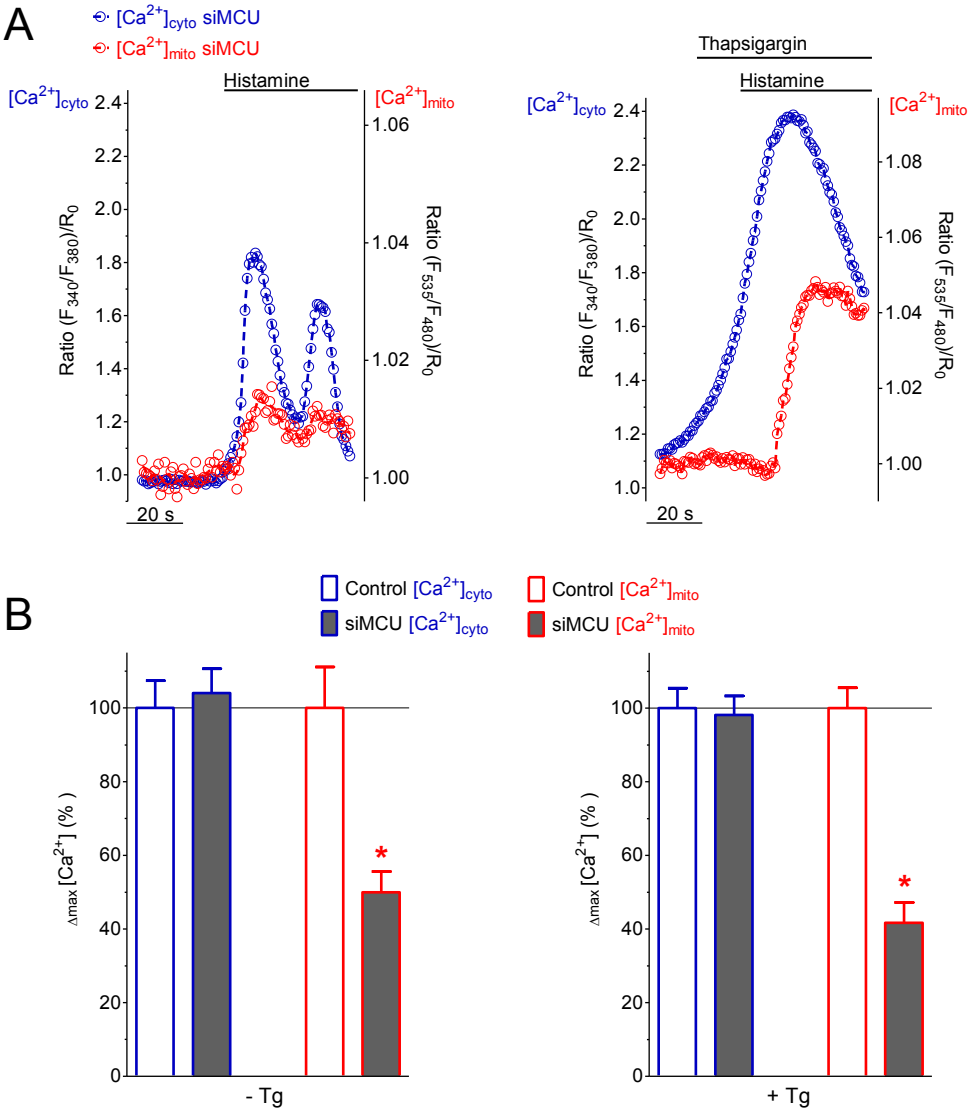

Figure 3.7 Transient knock-down of MCU results in a diminished mitochondrial Ca^{2+} uptake independently from SERCA activity *[modified and adopted from* (117)*]*

(**A**) Representative recordings of $[Ca^{2+}]_{cyto}$ (blue) and $[Ca^{2+}]_{mito}$ (red) in single individual HeLa cells transfected with siRNAs against MCU. Cells were treated with 100 µM histamine alone (left panel) or were pre-incubated with 1 µM thapsigargin (right panel) prior to histamine admission.

(**B**) Statistical evaluation of histamine-evoked cytosolic and mitochondrial Ca^{2+} signals in HeLa cells transfected with siRNA against MCU (siMCU, full columns). Experiments were performed in the absence (-Tg; n=24 for siMCU) or in the presence of thapsigargin pretreatment (+Tg; n=14 for siMCU). Open columns (control) are identical with those shown in Figure 3.5. Data show mean±s.e.m.*P< 0.05 versus Control $[Ca^{2+}]_{mito}$

3.2.4 SERCA inhibition following IP_3-mediated Ca^{2+} release abrogates the contribution of UCP2/3 to MCU-mediated mitochondrial Ca^{2+} uptake and switches to a Letm1/MCU-dependent uptake mode

SERCA inhibition prior to agonist stimulation had already partially emptied the internal Ca^{2+} store, which resulted in a higher histamine-evoked cytosolic Ca^{2+} signal. However, this signal developed slower and was transferred with a greater delay into mitochondria in comparison to IP_3-triggered Ca^{2+} signals without preceding SERCA blockade (**Figure 3.3**). This phenomenon suggests a shift in the mode/route of mitochondrial Ca^{2+} uptake. To test whether the occurrence of this shift is indeed the function of SERCA activity, a slightly different experimental protocol was applied, in which the SERCA-inhibitor thapsigargin was added after histamine. Continuous exposure to the IP_3-generating agonist in the absence of extracellular Ca^{2+}evoked a moderate cytosolic Ca^{2+} response, which was followed by a second smaller elevation of $[Ca^{2+}]_{cyto}$ upon thapsigargin admission (**Figure 3.8 A**). This second thapsigargin-induced increase of cytsolic Ca^{2+} levels triggered only small changes of $[Ca^{2+}]_{mito}$. On the contrary, if experiments were carried out in the presence of extracellular Ca^{2+}, SERCA inhibition induced prominent, longer-lasting Ca^{2+} elevations in both compartments (**Figure 3.8 B**), highlighting the involvement of SOCE that enhances mitochondrial Ca^{2+} accumulation. The latter experimental protocol was further used to investigate the contribution of UCP3, Letm1, and MCU to mitochondrial Ca^{2+} sequestration under this condition of intracellular Ca^{2+} mobilization.

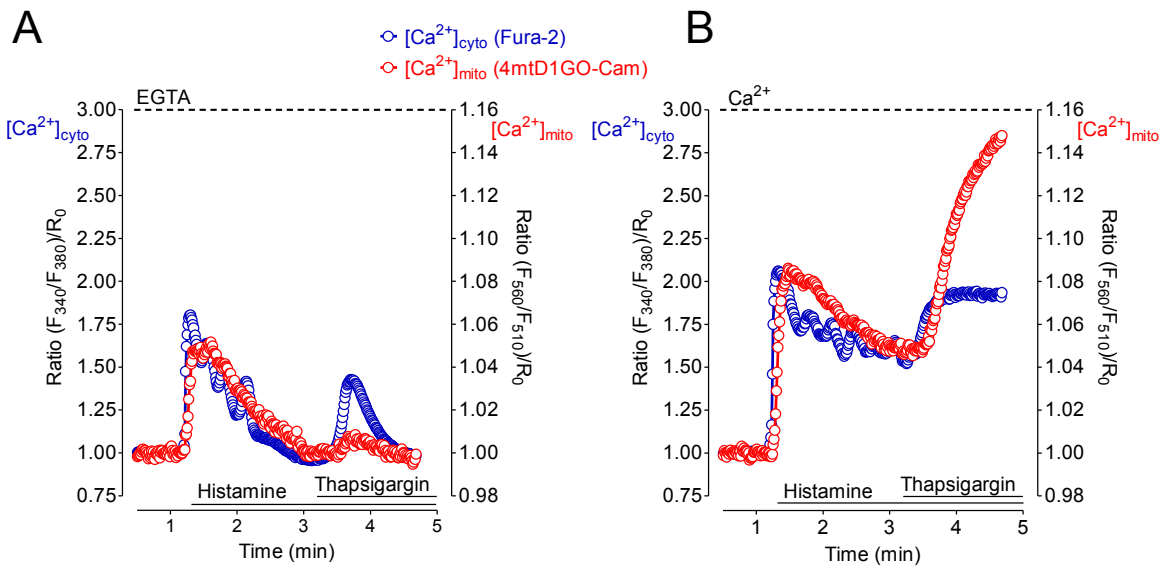

Figure 3.8 SERCA inhibition following cell stimulation with an IP_3-generating agonist results in an increase of $[Ca^{2+}]_{cyto}$ and $[Ca^{2+}]_{mito}$ ***[modified and adopted from* (117)*]***

Curves represent simultaneous measurement of $[Ca^{2+}]_{cyto}$ (blue) and $[Ca^{2+}]_{mito}$ (red) in HeLa cells loaded with fura-2/AM and transiently transfected with 4mtD1GO-Cam. Cells were stimulated with 100 µM histamine for 2 minutes before the addition of 1 µM thapsigargin

(**A**) In the absence of extracellular Ca^{2+} (EGTA)

(**B**) In the presence of 2 mM Ca^{2+} in the extracellular medium

Consistent with our previous work (110) and the experiments carried out in the absence of extracellular Ca^{2+} (**Figures 3.3 & 3.5**), cells depleted of UCP3 showed greatly reduced mitochondrial Ca^{2+} accumulation in response to histamine (**Figure 3.9**). The subsequent addition of thapsigargin evoked a substantial increase of $[Ca^{2+}]_{mito}$ that was not affected by the diminution of UCP3. On the contrary, the knockdown of Letm1 suppressed only the second, thapsigargin-induced rise of $[Ca^{2+}]_{mito}$, while it had no impact on the initial IP_3-mediated mitochondrial Ca^{2+} sequestration (**Figure 3.9**). These data indicate that SERCA inhibition switches the mode of mitochondrial Ca^{2+} uptake from a Letm1-independent to a Letm1-dependent one and, hence, explain the lacking contribution of UCP2/3 to mitochondrial Ca^{2+} uptake, if SERCA is inactive.

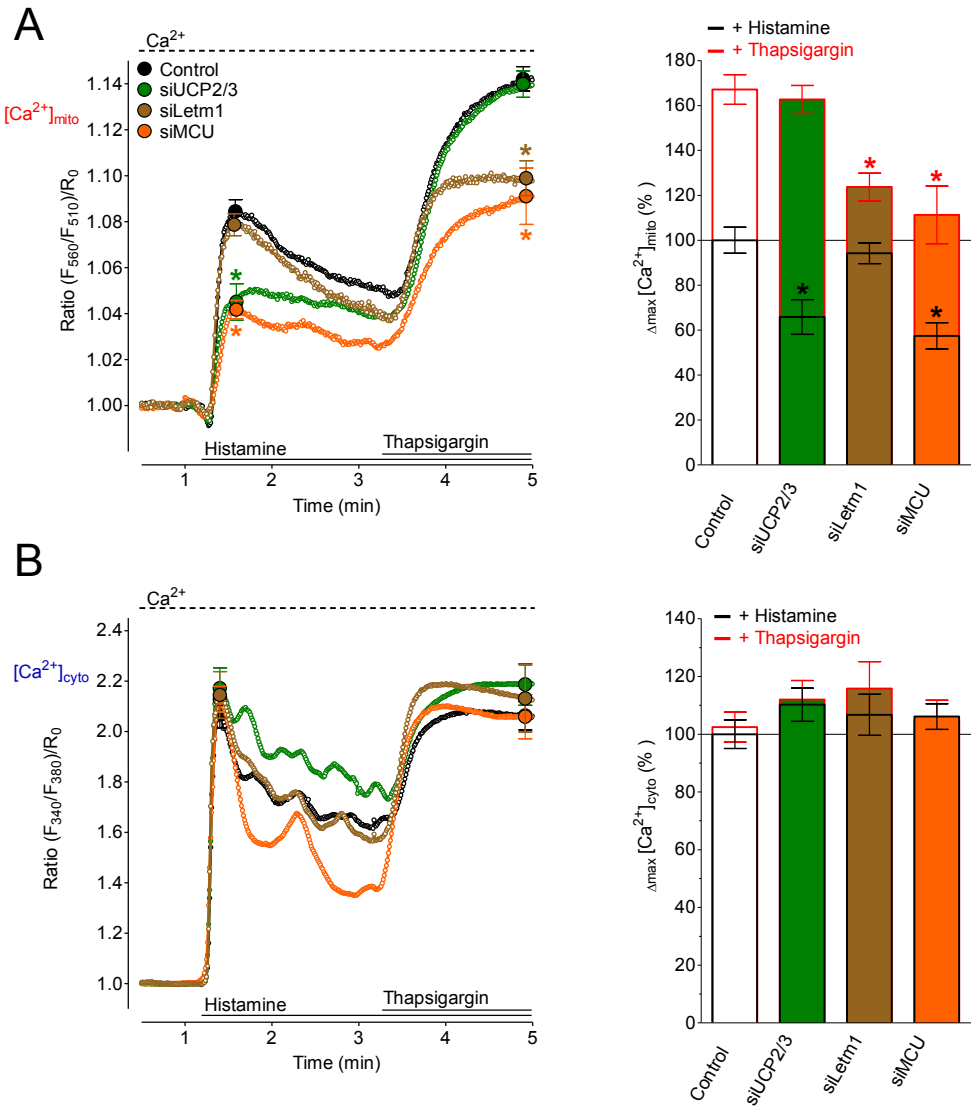

Figure 3.9 SERCA inhibition during cell stimulation with histamine switches the UCP2/3 and MCU-dependent mitochondrial Ca^{2+} uptake mode to a Letm1 and MCU-dependent one *[modified and adopted from* (117)*]*

HeLa cells were either transfected with an inoperative Control siRNA (black curves and white columns, n=18), or with siRNAs against UCP2 and UCP3 (green curves and green columns, n=18), or Letm1 (brown curves and brown columns, n=20) or MCU (orange curves and orange columns, n=19)

(**A**) Curves show mean±s.e.m. (*left panel*) and statistical data (*right panel*) of $[Ca^{2+}]_{mito}$ signals measured with 4mtD1GO-Cam upon cell treatment with 100 µM histamine and the subsequent addition of 1 µM thapsigargin in the presence of 2 mM Ca^{2+}. *P<0.05 versus respective Controls

(**B**) Respective cytosolic Ca^{2+} curves (left panel, mean±s.e.m) and statistical analysis of Δmax $[Ca^{2+}]_{cyto}$ values (right panel) from Fura-2 signals of HeLa cells that were treated as indicated in (A).

3.3 IP_3-mediated STIM1 oligomerization requires intact mitochondrial Ca^{2+} uptake

Current chapter is based on the study of Deak et al. 2014 (116).

As mentioned earlier, mitochondrial Ca^{2+} buffering has a strong influence on the activation and maintenance of store-operated Ca^{2+} entry *(see chapter 1.8)*. After investigating different "molecular aspects" of mitochondrial Ca^{2+} uptake, the further experimental work aimed to clarify the actual molecular mechanism(s) by which mitochondria, in particular mitochondrial Ca^{2+} buffering contributes to SOCE activation and maintenance under physiological conditions. The experimental approach differed from the "conventional" setups: instead of using chemical uncoupling compounds, mitochondrial Ca^{2+} uptake was selectively abrogated by siRNAs and the effect thereof was investigated on SOCE. For these experiments the HeLa SilenceX knockdown cell line was used, in which the level of MCU (MCU^{KD}) or UCP2 ($UCP2^{KD}$) was stably reduced.

3.3.1 Characterization of MCU^{KD} and UCP^{KD} cells

Firstly, the knock-down efficiency of MCU and UCP2 was validated with qPCR: mRNA levels of both proteins were strongly reduced in the respective cell lines (**Figure 3.10 A**). As next step, we investigated the mitochondrial Ca^{2+} handling of MCU^{KD} and $UCP2^{KD}$ cells that were transiently transfected with the mitochondrial Ca^{2+} probe 4mtD3cpv. We found that a stable knockdown of either of the two proteins strongly reduced mitochondrial sequestration of intracellularly released Ca^{2+} **(Figure 3.10 B).** On the other hand, knock-down of MCU, but not of UCP2 suppressed mitochondrial sequestration of Ca^{2+} entering via SOCE (**Figure 3.10 C**). These results are consistent with the previous observations in HeLa cells transiently depleted of MCU or UCP2 (**Figures 3.5 & 3.8**) and furthermore, they confirm our earlier findings demonstrating the exclusive involvement of UCP2/3 in mitochondrial Ca^{2+} sequestration upon IP_3-mediated intracellular Ca^{2+} release (110,113,115).

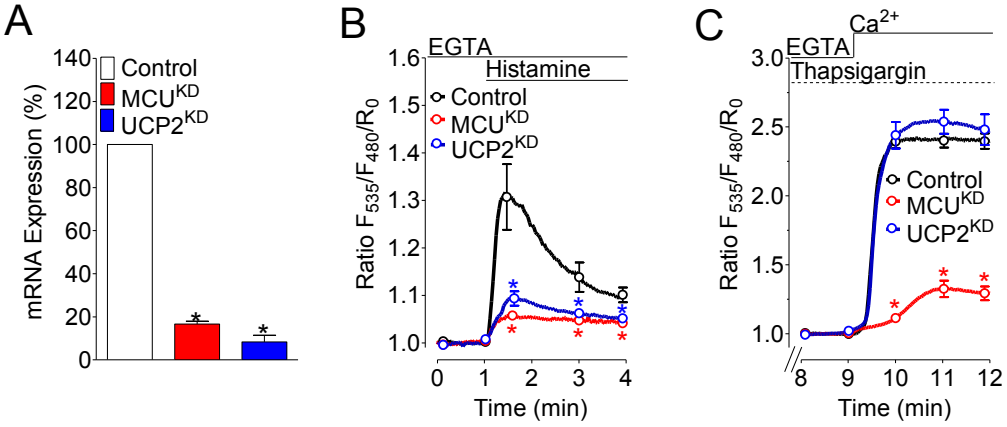

Figure 3.10 Characterization of mitochondrial Ca^{2+} handling in MCU^{KD} and $UCP2^{KD}$ cells *[modified and adopted from* (116)*]*

(**A**) Knock-down efficiency of MCU and UCP2 in the HeLa SilenceX knock-down cell lines (n=9 for each samples). *P<0.05 versus Control

(B) Mitochondrial Ca^{2+} signals upon stimulation with 100 µM histamine in the absence of extracellular Ca^{2+} were measured in Control (black, n=21), MCU^{KD} (red, n=19) and UCP^{KD} (blue, n=19) cells expressing 4mtD3CPV. Curves indicate mean ± s.e.m. *P<0.05 versus Control.

(C) Mitochondrial Ca^{2+} signals upon Ca^{2+} re-addmission following 1 µM thapsigargin treatment in the absence of extracellular Ca^{2+} were measured in the same cells shown in (B). Curves indicate mean ± s.e.m. *P<0.05 versus Control

As mitochondria play a central role in the cellular energy homeostasis (144,145), we tested, if stable silencing of either MCU or UCP2 alters the basal metabolic status of HeLa cells. For this purpose, the mitochondrial membrane potential, oxygen consumption rate, and cellular ATP content of the stable knockdown cells were measured (**Figure 3.11**). All of these variables remained unaffected by the reduction of the respective proteins. Moreover, the morphology of mitochondria, ER structure and the contact sites between these organelles (**Figure 3.12**) were not altered by the stable knock-down of MCU or UCP2.

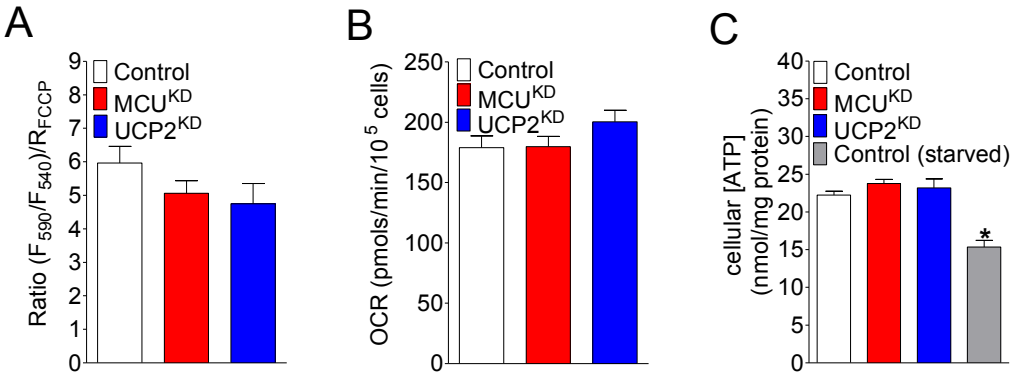

Figure 3.11 Characterization of metabolic status in MCU^{KD} and UCP2^{KD} cells

(A) Mitochondrial membrane potential was measured using the ratiometric dye JC-1 (n=3 for each cell line). The basal fluorescence ratio was normalized to the ratio after 10 µM FCCP addition. Bar charts indicate mean ± s.e.m

(B) The oxygen consumption rate in Control (n=30 wells), MCU^{KD} (n=32 wells) and UCP2^{KD} (n=30 wells) were measured using the Seahorse® Flux analyser. Bar charts indicate mean ± s.e.m

(C) Bar charts represent the whole cellular ATP content of Control (n=4), MCU^{KD} (n=6) and UCP2^{KD} (n=5) cells. The grey column indicates the ATP content of Control cells that were kept for 30 minutes in glucose-free medium (starved; n=4). Bar charts indicate mean ± s.e.m; *P<0.05 versus Control

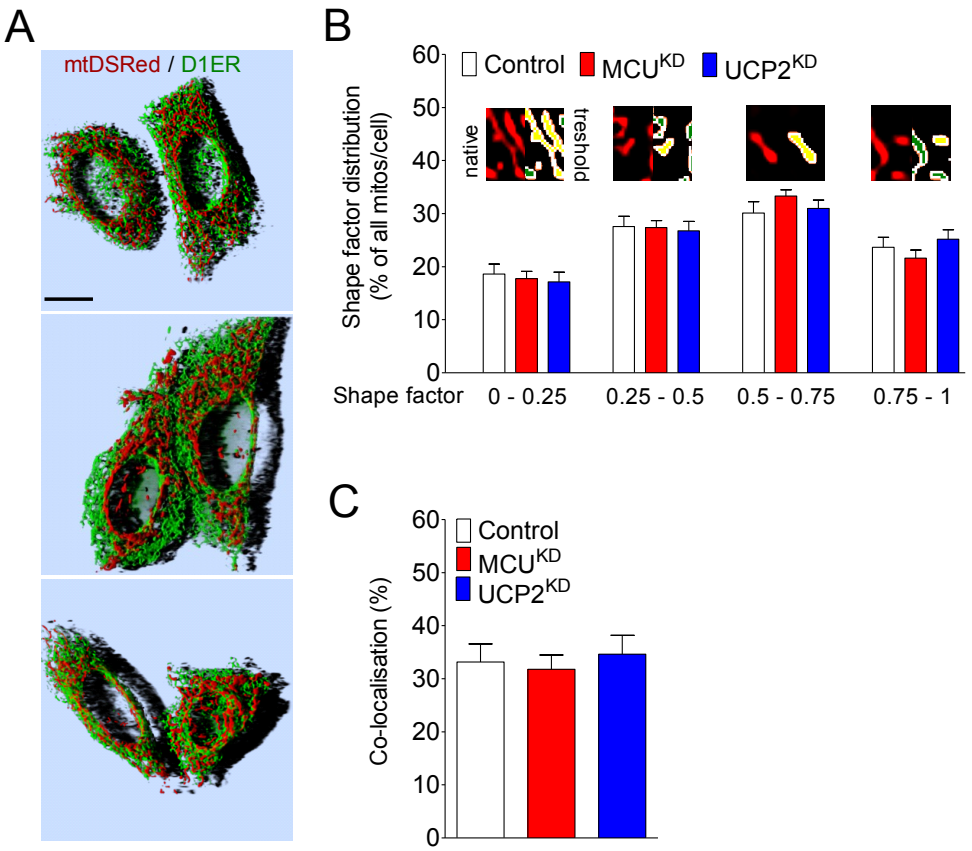

Figure 3.12 Characterization of organelle morphology in MCU^{KD} and UCP2^{KD} cells *[modified and adopted from (116)]*

Confocal analysis of mitochondrial (red) and ER structures (lgreen) in HeLa cells co-expressing mtDsRed and D1ER.

(A) Images are representative for Control (top), MCU^{KD} (middle) and UCP2^{KD} (bottom). Scale bar is 10 µm.

(B) Quantitative mitochondrial shape analysis based on shape factor values corresponding to mitochondrial morphology in Control (white columns, n=13), MCU^{KD} (red columns, n=14) and UCP2^{KD} (blue columns, n=16) cells. Shape factor values range between 0-1, where 0 stands for large, tubular interconnected mitochondria, whereas 1 corresponds to small, fragmented ones. Bar charts show distribution (mean ± s.e.m.) of mitochondrial shape factors calculated for all mitochondria within the middle plane of individual cells.

(C) Co-localisation between ER and mitochondria in the different cell types (Control, MCU^{KD} and UCP2^{KD}) were defined as the percentage values of pixels that contain both fluorophores.

In summary, these data demonstrate that the lack of MCU or UCP2 is restricted to influence distinct modes of mitochondrial Ca^{2+} uptake. Therefore, MCU^{KD} and $UCP2^{KD}$ cells can serve as suitable models to specifically investigate the role of mitochondrial Ca^{2+} sequestration in the regulation of SOCE. In addition, due to the selective engagement of UCP2 in mitochondrial Ca^{2+} sequestration depending on the source of Ca^{2+} (114,115), these cell models allowed us to separately examine whether mitochondrial buffering of intracellularly released or entering Ca^{2+} contributes to SOCE activation.

3.3.2 Stable knock-down of either MCU or UCP2 inhibits mitochondrial Ca^{2+} uptake and impairs STIM1 oligomerization upon IP_3-mediated Ca^{2+} release

The initial step of SOCE activation is accomplished by the formation of STIM1 oligomers following ER Ca^{2+} depletion (31). The dynamic process of STIM1 oligomerization can be visualized and quantified by measuring Förster resonance energy transfer (FRET) between STIM1 proteins fused to either cyan or yellow fluorescent proteins (CFP or YFP), respectively (42,63,146). We used this approach to investigate, whether impaired mitochondrial Ca^{2+} uptake in MCU^{KD} and $UCP2^{KD}$ cells upon ER Ca^{2+} mobilization under physiological conditions affects STIM1 oligomerization (**Figure 3.13**). Cell treatment with histamine in the presence of extracellular Ca^{2+} resulted in a moderate, but significant increase of the FRET signal between CFP-STIM1 and YFP-STIM1 in control cells. However, this increase was almost absent in the knock-down cells (**Figure 3.13 A**). As STIM1 oligomerization/de-oligomerization dynamics is known to be tightly regulated by the filling state of the ER Ca^{2+} pool (64,65), we monitored the changes of $[Ca^{2+}]_{ER}$ as well in the same experimental protocol. The measurement of $[Ca^{2+}]_{ER}$ in response to histamine using D1ER, the ER-targeted genetically encoded Ca^{2+} probe (142), revealed that the reduction in the global ER Ca^{2+} concentration was slightly slower in the knock-down cells compared with that of the control cells (**Figure 3.13 B**). To evoke a strong depletion of ER Ca^{2+} stores, the SERCA inhibitor 2,5-di-t-butyl-1,4-benzohydroquinone (BHQ) was added subsequently to histamine, which considerably augmented STIM1 oligomerization in all three cell types **(Figure 3.13 C & D)**.

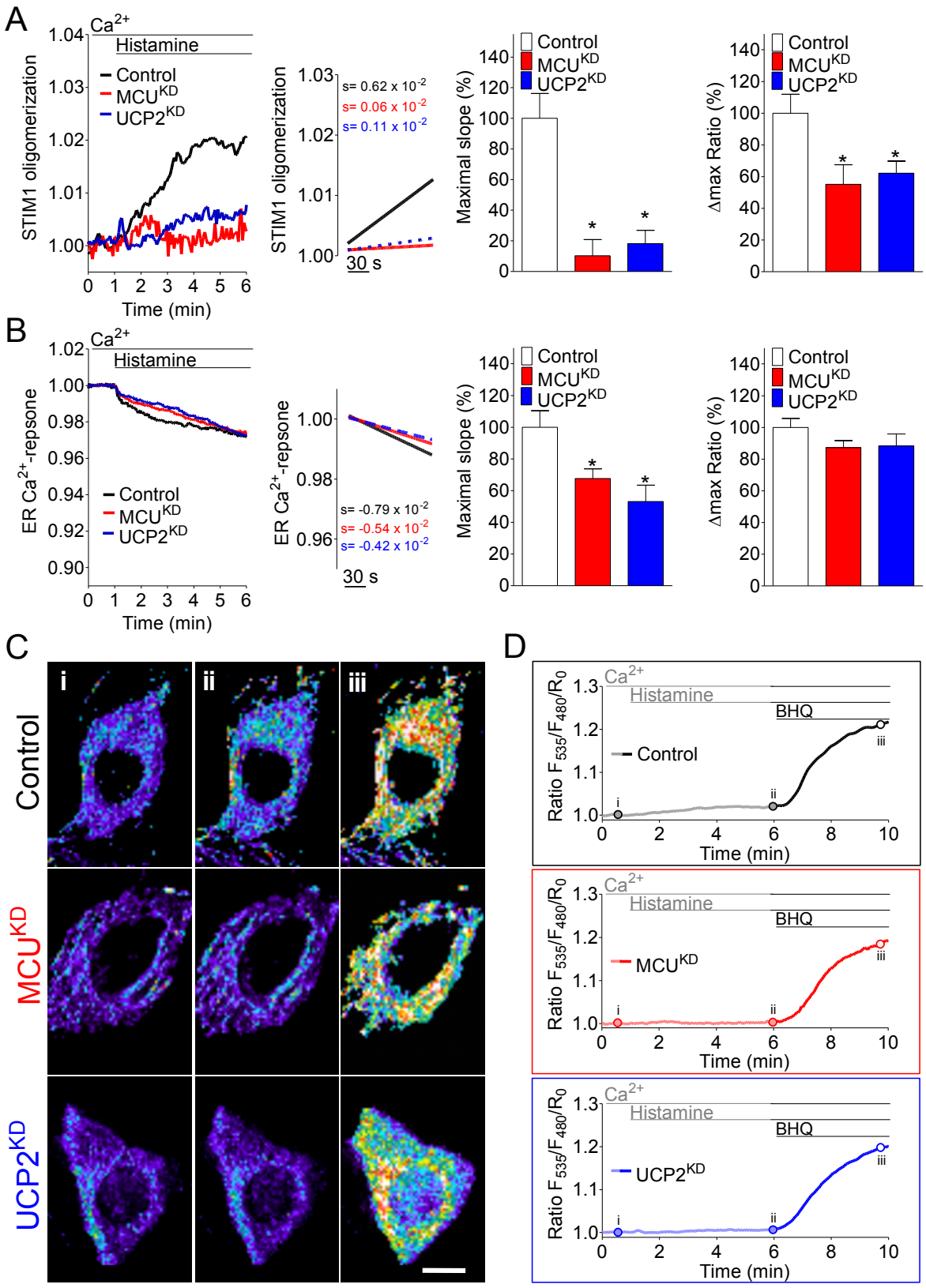

Figure 3.13 IP_3-triggered STIM1 oligomerization is impaired in MCU^{KD} and $UCP2^{KD}$ cells *[modified and adopted from* (116)*]*

(A)-(B) *Left-most panels:* Dynamic changes in the ratio of F_{535}/F_{480} [STIM1 oligomerization (A) or ER Ca^{2+}-response (B) respectively] over time, normalized to the basal ratio (R_0). *Middle-left panels*: Curves were fitted with straight lines using linear regression to assess maximal slope (s) of the increase (A) or decrease (B) of the ratio $F_{535}/F_{480}/R_0$. *Middle-right panels:* Bar charts show the mean ± s.e.m. of the maximal slope normalized to Control (set at 100%). *Right-most panels:*

Bar charts indicate the mean ± s.e.m. of Δmax ratio $F_{535}/F_{480}/R_0$ normalized to Control (set at 100%). STIM1 oligomerization / ER Ca^{2+}-release was induced by the admission of 100 µM histamine in the presence of extracellular Ca^{2+}; *P<0.05 versus Control

(A) STIM1 oligomerization was visualized in Control (black, n=35), MCU^{KD} (red, n=37) and $UCP2^{KD}$ (blue, n=33) cells by measuring intermolecular FRET between CFP-STIM1 and YFP-STIM1.

(B) Dynamics of ER Ca^{2+} depletion (ER Ca^{2+} response) was monitored in Control/MCU^{KD}/UCP^{KD} (n=33/33/35) cells expressing D1ER

(C) Respective pseudocolor CFP/YFP FRET images of Control, MCU^{KD} and $UCP2^{KD}$ cells in basal condition (i) upon 100 µM histamine (ii) and upon 15 µM BHQ (iii) addition. Increased FRET signals appear as red pixels. Scale bar represents 10 µm

(D) Time-lapse FRET measurement of STIM1 oligomerization in Control (upper panel) MCU^{KD} (middle panel) and $UCP2^{KD}$ cells (lower panel) shown in (C). The thin regions of the curves (0-6 minutes) are identical to those shown in the left-most panel of (A) without y-axis magnification

These findings indicate that IP_3-mediated ER Ca^{2+} depletion and the subsequent oligomerization of STIM1 are facilitated by MCU- and UCP2-reliant mitochondrial Ca^{2+} uptake. Notably, after approximately 4 minutes of histamine treatment the degree of ER Ca^{2+} depletion in MCU^{KD} and $UCP2^{KD}$ cells reached that of control cells **(Fig. 3.13 B),** whereas the respective STIM1 FRET signals in the knock-down cells remained strongly reduced (**Fig. 3.13 A**). This suggests that mitochondrial Ca^{2+} sequestration contributes to STIM1 activation not only by shaping ER Ca^{2+} response.

3.3.3 The contribution of mitochondrial Ca^{2+} uptake to STIM1 oligomerization depends on the mode of Ca^{2+} mobilization

To further characterize the role of mitochondrial Ca^{2+}-buffering in IP_3-mediated STIM1 activation and ER Ca^{2+}-depletion, the same set of experiments shown in Figure 3.13 were repeated, but extracellular Ca^{2+} was removed and replaced by EGTA. Cell stimulation with histamine in this setup led to an enhanced and rapid STIM1 oligomerization **(Figure 3.14 A)** due to a more pronounced release of Ca^{2+} from ER **(Figure 3.14 B).** Although the rate of ER Ca^{2+} depletion was the same in all three cell lines under these conditions **(Figure 3.14 B)**, STIM1 oligomerization was clearly delayed in MCU^{KD} and $UCP2^{KD}$ cells compared with that of the control cells **(Figure 3.14 A)**.

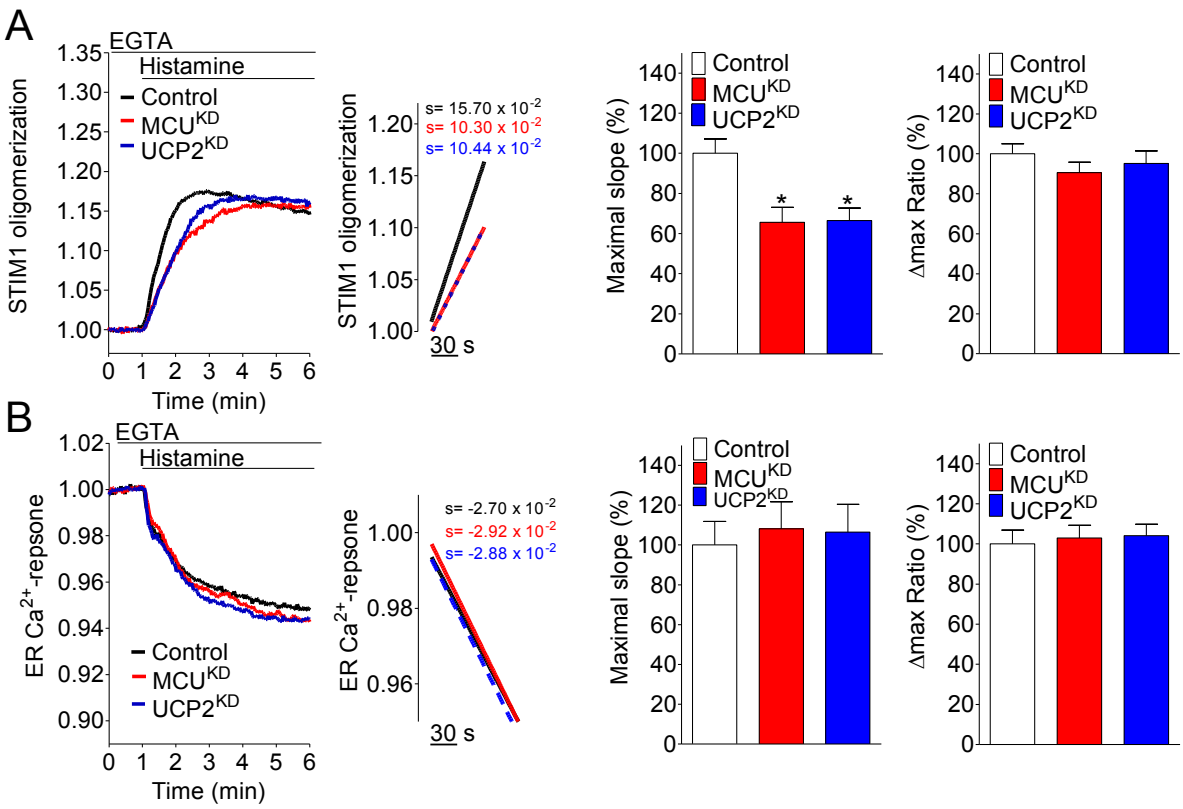

Figure 3.14 Enhanced STIM1 oligomerization is decelerated in MCU^{KD} and UCP2^{KD} cells *[modified and adopted from* (116)*]*

Left-most panels: Dynamic changes in the ratio of F_{535}/F_{480} [STIM1 oligomerization (A) or ER Ca^{2+}-response (B) respectively] over time, normalized to the basal ratio (R_0). *Middle-left panels*: Curves were fitted with straight lines using linear regression to assess maximal slope (s) of the increase (A) or decrease (B) of the ratio $F_{535}/F_{480}/R_0$. *Middle-right panels:* Bar charts show the mean ± s.e.m. of the maximal slope normalized to Control (set at 100%) *Right-most panels:* Bar charts indicate the mean ± s.e.m. of Δmax ratio $F_{535}/F_{480}/R_0$ normalized to Control (set at 100%).

(A) Control/MCU^{KD}/UCP2^{KD} cells (n=65/55/55) co-expressing YFP-STIM1 and CFP-STIM1 were stimulated with 100 µM histamine in the absence of extracellular Ca^{2+} (EGTA). *P<0.05 versus Control

(B) ER Ca^{2+}-response of Control/MCU^{KD}/UCP2^{KD} (n=31/36/27) cells expressing D1ER in the same experimental protocol as in (A)

However, neither STIM1 oligomerization **(Figure 3.15 A),** nor ER Ca^{2+} release **(Figure 3.15 B)** was affected by MCU or UCP2 knock-down, if ER Ca^{2+} was mobilized by the SERCA inhibitor BHQ. These findings indicate a stimulus-specific contribution of mitochondrial Ca^{2+}-buffering to STIM1 oligomerization. Moreover, as ER Ca^{2+} responses were insensitive to MCU or UCP2 silencing under both of these conditions **(Figures 3.14 and 3.15)**, this confirms that mitochondrial Ca^{2+} uptake promotes STIM1 activation by a mechanism other than the control of ER Ca^{2+}-responses only.

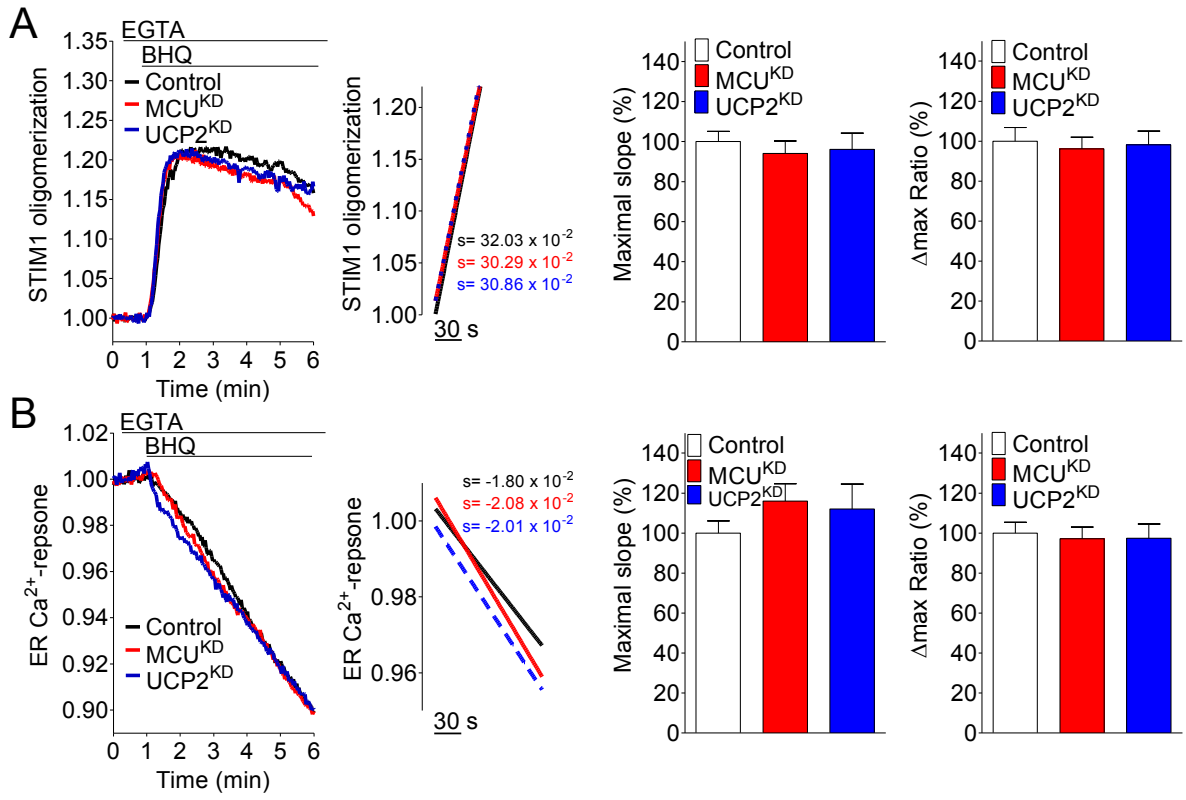

Figure 3.15 Stimulus-specific dependency of STIM1 oligomerization on mitochondrial Ca^{2+} uptake *[modified and adopted from* (116)*]*

Left-most panels: Dynamic changes in the ratio of F_{535}/F_{480} [STIM1 oligomerization (A) or ER Ca^{2+}-response (B) respectively] over time, normalized to the basal ratio (R_0). *Middle-left panels*: Curves were fitted with straight lines using linear regression to assess maximal slope (s) of the increase (A) or decrease (B) of the ratio $F_{535}/F_{480}/R_0$. *Middle-right panels:* Bar charts show the mean ± s.e.m. of the maximal slope normalized to Control (set at 100%) *Right-most panels:* Bar charts indicate the mean ± s.e.m. of Δmax ratio $F_{535}/F_{480}/R_0$ normalized to Control (set at 100%).

(A) Control/MCU^{KD}/$UCP2^{KD}$ cells (n=22/24/22) co-expressing YFP-STIM1 and CFP-STIM1 were stimulated with 15 µM BHQ in the absence of extracellular Ca^{2+} (EGTA)

(B) ER Ca^{2+}-response of Control/MCU^{KD}/$UCP2^{KD}$ (n=35/45/38) cells expressing D1ER in the same experimental protocol as in (A)

3.3.4 Augmented cytosolic Ca^{2+} buffering with BAPTA diminishes the contribution of mitochondrial Ca^{2+} uptake to IP_3-induced STIM1 oligomerization

Global and local cytosolic Ca^{2+} elevations were shown to impair STIM1 activation independently of $[Ca^{2+}]_{ER}$ (64). Accordingly, we hypothesized that upon IP_3-mediated ER Ca^{2+} release mitochondrial buffering of cytosolic Ca^{2+} might counteract this negative feedback effect and, thus, facilitate STIM1 activation. In order to experimentally test this assumption, we examined STIM1 oligomerization and ER Ca^{2+} release in cells loaded with the chemical Ca^{2+} chelator 1,2-bis(2-aminophenoxy)ethane-N,N,N′,N′-tetraacetic acid

tetrakis (acetoxymethyl ester) (BAPTA-AM). Given to cells, the compound enters through the plasma membrane, accumulates in the cytosol and prevents the formation of high-concentration cytosolic Ca^{2+} micro-domains (147). In BAPTA-loaded cells both STIM1 oligomerization **(Figure 3.16 A)** and ER Ca^{2+} depletion **(Figure 3.16 B)** were rapid and occurred transiently in response to histamine, while the respective FRET responses of Control MCU^{KD} and $UCP2^{KD}$ cells did not significantly differ from each other.

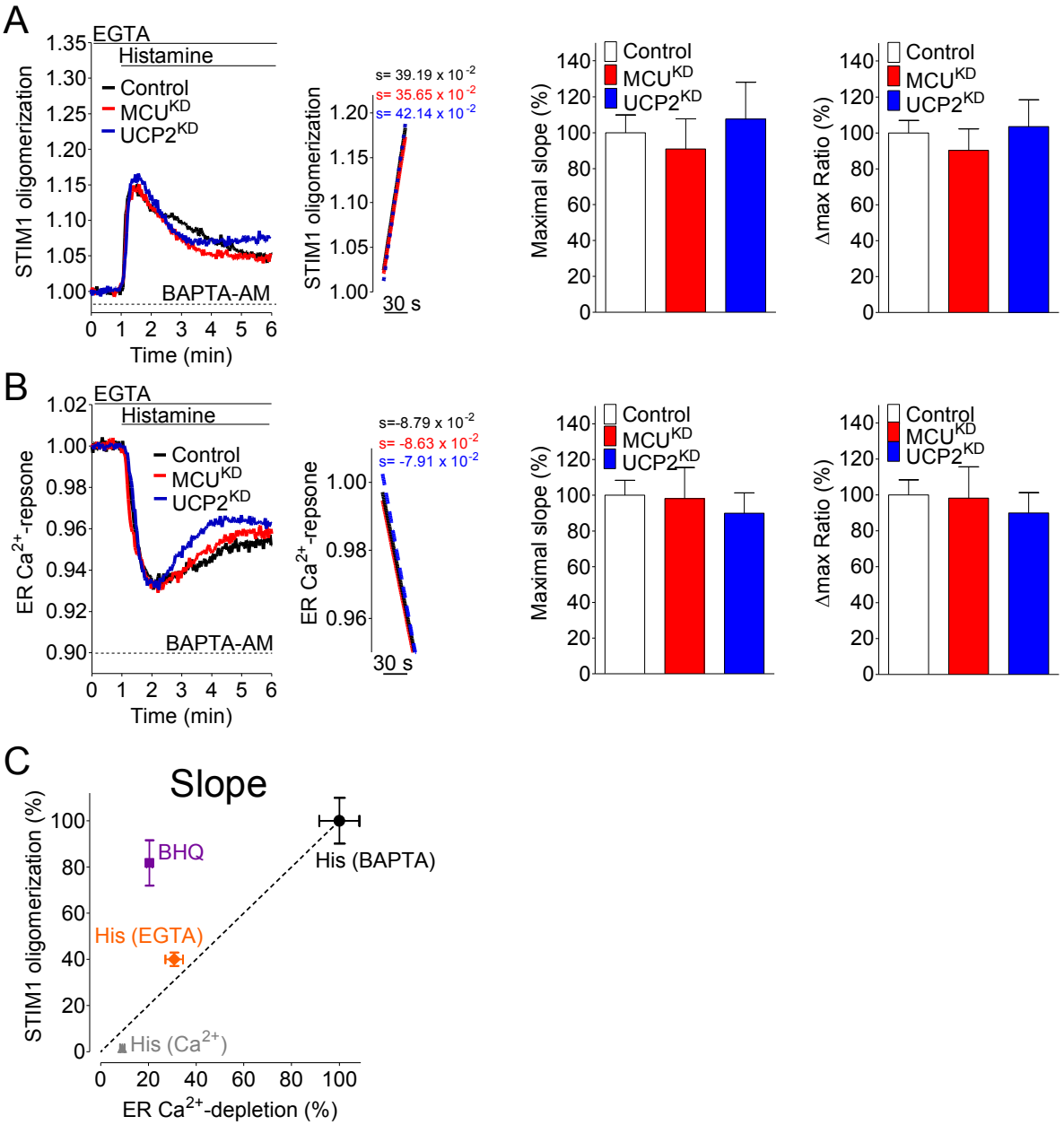

Figure 3.16 IP_3-mediated STIM1 oligomerization does not require intact mitochondrial Ca^{2+} uptake in BAPTA-AM loaded cells *[modified and adopted from* (116)*]*

(**A**)-(**B**) *Left-most panels:* Dynamic changes in the ratio of F_{535}/F_{480} [STIM1 oligomerization (A) or ER Ca^{2+}-response (B) respectively] over time, normalized to the basal ratio (R_0). *Middle-left panels*: Curves were fitted with straight lines using

linear regression to assess maximal slope (s) of the increase (A) or decrease (B) of the ratio $F_{535}/F_{480}/R_0$. *Middle-right panels:* Bar charts show the mean ± s.e.m. of the maximal slope normalized to Control (set at 100%) *Right-most panels:* Bar charts indicate the mean ± s.e.m. of Δmax ratio $F_{535}/F_{480}/R_0$ normalized to Control (set at 100%).

(A) Prior to experiments Control/MCU^{KD}/$UCP2^{KD}$ cells (n=16/10/12) co-expressing YFP-STIM1 and CFP-STIM1 were exposed to 10 µM BAPTA-AM for 45 minutes and were stimulated with 100 µM histamine in a Ca^{2+}-free solution (EGTA)

(B) ER Ca^{2+}-response of Control/MCU^{KD}/$UCP2^{KD}$ (n=16/15/19) cells expressing D1ER in the same experimental protocol as in (A)

(**C**) Initial slopes of ER Ca^{2+} depletion (x-axis) were plotted against maximal slopes of STIM1 oligomerization (y-axis) of control cells that were treated with 100 µM histamine in the presence of 2 mM Ca^{2+} in the buffer (grey triangle, n=35 for STIM1 oligomerization; n=33 for ER Ca^{2+} response), 100 µM histamine in EGTA (orange diamond, n=65 for STIM1 oligomerization; n=31 for ER Ca^{2+} depletion), 15 µM BHQ in EGTA (purple square, n=22 for STIM1 oligomerization; n=35 for ER Ca^{2+} response), and 100 µM histamine in BAPTA-AM loaded cells (black circle, n=16 for each). Data represent means ± s.e.m. normalized to the maximal slopes in BAPTA-AM loaded cells, which were defined as 100 %.

The transient nature of both signals most likely reflects the SERCA-driven replenishment of the ER Ca^{2+} pool from the BAPTA-chelated cytosolic Ca^{2+}. Interestingly, comparing STIM1 oligomerization kinetics with that of the ER Ca^{2+} response, the "mirror-like" FRET signals suggests that once cytosolic Ca^{2+} is trapped by BAPTA, the rate of STIM1 is a function of ER Ca^{2+} content. Nevertheless, BAPTA-AM loading abolished the contribution of mitochondrial Ca^{2+} uptake to histamine-induced STIM1 oligomerization. These observations point to a possible role of mitochondria in shaping high-concentration cytosolic Ca^{2+} micro-domains, which negatively regulate STIM1 activation upon IP_3-mediated Ca^{2+} mobilization independently of the ER Ca^{2+} level. A relative independency of STIM1 activation from the speed of ER Ca^{2+} depletion becomes obvious by correlating the BHQ-induced initial maximal slope of STIM1 oligomerization with the ER Ca^{2+} depletion kinetics (**Figure 3.16 C**). Although the SERCA inhibitor evoked a slow ER Ca^{2+} depletion (**Figures 3.15 B & 3.16 C**), the kinetics of STIM1 oligomerization were quite fast (**Figures 3.15 A & 3.16 C**). This mismatch further points to a role of cytosolic Ca^{2+} in the regulation of STIM1 activation.

3.3.5 SOCE activity upon stimulation with an IP_3-generating agonist is attenuated in cells reduced of MCU or UCP2

The impact of decelerated, IP_3-mediated STIM1 activation in MCU^{KD} and UCP^{KD} cells on Ca^{2+} entry was examined using the fura-2 technique. In wild type cells, treatment with

histamine in the presence of extracellular Ca^{2+} generated sustained cytosolic Ca^{2+} signals (**Figure 3.17 A & 3.18 C**), while in MCU- or UCP2-depleted cells the second phase of the cytosolic Ca^{2+} elevation was strongly reduced. Notably, in the absence of extracellular Ca^{2+}, histamine-evoked Ca^{2+} signals became transient (**Figure 3.17 B & 3.18 C**), indicating that a constant influx of Ca^{2+} from the extracellular area is required to maintain elevated cytosolic Ca^{2+} levels during stimulation.

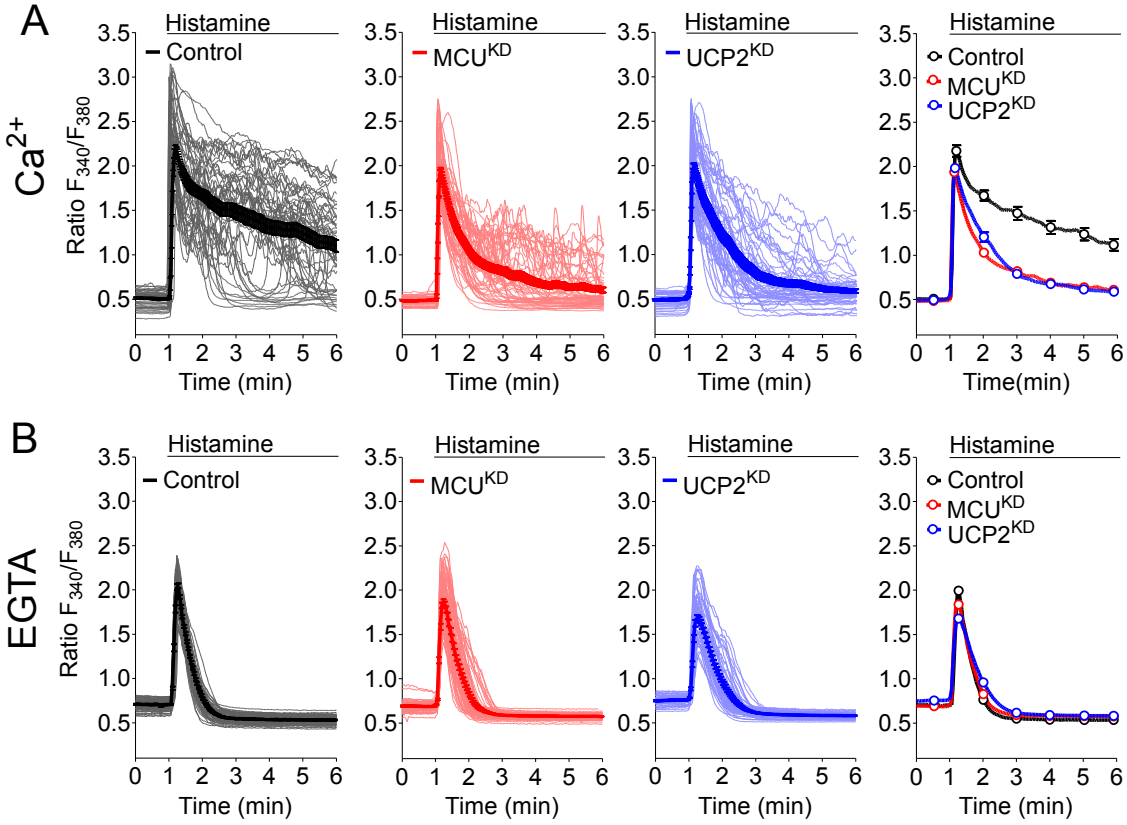

Figure 3.17 IP_3-triggered Ca^{2+} entry is attenuated in MCU^{KD} and $UCP2^{KD}$ cells *[modified and adopted from* (116)*]*

Curves indicate single-cell cytosolic Ca^{2+} signals (thin lines) and their respective mean ± S.E.M. (thick lines) of fura-2/am loaded Control (left panel), MCU^{KD} (middle-left panel) and $UCP2^{KD}$ (middle-right panel) cells, respectively. Right panel: data shows mean± s.e.m of the Ca^{2+} responses of Control (black), MCU^{KD} (red) and UCP^{KD} (blue) cells; *P<0.05 versus Control

(A) Cell stimulation with 100 µM histamine in the presence of extracellular Ca^{2+}. The number of Control/MCU^{KD}/$UCP2^{KD}$ cells are as follows: (n=51/57/60)

(B) Cell stimulation with 100 µM histamine in the absence of extracellular Ca^{2+} (EGTA). The numbers of Control/MCU^{KD}/$UCP2^{KD}$ cells are as follows: (n=76/76/65)

To verify whether the Ca^{2+} influx induced by IP_3-mediated ER depletion is indeed accomplished by the STIM1/Orai1-driven SOCE pathway, HeLa cells were transfected with Orai1(E106Q), a dominant negative form of the wild-type Orai1 protein (35). The glutamate/glutamine exchange in the Orai1 sequence yields a non-conducting CRAC-channel subunit, thus, Ca^{2+} responses upon stimulation of control cells expressing Orai1 (E106Q) showed a strongly reduced plateau phase in the presence of extracellular Ca^{2+} (**Figure 3.18 A & C**). Notably, in MCU^{KD} and $UCP2^{KD}$ cells the already transient cytosolic Ca^{2+} elevation in response to histamine remained unaffected by an additional expression of the dominant negative Orai1 (**Figure 3.18 A & C**). These results demonstrate that STIM1/Orai1-dependent SOCE is responsible for sustained cytosolic Ca^{2+} elevations in these cells. Moreover, these observations also indicate that SOCE is improperly activated in cells lacking the mitochondrial sequestration of intracellularly released Ca^{2+}. Similar results were obtained in all cell models (i.e. wild type, MCU^{KD} and $UCP2^{KD}$ cells) upon incubation with FCCP and oligomycin A prior to histamine-stimulation **(Figure 3.18 B & C)**. Interestingly, the sustained phase of the cytosolic Ca^{2+} signal in MCU- and UCP2-silenced cells in the absence of FCCP/oligomycin A was reduced to the same level as in control cells pre-exposed to the drugs (**Figure 3.18 C)**. This indicates that mitochondrial Ca^{2+} uptake is the molecular mechanism by which mitochondria contribute to SOCE under these conditions. To confirm additionally the reduced SOCE in MCU^{KD} and $UCP2^{KD}$ cells loaded with Fura-2, the rate of Mn^{2+}-influx was measured (**Figure 3.18 C**). CRAC channels are relatively permeable to Mn^{2+}, thus this divalent cation can permeate the cells via SOCE, and binds to Fura-2 with a very high affinity. As a result, the quenching of Fura-2 fluorescence caused by the entry of extracellular Mn^{2+} into the cells represents a measurement of SOCE activity (148). Cytosolic fura-2 fluorescence in response to histamine was quenched at a significantly slower rate by Mn^{2+} in MCU^{KD} and $UCP2^{KD}$ compared with controls cells, indicating that SOCE was indeed reduced in cells lacking mitochondrial Ca^{2+} uptake (**Figure 3.18 D**).

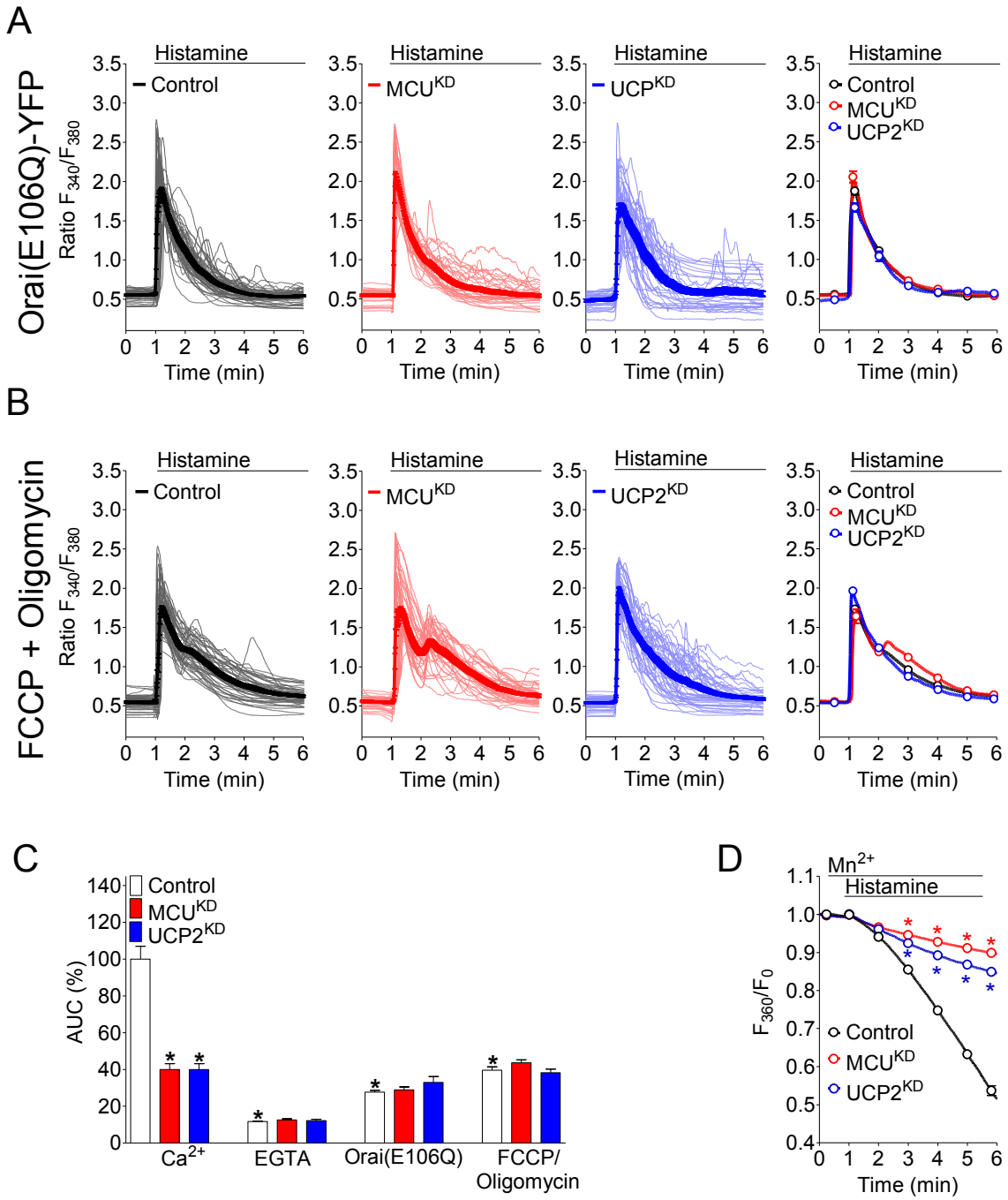

Figure 3.18 Expression of dominant negative Ora1 or mitochondrial depolarization did not further reduce SOCE in MCU^{KD} and UCP^{KD} cells *[modified and adopted from* (116)*]*

(**A**)-(**B**) Curves indicate single-cell cytosolic Ca^{2+} signals (thin lines) and their respective mean ± S.E.M. (thick lines) of fura-2/am loaded Control (left panel), MCU^{KD} (middle-left panel) and UCP2^{KD} (middle-right panel) cells, respectively. Ca^{2+} signals were evoked with 100 µM histamine in the presence of extracellular Ca^{2+}. Right panel: data shows mean±s.e.m of the Ca^{2+} responses of Control (black), MCU^{KD} (red) and UCP^{KD} (blue) cells

(**A**) Cytosolic Ca^{2+} signals of Control/MCU^{KD}/UCP2^{KD} cells (n=43/39/36) expressing Orai(E106Q)-YFP

(**B**) Control/MCU^{KD}/UCP2^{KD} cells were pretreated with FCCP + oligomycin (2µM each) prior to stimulation (n=54/40/56)

(**C**) The area under the curve (AUC) corresponding to respective cytosolic Ca^{2+} responses shown in Figure 3.17 and Figure 3.18 were calculated for each sample and normalized to the control cytosolic Ca^{2+} responses in the presence of 2

mM Ca^{2+} in the extracellular medium (set at 100%). The data show the mean ± s.e.m. The number of Control/MCU^{KD}/$UCP2^{KD}$ cells for each conditions are as follows: Ca^{2+} (n=51/57/60) EGTA (n= 76/76/65); Orai (E106Q) (n=43/39/36); FCCP/Oligomycin (n=54/40/56) *P<0.05 versus Control

(**D**) Perfusion of 100 µM Mn^{2+} quenched cytosolic fura-2 fluorescence in Control/MCU^{KD}/$UCP2^{KD}$ cells (n=43/56/52) upon treatment with 100 µM histamine. Data show the mean±s.e.m. of normalized fluorescent intensities measured at 360 nm excitation (F_{360}/F_0) *P<0.05 versus Control (unpaired Student´s *t*-test)

3.3.6 Re-expression of MCU in MCU^{KD} cells restores both IP_3-mediated mitochondrial Ca^{2+} uptake and sustained cytosolic Ca^{2+} elevations

Our findings so far unveiled that impaired IP_3-mediated mitochondrial Ca^{2+} uptake led to the suppression of SOCE and resulted in transient cytosolic Ca^{2+} response upon stimulation with histamine. As a next step, we investigated, if the restoration of mitochondrial Ca^{2+} buffering rescues the sustained phase of cytosolic Ca^{2+} signal. For this purpose Ca^{2+} responses of both compartments (mitochondrial matrix and cytosol) were measured simultaneously using the red-shifted mitochondria-targeted cameleon (4mtD1GO) in combination with fura-2 (123). This approach revealed a positive correlation between mitochondrial Ca^{2+} uptake and the plateau phase of $[Ca^{2+}]_{cyto}$ in response to histamine (**Figure 3.19 A & B**). Notably, due to oscillating cytosolic Ca^{2+} responses the correlation was rather weak. However, a transient re-expression of MCU in MCU^{KD} cells efficiently increased mRNA levels of MCU (**Figure 3.19 C**) and restored both mitochondrial Ca^{2+} uptake and the plateau phase of the cytosolic Ca^{2+} signal in the same individual cells (**Figure 3.19 A & B**). Thus, these results confirm that mitochondrial Ca^{2+} uptake contributes to SOCE upon cell stimulation with histamine.

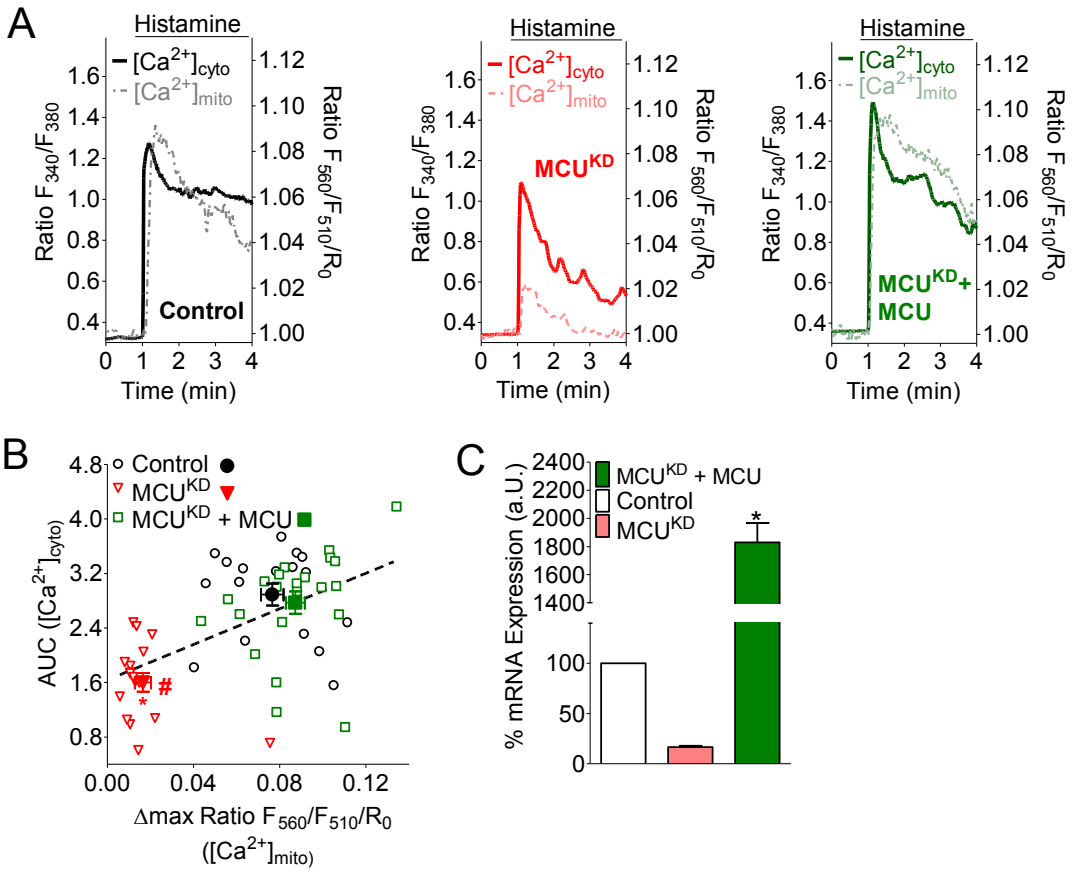

Figure 3.19 Re-expression of MCU in MCU^{KD} cells restores both IP$_3$-mediated mitochondrial Ca^{2+} uptake and SOCE´*[modified and adopted from* (116)*]*

(A) Representative cytosolic (thick lines) and mitochondrial (thin lines) Ca^{2+} signals from the same individual 4mtD1GO-expressing and fura-2/am-loaded control cells (left panel, black), MCU^{KD} cells (middle panel, red) and MCU-transfected MCU^{KD} cells (right panel, green)

(B) Scatter plot correlating cytosolic and mitochondrial Ca^{2+} responses (black dotted line) shown in (A). The values of the area under the curve (AUC) of cytosolic Ca^{2+} signals (arbitrary units; y-axis) were plotted against peak mitochondrial Ca^{2+} uptake (Δmax Ratio $F_{560}/F_{510}/R_0$; x-axis) derived from the same individual Control (open, black symbols, n=17), MCU^{KD} (open, red symbols, n=17) and MCU^{KD} + MCU (open, green symbols, n=22) cells. Filled symbols represent mean±s.e.m. *P<0.05 versus Control; #P<0.05 versus Control. (unpaired Student´s *t*-test)

(**C**) Relative mRNA levels (arbitrary units) of MCU in control cells (n=9) and MCU^{KD} cells (n=9) as shown in Figure 3.10, as well as MCU^{KD} cells expressing MCU (green column, n=9). Data shown mean±s.e.m; *P<0.05 versus Control (unpaired Student´s *t*-test)

3.3.7 MCU-mediated mitochondrial buffering of entering Ca^{2+} is essential for the maintenance of SOCE

A classical protocol to image SOCE is based on a complete depletion of the ER Ca^{2+} store with a SERCA inhibitor in the absence of extracellular Ca^{2+}, which is followed by the subsequent admission of Ca^{2+}. This leads to a pronounced elevation of $[Ca^{2+}]_{cyto}$, driven

predominately by SOCE within these pre-stimulated cells (114) (**Figure 3.20**). The initial phase of this cytosolic SOCE signal was neither affected in MCU^{KD} nor in $UCP2^{KD}$ cells (**Figure 3.20**). This is in line with our earlier observation demonstrating that STIM1 oligomerization triggered by SERCA blockade is unaffected in the knockdown cells (**Figure 3.15**). On the contrary, preincubation of cells with FCCP/oligomycin A prior to Ca^{2+} readmission in the same experimental protocol suppressed cytosolic Ca^{2+} elevations to the same level in all three cell types (**Figure 3.20**) , indicating that SOCE triggered by SERCA inhibition requires intact mitochondria, but not mitochondrial Ca^{2+} buffering for activation. However, exclusively in MCU^{KD} cells, in which a reduced mitochondrial accumulation of entering Ca^{2+} was observed **(Figure 3.10 C)**, the thapsigargin-induced SOCE signal was almost completely terminated within several minutes (**Figure 3.20**). This finding suggests that intact MCU-dependent mitochondrial buffering of entering Ca^{2+} is required for SOCE to prevent its fast deactivation, even if the Ca^{2+} entry pathway is maximally activated by an irreversible SERCA inhibition.

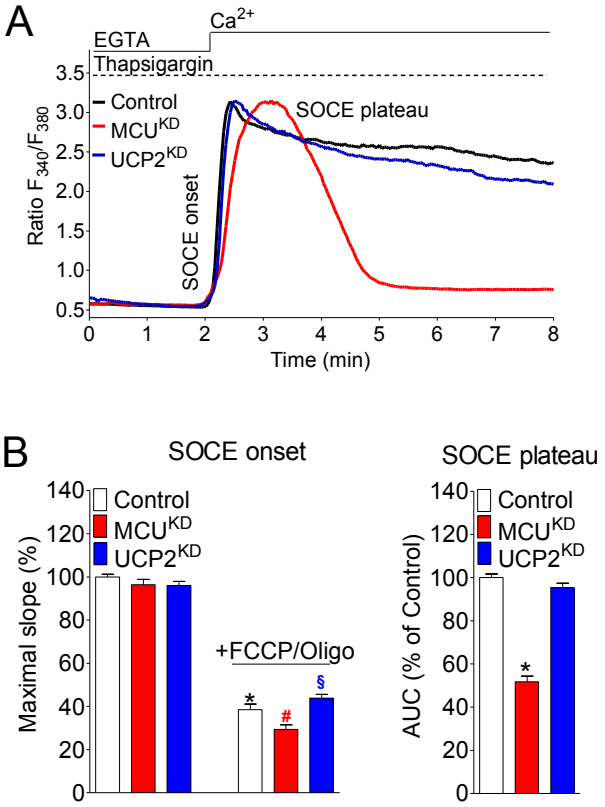

Figure 3.20 Thapsigargin-induced SOCE relies on MCU-dependent mitochondrial Ca^{2+} buffering to remain active ***[modified and adopted from* (116)*]***

(A) Curves represent cytosolic Ca^{2+} responses of control, MCU^{KD} and $UCP2^{KD}$ cells upon addition of 2 mM Ca^{2+}. Cells were pre-stimulated with 1 µM thapsigargin to induce depletion of the ER Ca^{2+} store.

(B) *Left panel:* Curves were fitted with straight lines using linear regression to assess maximal slope of thr increase in $[Ca^{2+}]_{cyto}$ (SOCE onset) upon Ca^{2+} addition. As a negative control, cells were exposed to FCCP and oligomycin (2 µM each) prior to the addition of Ca^{2+}. Data show the mean±s.e.m. normalized to Control (set at 100%). The number of Control/MCU^{KD}/$UCP2^{KD}$ cells for each condition are: untreated (n=104/93/91); +FCCP/oligomycin (n= 90/77/99). *Right panel:* Values of the area under the curve (AUC) of SOCE-driven Ca^{2+} signals were calculated to quantify inactivation (SOCE plateau). Data show the mean±s.e.m. normalized to Control (set at 100%); $^{*}P<0.05$ versus Control; $^{\#}P<0.05$ versus MCU^{KD}; $^{\S}P<0.05$ versus $UCP2^{KD}$ (unpaired Student´s *t*-test)

4. DISCUSSION

4.1 Organelle-associated Ca^{2+} measurement with a red-shifted cameleon and fura-2AM: a novel approach to correlate mitochondrial and cytosolic Ca^{2+} responses on a single-cell level

Examination of mitochondrial Ca^{2+} signals in intact cells requires sophisticated methods. In order to study and visualize the complex process of mitochondrial Ca^{2+} handling, various chemical and genetically encoded Ca^{2+} sensors, as well as electrophysiological techniques have been developed and utilized over the past decades (149). Chemical indicators exhibit altered fluorescent properties, when bound to Ca^{2+} and are usually loaded into permeabilized or intact cells by passive incubation. One of the most popular chemical Ca^{2+} indicators used to assess mitochondrial Ca^{2+} uptake is Rhod-2. Rhod-2 is a positively charged dye that accumulates within respiring mitochondria and responds with increased fluorescence upon $[Ca^{2+}]_{mito}$ elevation (150). Furthermore, as shown by Szanda et al Rhod-2 in combination with another Ca^{2+} sensitive dye, the Fluo-4, enables a real-time monitoring of mitochondrial and cytosolic Ca^{2+} rises within the same individual cells (151). Similarly to this approach, Csordas et al. used the combination of fura-2FF and Rhod-2 to simultaneously measure compartmentalized Ca^{2+} signals in suspensions of permeabilized mast cells (152). However, the application of chemical indicators bears certain limitations. As Rhod-2 is not a ratiometric Ca^{2+} indicator, the exact quantification of mitochondrial Ca^{2+} signals is often difficult. In addition to that, under most conditions, significant amounts of Rhod-2 can also be found in the cytosol and other extramitochondrial cellular compartments (150), which makes the analysis of organelle-associated Ca^{2+} signals problematic.

In case of the genetically encoded Ca^{2+} indicators, the appropriate mitochondrial matrix-targeting is ensured by specific mitochondrial target sequences (134). As described in *chapter 2.10.2*, these sensors, including single FP- or FRET-based probes, are reliable tools to visualize mitochondrial Ca^{2+} signals, but none of them are suitable for a co-imaging with the cytosolic Ca^{2+} indicator, fura-2, because of a significant overlap in the excitation and emission spectra. In order to resolve this problem, CFP and YFP, the most commonly used FRET donor/acceptor fluorophore pair in cameleons was replaced by GFP (cp173-mEGFP) and OFP (mKOk), respectively. This exchange made the novel red-shifted genetically encoded Ca^{2+} sensor fully compatible with fura-2 (**Figure 3.1 B**). Fura-

2am is the most popular chemical Ca^{2+} indicator employed to monitor changes of the cytosolic Ca^{2+} concentration in a confident manner. The reliability and usability of this indicator is based on its low toxicity, good cell loading properties and, importantly, pronounced ratiometric changes of its fluorescence signals in response to Ca^{2+} (153). Nevertheless, the combination of fura-2 with CFP/YFP-based FRET probes is problematic, because of the occurrence of spectral bleed-through (154). With the imaging system used in this study, we recognized that particularly the prominent fura-2 fluorescence contaminates CFP and YFP/FRET channels, as the violet excitation light of 435 nm still stimulates fluorescence of the chemical Ca^{2+} indicator. Accordingly, red-shifted FRET probes should be better compatible with the ultra violet (UV) -excitable fura-2.

A variety of fluorophore pairs suitable for FRET imaging have been tested to construct new genetically encoded probes, including ones based on orange and red fluorescent proteins (155). Such sensors were recently constructed to measure the translocation of annexin A4 (156) or caspase-3 activity (157), but to our knowledge such FRET pairs have not been used for the construction of red-shifted cameleons so far. Recently, a genetically encoded red-shifted ATP sensor containing cp173-mEGFP and the orange fluorescent variant mKOk was successfully used in combination with fura-2 to correlate $[Ca^{2+}]_{cyto}$ with changes of cytosolic or mitochondrial ATP levels (158). We took advantage of this study and designed an analogous red-shifted Ca^{2+} reporter probe, which was effectively targeted to the mitochondrial matrix by fusing the “4mt” sequence to its N-terminus. Serving as Ca^{2+} sensing and interacting site the, D1 domain was built in the probe, which should allow monitoring of Ca^{2+} over a wide range of concentration (142). Expressing 4mtD1GO in mammalian cells (HeLa and EA.hy26) loaded with fura-2am, simultaneous mitochondrial and cytosolic Ca^{2+} signals were successfully recorded and correlated on a single-cell level.

4.2 SERCA activity determines the mode and mediators of mitochondrial Ca^{2+} uptake

By correlating the two organelle-associated Ca^{2+} responses, we aimed to investigate the functional coupling between cytosolic and mitochondrial Ca^{2+} signals. Our findings revealed that IP_3-mediated rapid cytoplasmic Ca^{2+} rises that are associated with the generation of high-concentration Ca^{2+} micro-domains at the surface of mitochondria (159) were transferred into these organelles via an UCP3- and MCU-dependent, but Letm1-

independent pathway (**Figure 4.1 A**). However, if Ca^{2+} mobilization was decelerated by SERCA inhibition, which increased the leakage of Ca^{2+} from the ER and thus, probably prevented the formation of the inter-organelle Ca^{2+} micro-domains, mitochondrial Ca^{2+} accumulation was accomplished via an UCP3-independent, but Letm1- and MCU-reliant route (**Figure 4.1 B**).

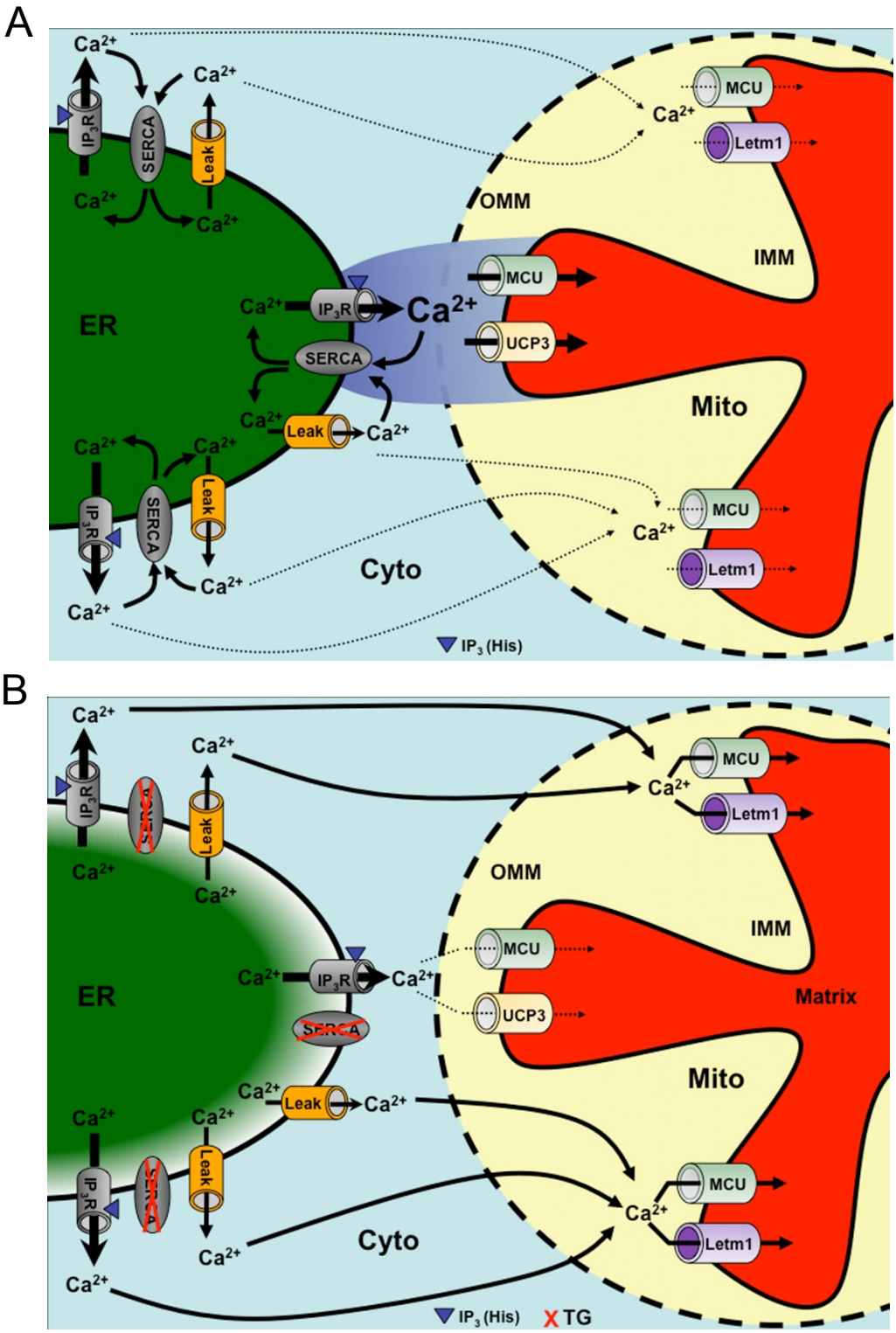

Figure 4.1 Schematic illustration of a hypothetical switch in the mitochondrial Ca^{2+} uptake mode triggered by SERCA inhibition upon IP_3-mediated Ca^{2+} release

(**A**) SERCA counteracts the leaking of Ca^{2+} from the ER and recycles Ca^{2+} back into the lumen. By this, SERCA supports the generation of high Ca^{2+} microdomains upon IP_3-mediated ER Ca^{2+} release. Under these conditions Ca^{2+} "hot spots" formed in the vicinity of mitochondrial Ca^{2+} uptake sites are sensed by UCP2/3 and MCU, which mediate the transfer of Ca^{2+} across the IMM. Arrows indicate Ca^{2+} fluxes

(**B**) Impaired SERCA activity yields partial ER Ca^{2+} depletion, which hinders the generation of high Ca^{2+} microdomains at mitochondrial contact sites. Under these conditions the global slow cytosolic Ca^{2+} elevation is partially transferred into mitochondria by a Letm1 and MCU-dependent pathway. Arrows indicate Ca^{2+} fluxes

Basically, the results indicate that a modification of the IP_3-mediated Ca^{2+} release by SERCA inhibition significantly alters the molecular characteristics of mitochondrial Ca^{2+} uptake. At a first glance, these findings are not surprising, considering the central role of ER Ca^{2+} pumps in the control of the cellular Ca^{2+} homeostasis (160,161). Virtually, in all cells, SERCA activity is necessary to maintain high Ca^{2+} levels within the ER: the pump counteracts the Ca^{2+} leakage and replenishes the ER Ca^{2+} pool upon events of ER Ca^{2+} release (162). In agreement with that, it is predictable that a combination of the SERCA inhibitor with an IP_3-generating agonist would yield increased global cytosolic and mitochondrial Ca^{2+} signals, as confirmed by the results shown in **Figure 3.3**.

According to our hypothesis, the switch in the mode of mitochondrial Ca^{2+} uptake upon SERCA inhibition occurs because of an attenuation of high-concentration Ca^{2+} micro-domains in the inter-organelle gap. The existence of such high-concentration Ca^{2+} concentration micro-domains (or also referred to as Ca^{2+} hot spots) has been verified some time ago. Functional evidence demonstrate their fundamental role in activating low Ca^{2+} sensitive mitochondrial Ca^{2+} uniport upon IP_3-mediated ER Ca^{2+} release (163,164). Moreover, in sophisticated studies, the Ca^{2+} hot spots on sites of mitochondrial Ca^{2+} uptake have recently been successfully visualized (159,165). Although local Ca^{2+} hot spots were not measured in the present work, it is likely that an acute blockade of ER Ca^{2+} pumps prior to or during the activation of the IP_3-mediated pathway also considerably impedes the formation of such local Ca^{2+} domains. In agreement with this assumption, our data demonstrate that the loss of SERCA activity in the HeLa cells instantly results in a slow and moderate cytosolic Ca^{2+} elevation that is accompanied with a tiny but measurable increase in $[Ca^{2+}]_{mito}$ (**Figure 3.3**) However, the ER Ca^{2+} leakage might be locally facilitated by neighboring mitochondria that sequester and buffer the leaked Ca^{2+} from the inter-organelle gap and thus, maintain the great Ca^{2+} gradient. This might result in an

accelerated local ER Ca^{2+} depletion in ER regions that are in the vicinity of mitochondria. Such a scenario would explain the decelerated cytosolic Ca^{2+} rise in response to IP_3-mediated Ca^{2+} mobilization upon a short preincubation with a SERCA inhibitor. Under such conditions, the IP_3-triggered formation of inter-organelle Ca^{2+} hot spots is hampered. Thus, a mitochondrial Ca^{2+} carrier such as UCP3, which might require high Ca^{2+} domains to be activated due to its low Ca^{2+} sensitivity (114), is inactive.

As shown in **Figure 3.4** a clear delay occurs between cytosolic and respective mitochondrial Ca^{2+} signals. This time gap was particularly increased, if the IP_3-mediated cytosolic Ca^{2+} elevation had been decelerated by SERCA inhibition. Accordingly, we assumed that this slow and delayed mitochondrial Ca^{2+} accumulation exhibits a specific mode of Ca^{2+} transfer across the IMM, which is different from mitochondrial Ca^{2+} uptake during fast IP_3-mediated ER Ca^{2+} release. This "slow", presumably highly sensitive type of mitochondrial Ca^{2+} accumulation in the presence of thapsigargin might be comparable with mitochondrial uptake of Ca^{2+} entering the cell via the SOCE pathway (113). Notably, it was shown that mitochondria in HeLa cells are not exposed to Ca^{2+} hot spots in response to SOCE (159). Letm1 as well as UCP2/3 were described to accomplish the transfer of Ca^{2+} into mitochondria, while their functioning and contribution to mitochondrial Ca^{2+} uptake is debated (111,166,167). Despite strong functional data, the concerns against the idea that Letm1 and UCP2/3 indeed accomplish a transfer of Ca^{2+} across the IMM, are primarily based on the postulation of a unique, ubiquitous Ca^{2+} uniporter being a low sensitive Ca^{2+} channel protein that is activated exclusively by high-concentration Ca^{2+} signals. MCU, a recently identified protein, was shown to fulfill some of the criteria that have been expected for a protein that accomplishes mitochondrial Ca^{2+} uniport (97,98). Our findings are not in contradiction with these landmark publications. Accordingly, an siRNA-mediated knockdown of MCU attenuated mitochondrial Ca^{2+} signals independently from the mode of Ca^{2+} mobilization. This indicates that MCU contributes to both "modes" of mitochondrial Ca^{2+} uptake shown herein (**Figure 4.1**), while the contribution of UCP2 or Letm1 is selectively determined by the rate and extent of Ca^{2+} accumulation at the sites of mitochondrial Ca^{2+} uptake.

4.3 Mitochondrial Ca^{2+} uptake facilitates STIM1 activation depending on the mode of Ca^{2+} mobilization from the ER

In line with earlier observations, present data confirms that MCU is generally involved in mitochondrial Ca^{2+} uptake regardless the sources of Ca^{2+} (**Figure 3.10**) (115,117), whereas UCP2 was found to be involved in mitochondrial Ca^{2+} sequestration upon intracellular Ca^{2+} release, but not in the buffering of entering Ca^{2+} (**Figure 3.10**) [see also in (97,113,168)]. Although it has been hypothesized that UCP2 and UCP3 are preferentially located within mitochondrial Ca^{2+} uptake sites that face spots of ER Ca^{2+} release (114), the exact reason, why the knock-down of these proteins exclusively diminishes mitochondrial uptake of Ca^{2+} that is mobilized from the ER, is still unknown. Interestingly, UCP2 depletion reduced mitochondrial Ca^{2+} uptake upon cell treatment with histamine to the same extent as a stable knock-down of MCU (**Figure 3.10**), the proposed pore-forming subunit of a mitochondrial Ca^{2+} channel (97). Notably, our recent study identified three biophysically distinct mitochondrial Ca^{2+} channel currents, of which only the most abundant one depends on the presence of MCU (169). These findings show that actually both UCP2 and MCU are necessary to accomplish IP_3-mediated mitochondrial Ca^{2+} uptake in HeLa cells, thus, pointing to a possible functional interrelation of these proteins. The functional interrelationships between these proteins require further investigations. Yet, the utilization of MCU^{KD} and $UCP2^{KD}$ cell models enabled us to specify, whether local mitochondrial buffering of Ca^{2+} entering via SOCE or mitochondrial sequestration of Ca^{2+} released from ER facilitates SOCE activation and maintenance.

Interestingly, a knock-down of UCP2, which in contrast to MCU is not essential for mitochondrial sequestration of entering Ca^{2+} (117), mimicked the inhibitory effect of MCU knock-down on IP_3-triggered STIM1 activation **(Figures 3.13 & 3.14)** and, in turn, SOCE **(Figure 3.17).** These findings indicate that mitochondrial Ca^{2+} buffering at the mouth of IP_3 receptors is the major mechanism by which mitochondria contribute to SOCE activation under physiological stimulation. Accordingly, our findings partially confirm a model of how mitochondria regulate SOCE in immune cells, introduced by Anant Parekh and colleagues before STIM1 and Orai1 were described (78). As already mentioned in *chapter 1.8*, energized mitochondria and, hence, increased mitochondrial Ca^{2+} buffering augments Ca^{2+} release activated Ca^{2+} current (I_{CRAC}), the electrophysiological correlate of SOCE (6). They concluded that local mitochondrial Ca^{2+} buffering at sites of ER Ca^{2+}

release facilitates store depletion and, thus, significantly support SOCE activation by IP_3 (78). Several (whole-cell) patch clamp studies in immune cells have indicated that Ca^{2+} chelating compounds such as BAPTA or EGTA need to be added to the pipette solution to evoke a pronounced I_{CRAC} (78,79,83). However, under such conditions of an artificially increased intracellular Ca^{2+} buffer capacity, the mitochondrial contribution is not relevant for SOCE/I_{CRAC} (78). In agreement with these findings, our data confirm that STIM1 oligomerization, which represents a key step in SOCE activation, becomes independent of MCU- and UCP2-mediated mitochondrial Ca^{2+} buffering upon histamine stimulation in cells loaded with BAPTA-AM (**Figure 3. 16**). When Ca^{2+} was mobilized by SERCA inhibition, which is known to efficiently deplete the store through Ca^{2+} leakage, STIM1 oligomerization remained largely unaffected by a knock-down of MCU and UCP2 **(Figure 3.15)**, indicating that intact mitochondrial Ca^{2+} uptake is not required for SOCE activation under these conditions. SERCA inhibition does not promote the formation of high Ca^{2+} micro-domains (117) (159), which are pivotal to activate the low Ca^{2+} sensitive mitochondrial Ca^{2+} uptake pathway (170). Studies using both chemical indicators (171) and genetically encoded Ca^{2+} probes (81) revealed that SERCA inhibition evoked only small and delayed mitochondrial Ca^{2+} signals. Accordingly, we can assume that due to a lack of an efficient activation of mitochondrial Ca^{2+} uptake under these conditions, the contribution of MCU and UCP2 to STIM oligomerization is irrelevant.

Experiments, in which the ER-targeted cameleon D1ER was used (142), revealed that the ER Ca^{2+} homeostasis is controlled by mitochondria in a rather complex manner. Upon IP_3-mediated cell stimulation, mitochondria are able to recycle Ca^{2+} that has been released from intracellular stores (172) and shuttle entering Ca^{2+} to ER Ca^{2+} reuptake sites (81,172). This facilitates ER Ca^{2+} refilling, which counteracts store depletion and, thus, SOCE activation. The data show that D1ER signals are only slightly affected in MCU^{KD} or $UCP2^{KD}$ cells, if Ca^{2+} is mobilized with histamine in the presence of extracellular Ca^{2+} **(Figure 3.13)**, indicating that reduced mitochondrial Ca^{2+} uptake to some extent attenuates the kinetics of IP_3-mediated ER Ca^{2+} depletion. This observation conflicts with the idea that mitochondria recycle released Ca^{2+} back to the ER (172), whereas it confirms the assumption that local mitochondrial Ca^{2+} buffering facilitates IP_3-mediated ER Ca^{2+} depletion (78). Interestingly, we found no differences in the kinetics of ER Ca^{2+} depletion between the three cell lines, when ER Ca^{2+} was mobilized with histamine in the absence of extracellular Ca^{2+} **(Figure 3.14 B)**. However, STIM1 oligomerization was clearly delayed

in MCU^{KD} and $UCP2^{KD}$ cells under these conditions **(Figure 3.14 A)** raising the question of why a difference in STIM1 activation occurs despite the same rate of ER Ca^{2+} depletion. This discrepancy might depend on the different Ca^{2+} binding affinities of D1ER and the EF-hand motif of STIM1. *In vitro* calibration of D1ER revealed a dissociation constant (Kd) of 60 µM (142), while the Kd of the Ca^{2+} probe was estimated to be approximately 220 µM *in vivo*(173). The Kd of the EF-hand domain of STIM1 ranges between 200 – 600 µM (174). Based on these clear differences it appears feasible that small changes of $[Ca^{2+}]_{ER}$ are sensed by STIM1, but not with D1ER. An alternative explanation of these findings suggests that mitochondrial Ca^{2+} buffering facilitates the reduction of $[Ca^{2+}]_{ER}$ primarily within sub-compartments of the ER that are sensed by STIM1, while the global ER Ca^{2+} concentration remains unaffected.

In addition, our data unveiled a clear discrepancy between the kinetics of ER Ca^{2+} depletion and STIM1 oligomerization in response to BHQ (**Figure 3.15**). Under these conditions STIM1 oligomerization was fast, despite slow ER Ca^{2+} depletion. In one of our earlier studies (confirmed by others as well) STIM1 punctae formation and oligomerization was shown to be under the control of cytosolic Ca^{2+} (64,65). As slow ER Ca^{2+} depletion with a SERCA inhibitor does not generate high cytosolic Ca^{2+} micro-domains on the ER surface, STIM1 oligomerization under these conditions is independent of mitochondrial Ca^{2+} uptake. Accordingly, the lack of cytosolic Ca^{2+} hot spot formation upon SERCA inhibition promotes STIM1 activation. Based on our findings, we established a model, how mitochondria regulate STIM1 activation under physiological mode of cell stimulation. Upon ER Ca^{2+} mobilization with an IP_3-generating agonist, UCP2- and MCU-dependent mitochondrial Ca^{2+} buffering is essential for STIM1 oligomerization. Mitochondrial Ca^{2+} buffering thereby predominately shapes cytosolic Ca^{2+} micro-domains in the vicinity of the ER, which negatively interfere with STIM1 activation (**Figure 4.2 A**).

However, the findings unveil another interesting aspect of the mitochondria – SOCE relationship. The data convincingly demonstrate the necessity of MCU-dependent mitochondrial Ca^{2+} uptake to keep SOCE active, once it is triggered by irreversible SERCA inhibition (**Figure 4.2 B**). Although this latter phenomenon appears upon "unphysiological" SOCE activation, the finding itself is striking in view of an earlier study, which questioned the formation of high Ca^{2+} micro-domains on mitochondria upon SOCE in HeLa cells (159). Therefore, it is tempting to speculate that the MCU-dependent transfer

of entering Ca^{2+} into mitochondria controls SOCE maintenance by a mechanism other than shaping subplasmalemmal Ca^{2+} hot-spots.

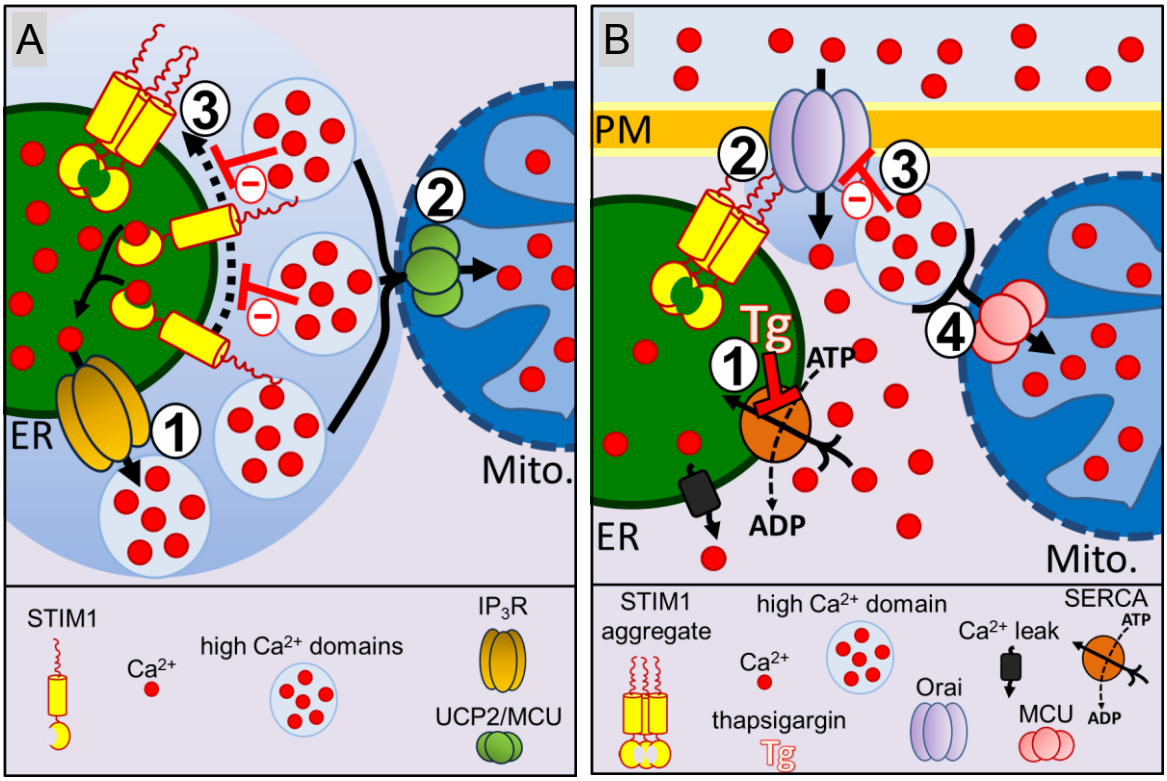

Figure 4.2 Model for a stimulus-specific mitochondrial regulation of STIM1 activation and SOCE

(**A**) The impact of UCP2- and MCU-dependent mitochondrial Ca^{2+} uptake on STIM1 activation. Dashed arrow - STIM1 oligomerization; solid arrows - Ca^{2+} movements (1) IP_3-mediated Ca^{2+} release causes a reduction in the Ca^{2+} content of the ER, which triggers STIM1 oligomerization. However, local high-concentration Ca^{2+} micro-domains on the cytosolic side of the ER membrane restrain the formation of STIM1 oligomers. (2) Mitochondria (mito.) adjacent to sites of ER Ca^{2+} release act to sequester Ca^{2+} by a UCP2- and MCU-dependent pathway, which dissipates high-concentration Ca^{2+} micro-domains and, hence, facilitates STIM1 oligomerization. (3) Accordingly, STIM1 oligomerization upon IP_3-mediated Ca^{2+} mobilization requires mitochondrial Ca^{2+} uptake, as Ca^{2+} buffering by the mitochondria results in both an efficient depletion of Ca^{2+} from the ER and, importantly, the dissipation of local cytosolic Ca^{2+} micro-domains at the ER surface. (**B**) MCU-dependent mitochondrial Ca^{2+} uptake counteracts Ca^{2+}-dependent SOCE inactivation. Solid arrows - Ca^{2+} movements. (1) SERCA inhibition with thapsigargin induces strong ER Ca^{2+} depletion, leading to STIM1 oligomerization and punctae formation in superficial ER domains. (2) STIM1 aggregates interfere with plasma membrane (PM) Ca^{2+} channels such as Orai1, which leads to strong SOCE activation. (3) Upon Ca^{2+} addition to thapsigargin-treated cells, SOCE induces an increase of global and local cytosolic Ca^{2+} levels, and Ca^{2+} negatively impacts on SOCE. (4) MCU-dependent mitochondrial sequestration of entering Ca^{2+} is irrelevant for thapsigargin-induced SOCE activation, but essential to maintain SOCE – probably by abrogating the (slow) Ca^{2+}-dependent in activation of this Ca^{2+} entry pathway.

Recently, a MCU knock-out mouse was generated (100). Interestingly, MCU depletion yielded in a rather inconspicuous phenotype, which is comparable with that of UCP2 or

UCP3 knock-out mice (175). The lack of MCU was however associated with reduced Ca^{2+}-stimulated mitochondrial ATP generation and skeletal muscle work (100). Typical STIM1 related functions such as T-cell activation and skeleton muscle physiology (176) have not been specifically examined in MCU knock-out mice so far. However, the clear inability of mitochondria to respond to Ca^{2+} elevations with increased ATP generation in MCU knock-out cells and our findings, which demonstrate the importance of MCU in SOCE activation and maintenance point to mitochondrial ATP as a potential regulator of SOCE. Indeed, it has been suggested that ATP facilitates SOCE by activating certain kinases (60) and/or increasing the local Ca^{2+} buffer capacity (177). Additional studies are necessary to entirely characterize molecular mechanisms by which mitochondrial Ca^{2+} handling and the metabolic activity of the organelle interfere with SOCE activation, maintenance and termination in different cell types.

In summary, our findings, reveal that under physiological conditions of IP_3-mediated Ca^{2+} mobilization the transfer of Ca^{2+} from the ER into mitochondria is essential for efficient STIM1 oligomerization and SOCE activation. Considering versatile functions of STIM1 (178,179), the identification of any molecular mechanism by which mitochondria regulate the activation of this protein under physiological conditions of cell stimulation will help to improve our understanding of other STIM1-dependent cell signaling events as well.

4.4 Concluding remarks

The primary focus of the current work was to elaborate the functional relationship between SOCE and mitochondrial Ca^{2+} sequestration. Initially, a new method was established that allows real-time recording of mitochondrial and cytosolic signals of single cells. Combining a mitochondrial-targeted FRET-based Ca^{2+} probe (4mtD1GO) with a chemical Ca^{2+} indicator (fura-2am), the coupling of organelle-associated Ca^{2+} signals was evaluated by fluorescence microscope. Using this technique, two molecularly distinct mitochondrial Ca^{2+} uptake routes determined by SERCA activity were described. Upon IP_3-mediated Ca^{2+} mobilization from the ER, the transfer of Ca^{2+} into the mitochondrial matrix was mediated by MCU and UCP2. Once SERCA had been blocked shortly prior to IP_3-triggered Ca^{2+} release, MCU and Letm1 were responsible for mitochondrial Ca^{2+} accumulation. The dissection of these two molecularly distinct mitochondrial Ca^{2+} uptake routes points to the complexity of the mitochondrial Ca^{2+} uptake machinery. Furthermore, it reflects how exceptionally finely mitochondria can decode incoming Ca^{2+} signal inputs.

Taking advantage of these findings, additional FRET and Ca^{2+} measurements were performed in HeLa cells stably depleted of MCU or UCP2, in order to directly examine how mitochondrial Ca^{2+} buffering controls SOCE. This was a completely new approach to study the functional interaction between the two "Ca^{2+} signaling systems". As described herein, these experiments unveiled a stimulus-specific contribution of mitochondrial Ca^{2+} uptake to STIM1 oligomerization. Moreover, MCU-dependent mitochondrial Ca^{2+} buffering was demonstrated to be essential to maintain SOCE activation. These findings expanded our existing knowledge of the mitochondria-SOCE relationship and specified the signaling mechanism, where mitochondria interfere with STIM1 and SOCE signaling.

What gives the actuality and relevance of this work is that the significance of SOCE in physiology and pathology is recently being recognized. The number of studies describing diseases and pathological condition related to SOCE has dramatically increased in the past few years. Once in the near future, it is feasible that different components of SOCE might prove as potential drug targets. Therefore, an in-depth analysis and exploration of the underlying signaling mechanisms such as the direct mitochondrial regulation of SOCE helps us to achieve these goals.

5. REFERENCES

1. Berridge MJ, Bootman MD, Roderick HL. Calcium signalling: dynamics, homeostasis and remodelling. Nat Rev Mol Cell Biol. 2003;4(7):517-29.

2. Berridge MJ, Irvine RF. Inositol trisphosphate, a novel second messenger in cellular signal transduction. Nature. 1984;312(5992):315-21.

3. Putney JW. A model for receptor-regulated calcium entry. Cell Calcium. 1986;7(1):1-2.

4. Putney JW. Origins of the concept of store-operated calcium entry. Frontiers in bioscience (Scholar edition). 2011;3:980-4.

5. Putney JW. Capacitative calcium entry revisited. Cell Calcium. 1990;11(10):611-24.

6. Hoth M, Penner R. Depletion of intracellular calcium stores activates a calcium current in mast cells. Nature. 1992;355(6358):353-6.

7. Zweifach A, Lewis RS. Mitogen-regulated Ca^{2+} current of T lymphocytes is activated by depletion of intracellular Ca^{2+} stores. Proc Natl Acad Sci U S A. 1993;90(13):6295-9.

8. Hoth M, Fanger CM, Lewis RS. Mitochondrial regulation of store-operated calcium signaling in T lymphocytes. J Cell Biol. 1997;137(3):633-48.

9. Naghdi S, Waldeck-Weiermair M, Fertschai I, Poteser M, Graier WF, Malli R. Mitochondrial Ca^{2+} uptake and not mitochondrial motility is required for STIM1-Orai1-dependent store-operated Ca^{2+} entry. J Cell Sci. 2010;123(Pt 15):2553-64.

10. Roos J, DiGregorio PJ, Yeromin AV, Ohlsen K, Lioudyno M, Zhang S et al. STIM1, an essential and conserved component of store-operated Ca^{2+} channel function. J Cell Biol. 2005;169(3):435-45.

11. Liou J, Kim ML, Heo WD, Jones JT, Myers JW, Ferrell JE et al. STIM is a Ca^{2+} sensor essential for Ca^{2+}-store-depletion-triggered Ca^{2+} influx. Curr Biol. 2005;15(13):1235-41.

12. Feske S, Gwack Y, Prakriya M, Srikanth S, Puppel SH, Tanasa B et al. A mutation in Orai1 causes immune deficiency by abrogating CRAC channel function. Nature. 2006;441(7090):179-85.

13. Zhang SL, Yeromin AV, Zhang XHF, Yu Y, Safrina O, Penna A et al. Genome-wide RNAi screen of Ca^{2+} influx identifies genes that regulate Ca^{2+} release-activated Ca^{2+} channel activity. Proc Natl Acad Sci U S A. 2006;103(24):9357-62.

14. Williams RT, Manji SS, Parker NJ, Hancock MS, Van Stekelenburg L, Eid JP et al. Identification and characterization of the STIM (stromal interaction molecule) gene family: coding for a novel class of transmembrane proteins. Biochem J. 2001;357(Pt 3):673-85.

15. Oritani K, Kincade PW. Identification of stromal cell products that interact with pre-B cells. J Cell Biol. 1996;134(3):771-82.

16. Sabbioni S, Veronese A, Trubia M, Taramelli R, Barbanti-Brodano G, Croce CM et al. Exon structure and promoter identification of STIM1 (alias GOK), a human gene causing growth arrest of the human tumor cell lines G401 and RD. Cytogenet Cell Genet. 1999;86(3-4):214-8.

17. Sabbioni S, Barbanti-Brodano G, Croce CM, Negrini M. GOK: a gene at 11p15 involved in rhabdomyosarcoma and rhabdoid tumor development. Cancer Res. 1997;57(20):4493-7.

18. Soboloff J, Spassova MA, Hewavitharana T, He LP, Xu W, Johnstone LS et al. STIM2 is an inhibitor of STIM1-mediated store-operated Ca^{2+} Entry. Curr Biol. 2006;16(14):1465-70.

19. Brandman O, Liou J, Park WS, Meyer T. STIM2 is a feedback regulator that stabilizes basal cytosolic and endoplasmic reticulum Ca^{2+} levels. Cell. 2007;131(7):1327-39.

20. Berna-Erro A, Braun A, Kraft R, Kleinschnitz C, Schuhmann MK, Stegner D et al. STIM2 regulates capacitive Ca^{2+} entry in neurons and plays a key role in hypoxic neuronal cell death. Science signaling. 2009;2(93):ra67.

21. Gruszczynska-Biegala J, Kuznicki J. Native STIM2 and ORAI1 proteins form a calcium-sensitive and thapsigargin-insensitive complex in cortical neurons. J Neurochem. 2013;126(6):727-38.

22. Collins HE, Zhu-Mauldin X, Marchase RB, Chatham JC. STIM1/Orai1-mediated SOCE: current perspectives and potential roles in cardiac function and pathology. Am J Physiol Heart Circ Physiol. 2013;305(4):H446-58.

23. Cahalan MD. STIMulating store-operated Ca^{2+} entry. Nat Cell Biol. 2009;11(6):669-77.

24. Stathopulos PB, Zheng L, Li GY, Plevin MJ, Ikura M. Structural and mechanistic insights into STIM1-mediated initiation of store-operated calcium entry. Cell. 2008;135(1):110-22.

25. Yang X, Jin H, Cai X, Li S, Shen Y. Structural and mechanistic insights into the activation of Stromal interaction molecule 1 (STIM1). Proc Natl Acad Sci U S A. 2012;109(15):5657-62.

26. Bird GS, Hwang SY, Smyth JT, Fukushima M, Boyles RR, Putney JW. STIM1 is a calcium sensor specialized for digital signaling. Curr Biol. 2009;19(20):1724-9.

27. Bandyopadhyay BC, Pingle SC, Ahern GP. Store-operated Ca^{2+} signaling in dendritic cells occurs independently of STIM1. J Leukoc Biol. 2011;89(1):57-62.

28. Covington ED, Wu MM, Lewis RS. Essential role for the CRAC activation domain in store-dependent oligomerization of STIM1. Mol Biol Cell. 2010;21(11):1897-907.

29. Baba Y, Hayashi K, Fujii Y, Mizushima A, Watarai H, Wakamori M et al. Coupling of STIM1 to store-operated Ca^{2+} entry through its constitutive and inducible movement in the endoplasmic reticulum. Proc Natl Acad Sci U S A. 2006;103(45):16704-9.

30. Wu MM, Buchanan J, Luik RM, Lewis RS. Ca^{2+} store depletion causes STIM1 to accumulate in ER regions closely associated with the plasma membrane. J Cell Biol. 2006;174(6):803-13.

31. Luik RM, Wang B, Prakriya M, Wu MM, Lewis RS. Oligomerization of STIM1 couples ER calcium depletion to CRAC channel activation. Nature. 2008;454(7203):538-42.

32. Várnai P, Hunyady L, Balla T. STIM and Orai: the long-awaited constituents of store-operated calcium entry. Trends Pharmacol Sci. 2009;30(3):118-28.

33. Huang GN, Zeng W, Kim JY, Yuan JP, Han L, Muallem S et al. STIM1 carboxyl-terminus activates native SOC, I_{CRAC} and TRPC1 channels. Nat Cell Biol. 2006;8(9):1003-10.

34. Cheng KT, Ong HL, Liu X, Ambudkar IS. Contribution and regulation of TRPC channels in store-operated Ca^{2+} entry. Current topics in membranes. 2013;71:149-79.

35. Vig M, Peinelt C, Beck A, Koomoa DL, Rabah D, Koblan-Huberson M et al. CRACM1 is a plasma membrane protein essential for store-operated Ca^{2+} entry. Science. 2006;312(5777):1220-3.

36. Hou X, Pedi L, Diver MM, Long SB. Crystal structure of the calcium release-activated calcium channel Orai. Science. 2012;338(6112):1308-13.

37. Derler I, Madl J, Schütz G, Romanin C. Structure, regulation and biophysics of I_{CRAC}, STIM/Orai1. Adv Exp Med Biol. 2012;740:383-410.

38. Demuro A, Penna A, Safrina O, Yeromin AV, Amcheslavsky A, Cahalan MD et al. Subunit stoichiometry of human Orai1 and Orai3 channels in closed and open states. Proc Natl Acad Sci U S A. 2011;108(43):17832-7.

39. Madl J, Weghuber J, Fritsch R, Derler I, Fahrner M, Frischauf I et al. Resting state Orai1 diffuses as homotetramer in the plasma membrane of live mammalian cells. J Biol Chem. 2010;285(52):41135-42.

40. Xu P, Lu J, Li Z, Yu X, Chen L, Xu T. Aggregation of STIM1 underneath the plasma membrane induces clustering of Orai1. Biochem Biophys Res Commun. 2006;350(4):969-76.

41. Várnai P, Tóth B, Tóth DJ, Hunyady L, Balla T. Visualization and manipulation of plasma membrane-endoplasmic reticulum contact sites indicates the presence of additional molecular components within the STIM1-Orai1 Complex. J Biol Chem. 2007;282(40):29678-90.

42. Muik M, Frischauf I, Derler I, Fahrner M, Bergsmann J, Eder P et al. Dynamic coupling of the putative coiled-coil domain of ORAI1 with STIM1 mediates ORAI1 channel activation. J Biol Chem. 2008;283(12):8014-22.

43. Navarro-Borelly L, Somasundaram A, Yamashita M, Ren D, Miller RJ, Prakriya M. STIM1-Orai1 interactions and Orai1 conformational changes revealed by live-cell FRET microscopy. J Physiol. 2008;586(Pt 22):5383-401.

44. Yeromin AV, Zhang SL, Jiang W, Yu Y, Safrina O, Cahalan MD. Molecular identification of the CRAC channel by altered ion selectivity in a mutant of Orai. Nature. 2006;443(7108):226-9.

45. Park CY, Hoover PJ, Mullins FM, Bachhawat P, Covington ED, Raunser S et al. STIM1 clusters and activates CRAC channels via direct binding of a cytosolic domain to Orai1. Cell. 2009;136(5):876-90.

46. Yuan JP, Zeng W, Dorwart MR, Choi YJ, Worley PF, Muallem S. SOAR and the polybasic STIM1 domains gate and regulate Orai channels. Nat Cell Biol. 2009;11(3):337-43.

47. Muik M, Fahrner M, Derler I, Schindl R, Bergsmann J, Frischauf I et al. A Cytosolic Homomerization and a Modulatory Domain within STIM1 C Terminus Determine Coupling to ORAI1 Channels. J Biol Chem. 2009;284(13):8421-6.

48. McNally BA, Somasundaram A, Yamashita M, Prakriya M. Gated regulation of CRAC channel ion selectivity by STIM1. Nature. 2012;482(7384):241-5.

49. Parekh AB, Putney JW. Store-operated calcium channels. Physiol Rev. 2005;85(2):757-810.

50. Zitt C, Zobel A, Obukhov AG, Harteneck C, Kalkbrenner F, Lückhoff A et al. Cloning and functional expression of a human Ca^{2+}-permeable cation channel activated by calcium store depletion. Neuron. 1996;16(6):1189-96.

51. Xu XZ, Li HS, Guggino WB, Montell C. Coassembly of TRP and TRPL produces a distinct store-operated conductance. Cell. 1997;89(7):1155-64.

52. Xu SZ, Beech DJ. TrpC1 is a membrane-spanning subunit of store-operated Ca^{2+} channels in native vascular smooth muscle cells. Circ Res. 2001;88(1):84-7.

53. Yuan JP, Zeng W, Huang GN, Worley PF, Muallem S. STIM1 heteromultimerizes TRPC channels to determine their function as store-operated channels. Nat Cell Biol. 2007;9(6):636-45.

54. Zeng W, Yuan JP, Kim MS, Choi YJ, Huang GN, Worley PF et al. STIM1 gates TRPC channels, but not Orai1, by electrostatic interaction. Mol Cell. 2008;32(3):439-48.

55. DeHaven WI, Jones BF, Petranka JG, Smyth JT, Tomita T, Bird GS et al. TRPC channels function independently of STIM1 and Orai1. J Physiol. 2009;587(Pt 10):2275-98.

56. Deng X, Wang Y, Zhou Y, Soboloff J, Gill DL. STIM and Orai: dynamic intermembrane coupling to control cellular calcium signals. J Biol Chem. 2009;284(34):22501-5.

57. Korzeniowski MK, Manjarrés IM, Varnai P, Balla T. Activation of STIM1-Orai1 involves an intramolecular switching mechanism. Science signaling. 2010;3(148):ra82.

58. Wang Y, Deng X, Gill DL. Calcium signaling by STIM and Orai: intimate coupling details revealed. Science signaling. 2010;3(148):pe42.

59. Ji W, Xu P, Li Z, Lu J, Liu L, Zhan Y et al. Functional stoichiometry of the unitary calcium-release-activated calcium channel. Proc Natl Acad Sci U S A. 2008;105(36):13668-73.

60. Lang F, Eylenstein A, Shumilina E. Regulation of Orai1/STIM1 by the kinases SGK1 and AMPK. Cell Calcium. 2012;52(5):347-54.

61. Pozo-Guisado E, Campbell DG, Deak M, Alvarez-Barrientos A, Morrice NA, Alvarez IS et al. Phosphorylation of STIM1 at ERK1/2 target sites modulates store-operated calcium entry. J Cell Sci. 2010;123(Pt 18):3084-93.

62. Manji SS, Parker NJ, Williams RT, van Stekelenburg L, Pearson RB, Dziadek M et al. STIM1: a novel phosphoprotein located at the cell surface. Biochim Biophys Acta. 2000;1481(1):147-55.

63. Deak AT, Groschner LN, Alam MR, Seles E, Bondarenko AI, Graier WF et al. The endocannabinoid N-arachidonoyl glycine (NAGly) inhibits store-operated Ca^{2+} entry by preventing STIM1-Orai1 interaction. J Cell Sci. 2013;126(Pt 4):879-88.

64. Malli R, Naghdi S, Romanin C, Graier WF. Cytosolic Ca^{2+} prevents the subplasmalemmal clustering of STIM1: an intrinsic mechanism to avoid Ca^{2+} overload. J Cell Sci. 2008;121(Pt 19):3133-9.

65. Shen WW, Frieden M, Demaurex N. Local cytosolic Ca^{2+} elevations are required for stromal interaction molecule 1 (STIM1) de-oligomerization and termination of store-operated Ca^{2+} entry. J Biol Chem. 2011;286(42):36448-59.

66. Zweifach A, Lewis RS. Slow calcium-dependent inactivation of depletion-activated calcium current. Store-dependent and -independent mechanisms. J Biol Chem. 1995;270(24):14445-51.

67. Shaw PJ, Feske S. Physiological and pathophysiological functions of SOCE in the immune system. Frontiers in bioscience (Elite edition). 2012;4:2253-68.

68. Soboloff J, Rothberg BS, Madesh M, Gill DL. STIM proteins: dynamic calcium signal transducers. Nat Rev Mol Cell Biol. 2012;13(9):549-65.

69. Feske S. CRAC channelopathies. Pflugers Arch. 2010;460(2):417-35.

70. Cope AP. Studies of T-cell activation in chronic inflammation. Arthritis Res. 2002;4 Suppl 3:S197-211.

71. Feske S. ORAI1 and STIM1 deficiency in human and mice: roles of store-operated Ca^{2+} entry in the immune system and beyond. Immunol Rev. 2009;231(1):189-209.

72. Pan Z, Brotto M, Ma J. Store-operated Ca^{2+} entry in muscle physiology and diseases. BMB reports. 2014;47(2):69-79.

73. Varga-Szabo D, Authi KS, Braun A, Bender M, Ambily A, Hassock SR et al. Store-operated Ca^{2+} entry in platelets occurs independently of transient receptor potential (TRP) C1. Pflugers Arch. 2008;457(2):377-87.

74. Sun S, Zhang H, Liu J, Popugaeva E, Xu NJ, Feske S et al. Reduced synaptic STIM2 expression and impaired store-operated calcium entry cause destabilization of mature spines in mutant presenilin mice. Neuron. 2014;82(1):79-93.

75. Feng M, Grice DM, Faddy HM, Nguyen N, Leitch S, Wang Y et al. Store-independent activation of Orai1 by SPCA2 in mammary tumors. Cell. 2010;143(1):84-98.

76. Weidinger C, Shaw PJ, Feske S. STIM1 and STIM2-mediated Ca^{2+} influx regulates antitumour immunity by CD8(+) T cells. EMBO molecular medicine. 2013;5(9):1311-21.

77. Watson R, Parekh AB. Mitochondrial regulation of CRAC channel-driven cellular responses. Cell Calcium. 2012;52(1):52-6.

78. Gilabert JA, Bakowski D, Parekh AB. Energized mitochondria increase the dynamic range over which inositol 1,4,5-trisphosphate activates store-operated calcium influx. EMBO J. 2001;20(11):2672-9.

79. Glitsch MD, Bakowski D, Parekh AB. Store-operated Ca^{2+} entry depends on mitochondrial Ca^{2+} uptake. EMBO J. 2002;21(24):6744-54.

80. Rizzuto R, Pozzan T. Microdomains of intracellular Ca^{2+}: molecular determinants and functional consequences. Physiol Rev. 2006;86(1):369-408.

81. Malli R, Frieden M, Trenker M, Graier WF. The role of mitochondria for Ca^{2+} refilling of the endoplasmic reticulum. J Biol Chem. 2005;280(13):12114-22.

82. Gilabert JA, Parekh AB. Respiring mitochondria determine the pattern of activation and inactivation of the store-operated Ca^{2+} current I_{CRAC}. EMBO J. 2000;19(23):6401-7.

83. Zweifach A, Lewis RS. Rapid inactivation of depletion-activated calcium current (I_{CRAC}) due to local calcium feedback. J Gen Physiol. 1995;105(2):209-26.

84. Mullins FM, Park CY, Dolmetsch RE, Lewis RS. STIM1 and calmodulin interact with Orai1 to induce Ca^{2+}-dependent inactivation of CRAC channels. Proc Natl Acad Sci U S A. 2009;106(36):15495-500.

85. Singaravelu K, Nelson C, Bakowski D, de Brito OM, Ng SW, Di Capite J et al. Mitofusin 2 regulates STIM1 migration from the Ca^{2+} store to the plasma membrane in cells with depolarized mitochondria. J Biol Chem. 2011;286(14):12189-201.

86. de Brito OM, Scorrano L. Mitofusin 2 tethers endoplasmic reticulum to mitochondria. Nature. 2008;456(7222):605-10.

87. Saris NEL, Carafoli E. A historical review of cellular calcium handling, with emphasis on mitochondria. Biochemistry. Biokhimiia. 2005;70(2):187-94.

88. Gunter TE, Pfeiffer DR. Mechanisms by which mitochondria transport calcium. Am J Physiol. 1990;258(5 Pt 1):C755-86.

89. Kevin Foskett J, Madesh M. Regulation of the mitochondrial Ca^{2+} uniporter by MICU1 and MICU2. Biochem Biophys Res Commun. 2014;

90. Castaldo P, Cataldi M, Magi S, Lariccia V, Arcangeli S, Amoroso S. Role of the mitochondrial sodium/calcium exchanger in neuronal physiology and in the pathogenesis of neurological diseases. Prog Neurobiol. 2009;87(1):58-79.

91. Palty R, Silverman WF, Hershfinkel M, Caporale T, Sensi SL, Parnis J et al. NCLX is an essential component of mitochondrial Na^{+}/Ca^{2+} exchange. Proc Natl Acad Sci U S A. 2010;107(1):436-41.

92. Villa A, García-Simón MI, Blanco P, Sesé B, Bogónez E, Satrustegui J. Affinity chromatography purification of mitochondrial inner membrane proteins with calcium transport activity. Biochim Biophys Acta. 1998;1373(2):347-59.

93. Ichas F, Jouaville LS, Mazat JP. Mitochondria are excitable organelles capable of generating and conveying electrical and calcium signals. Cell. 1997;89(7):1145-53.

94. Pendin D, Greotti E, Pozzan T. The elusive importance of being a mitochondrial Ca^{2+} uniporter. Cell Calcium. 2014;55(3):139-45.

95. Bragadin M, Pozzan T, Azzone GF. Activation energies and enthalpies during Ca^{2+} transport in rat liver mitochondria. FEBS Lett. 1979;104(2):347-51.

96. Kirichok Y, Krapivinsky G, Clapham DE. The mitochondrial calcium uniporter is a highly selective ion channel. Nature. 2004;427(6972):360-4.

97. De Stefani D, Raffaello A, Teardo E, Szabò I, Rizzuto R. A forty-kilodalton protein of the inner membrane is the mitochondrial calcium uniporter. Nature. 2011;476(7360):336-40.

98. Baughman JM, Perocchi F, Girgis HS, Plovanich M, Belcher-Timme CA, Sancak Y et al. Integrative genomics identifies MCU as an essential component of the mitochondrial calcium uniporter. Nature. 2011;476(7360):341-5.

99. Raffaello A, De Stefani D, Sabbadin D, Teardo E, Merli G, Picard A et al. The mitochondrial calcium uniporter is a multimer that can include a dominant-negative pore-forming subunit. EMBO J. 2013;32(17):2362-76.

100. Pan X, Liu J, Nguyen T, Liu C, Sun J, Teng Y et al. The physiological role of mitochondrial calcium revealed by mice lacking the mitochondrial calcium uniporter. Nat Cell Biol. 2013;15(12):1464-72.

101. Mallilankaraman K, Cárdenas C, Doonan PJ, Chandramoorthy HC, Irrinki KM, Golenár T et al. MCUR1 is an essential component of mitochondrial Ca^{2+} uptake that regulates cellular metabolism. Nat Cell Biol. 2012;14(12):1336-43.

102. Perocchi F, Gohil VM, Girgis HS, Bao XR, McCombs JE, Palmer AE et al. MICU1 encodes a mitochondrial EF hand protein required for Ca^{2+} uptake. Nature. 2010;467(7313):291-6.

103. Alam MR, Groschner LN, Parichatikanond W, Kuo L, Bondarenko AI, Rost R et al. Mitochondrial Ca2+ uptake 1 (MICU1) and mitochondrial Ca^{2+} uniporter (MCU) contribute to metabolism-secretion coupling in clonal pancreatic β-cells. J Biol Chem. 2012;287(41):34445-54.

104. Mallilankaraman K, Doonan P, Cárdenas C, Chandramoorthy HC, Müller M, Miller R et al. MICU1 Is an Essential Gatekeeper for MCU-Mediated Mitochondrial Ca^{2+} Uptake that Regulates Cell Survival. Cell. 2012;151(3):630-44.

105. Csordás G, Golenár T, Seifert EL, Kamer KJ, Sancak Y, Perocchi F et al. MICU1 controls both the threshold and cooperative activation of the mitochondrial Ca^{2+} uniporter. Cell Metab. 2013;17(6):976-87.

106. Plovanich M, Bogorad RL, Sancak Y, Kamer KJ, Strittmatter L, Li AA et al. MICU2, a Paralog of MICU1, Resides within the Mitochondrial Uniporter Complex to Regulate Calcium Handling. PloS one. 2013;8(2):e55785.

107. Patron M, Checchetto V, Raffaello A, Teardo E, Vecellio Reane D, Mantoan M et al. MICU1 and MICU2 finely tune the mitochondrial Ca^{2+} uniporter by exerting opposite effects on MCU activity. Mol Cell. 2014;53(5):726-37.

108. Nicholls DG, Rial E. A history of the first uncoupling protein, UCP1. J Bioenerg Biomembr. 1999;31(5):399-406.

109. Krauss S, Zhang CY, Lowell BB. The mitochondrial uncoupling-protein homologues. Nat Rev Mol Cell Biol. 2005;6(3):248-61.

110. Trenker M, Malli R, Fertschai I, Levak-Frank S, Graier WF. Uncoupling proteins 2 and 3 are fundamental for mitochondrial Ca^{2+} uniport. Nat Cell Biol. 2007;9(4):445-52.

111. Pizzo P, Drago I, Filadi R, Pozzan T. Mitochondrial Ca^{2+} homeostasis: mechanism, role, and tissue specificities. Pflugers Arch. 2012;464(1):3-17.

112. Brookes PS, Parker N, Buckingham JA, Vidal-Puig A, Halestrap AP, Gunter TE et al. UCPs--unlikely calcium porters. Nat Cell Biol. 2008;10(11):1235-7; author reply 1237.

113. Waldeck-Weiermair M, Malli R, Naghdi S, Trenker M, Kahn MJ, Graier WF. The contribution of UCP2 and UCP3 to mitochondrial Ca^{2+} uptake is differentially determined by the source of supplied Ca^{2+}. Cell Calcium. 2010;47(5):433-40.

114. Waldeck-Weiermair M, Duan X, Naghdi S, Khan MJ, Trenker M, Malli R et al. Uncoupling protein 3 adjusts mitochondrial Ca^{2+} uptake to high and low Ca^{2+} signals. Cell Calcium. 2010;48(5):288-301.

115. Waldeck-Weiermair M, Jean-Quartier C, Rost R, Khan MJ, Vishnu N, Bondarenko AI et al. Leucine zipper EF hand-containing transmembrane protein 1 (Letm1) and uncoupling proteins 2 and 3 (UCP2/3) contribute to two distinct mitochondrial Ca^{2+} uptake pathways. J Biol Chem. 2011;286(32):28444-55.

116. Deak AT, Blass S, Khan MJ, Groschner LN, Waldeck-Weiermair M, Hallström S et al. Inositol-1,4,5-trisphosphate (IP_3)-mediated STIM1 oligomerization requires intact mitochondrial Ca^{2+} uptake. J Cell Sci. 2014;

117. Waldeck-Weiermair M, Deak AT, Groschner LN, Alam MR, Jean-Quartier C, Malli R et al. Molecularly distinct routes of mitochondrial Ca^{2+} uptake are activated depending on the activity of the sarco/endoplasmic reticulum Ca^{2+} ATPase (SERCA). J Biol Chem. 2013;288(21):15367-79.

118. Jiang D, Zhao L, Clapham DE. Genome-wide RNAi screen identifies Letm1 as a mitochondrial Ca^{2+}/H^{+} antiporter. Science. 2009;326(5949):144-7.

119. Nowikovsky K, Froschauer EM, Zsurka G, Samaj J, Reipert S, Kolisek M et al. The LETM1/YOL027 gene family encodes a factor of the mitochondrial K^{+} homeostasis with a potential role in the Wolf-Hirschhorn syndrome. J Biol Chem. 2004;279(29):30307-15.

120. Jiang D, Zhao L, Clish CB, Clapham DE. Letm1, the mitochondrial Ca^{2+}/H^{+} antiporter, is essential for normal glucose metabolism and alters brain function in Wolf-Hirschhorn syndrome. Proc Natl Acad Sci U S A. 2013;110(24):E2249-54.

121. Tsai MF, Jiang D, Zhao L, Clapham D, Miller C. Functional reconstitution of the mitochondrial Ca^{2+}/H^{+} antiporter Letm1. J Gen Physiol. 2014;143(1):67-73.

122. Sancak Y, Markhard AL, Kitami T, Kovács-Bogdán E, Kamer KJ, Udeshi ND et al. EMRE is an Essential Component of the Mitochondrial Calcium Uniporter Complex. Science. 2013;342(6164):1379-82.

123. Waldeck-Weiermair M, Alam MR, Khan MJ, Deak AT, Vishnu N, Karsten F et al. Spatiotemporal Correlations between Cytosolic and Mitochondrial Ca^{2+} Signals Using a Novel Red-Shifted Mitochondrial Targeted Cameleon. PloS one. 2012;7(9):e45917.

124. Fu LW, Pan HL, Longhurst JC. Endogenous histamine stimulates ischemically sensitive abdominal visceral afferents through H_1 receptors. Am J Physiol. 1997;273(6 Pt 2):H2726-37.

125. Hasséssian H, Vaca L, Kunze DL. Blockade of the inward rectifier potassium current by the Ca^{2+}-ATPase inhibitor 2',5'-di(tert-butyl)-1,4-benzohydroquinone (BHQ). Br J Pharmacol. 1994;112(4):1118-22.

126. McLarnon JG. Purinergic mediated changes in Ca^{2+} mobilization and functional responses in microglia: effects of low levels of ATP. J Neurosci Res. 2005;81(3):349-56.

127. Christensen SB, Andersen A, Poulsen JC, Treiman M. Derivatives of thapsigargin as probes of its binding site on endoplasmic reticulum Ca^{2+} ATPase. Stereoselectivity and important functional groups. FEBS Lett. 1993;335(3):345-8.

128. Nagamune H, Fukushima Y, Takada J, Yoshida K, Unami A, Shimooka T et al. The lipophilic weak base (Z)-5-methyl-2-[2-(1-naphthyl)ethenyl]-4-piperidinopyridine (AU-1421) is a potent protonophore type cationic uncoupler of oxidative phosphorylation in mitochondria. Biochim Biophys Acta. 1993;1141(2-3):231-7.

129. Heytler PG, Prichard WW. A new class of uncoupling agents--carbonyl cyanide phenylhydrazones. Biochem Biophys Res Commun. 1962;7:272-5.

130. Paredes RM, Etzler JC, Watts LT, Zheng W, Lechleiter JD. Chemical calcium indicators. Methods. 2008;46(3):143-51.

131. Tang Q, Jin MW, Xiang JZ, Dong MQ, Sun HY, Lau CP et al. The membrane permeable calcium chelator BAPTA-AM directly blocks human ether a-go-go-related gene potassium channels stably expressed in HEK 293 cells. Biochem Pharmacol. 2007;74(11):1596-607.

132. Brauner P, Fridlender B. Use of chelating agents as terminators of alkaline phosphatase activity in enzyme-linked immunosorbent assay (ELISA) tests. J Immunol Methods. 1981;42(3):375-9.

133. Khan MJ, Rizwan Alam M, Waldeck-Weiermair M, Karsten F, Groschner L, Riederer M et al. Inhibition of autophagy rescues palmitic acid-induced necroptosis of endothelial cells. J Biol Chem. 2012;287(25):21110-20.

134. Rizzuto R, Simpson AW, Brini M, Pozzan T. Rapid changes of mitochondrial Ca^{2+} revealed by specifically targeted recombinant aequorin. Nature. 1992;358(6384):325-7.

135. Nagai T, Sawano A, Park ES, Miyawaki A. Circularly permuted green fluorescent proteins engineered to sense Ca^{2+}. Proc Natl Acad Sci U S A. 2001;98(6):3197-202.

136. Nakai J, Ohkura M, Imoto K. A high signal-to-noise Ca^{2+} probe composed of a single green fluorescent protein. Nat Biotechnol. 2001;19(2):137-41.

137. Zhao Y, Araki S, Wu J, Teramoto T, Chang YF, Nakano M et al. An expanded palette of genetically encoded Ca^{2+} indicators. Science. 2011;333(6051):1888-91.

138. Miyawaki A, Llopis J, Heim R, McCaffery JM, Adams JA, Ikura M et al. Fluorescent indicators for Ca^{2+} based on green fluorescent proteins and calmodulin. Nature. 1997;388(6645):882-7.

139. Palmer AE, Jin C, Reed JC, Tsien RY. Bcl-2-mediated alterations in endoplasmic reticulum Ca^{2+} analyzed with an improved genetically encoded fluorescent sensor. Proc Natl Acad Sci U S A. 2004;101(50):17404-9.

140. Palmer AE, Giacomello M, Kortemme T, Hires SA, Lev-Ram V, Baker D et al. Ca^{2+} indicators based on computationally redesigned calmodulin-peptide pairs. Chem Biol. 2006;13(5):521-30.

141. McCombs JE, Palmer AE. Measuring calcium dynamics in living cells with genetically encodable calcium indicators. Methods. 2008;46(3):152-9.

142. Palmer AE, Jin C, Reed JC, Tsien RY. Bcl-2-mediated alterations in endoplasmic reticulum Ca^{2+} analyzed with an improved genetically encoded fluorescent sensor. Proc Natl Acad Sci U S A. 2004;101(50):17404-9.

143. De Marchi U, Castelbou C, Demaurex N. Uncoupling protein 3 (UCP3) modulates the activity of Sarco/endoplasmic reticulum Ca^{2+}-ATPase (SERCA) by decreasing mitochondrial ATP production. J Biol Chem. 2011;286(37):32533-41.

144. Graier WF, Frieden M, Malli R. Mitochondria and Ca^{2+} signaling: old guests, new functions. Pflugers Arch. 2007;455(3):375-96.

145. Duchen MR. Mitochondria in health and disease: perspectives on a new mitochondrial biology. Mol Aspects Med. 2004;25(4):365-451.

146. Liou J, Fivaz M, Inoue T, Meyer T. Live-cell imaging reveals sequential oligomerization and local plasma membrane targeting of stromal interaction molecule 1 after Ca^{2+} store depletion. Proc Natl Acad Sci U S A. 2007;104(22):9301-6.

147. Parekh AB. Ca^{2+} microdomains near plasma membrane Ca^{2+} channels: impact on cell function. J Physiol. 2008;586(13):3043-54.

148. Hirata Y, Brotto M, Weisleder N, Chu Y, Lin P, Zhao X et al. Uncoupling store-operated Ca^{2+} entry and altered Ca^{2+} release from sarcoplasmic reticulum through silencing of junctophilin genes. Biophys J. 2006;90(12):4418-27.

149. Jean-Quartier C, Bondarenko AI, Alam MR, Trenker M, Waldeck-Weiermair M, Malli R et al. Studying mitochondrial Ca^{2+} uptake - a revisit. Mol Cell Endocrinol. 2012;353(1-2):114-27.

150. Bright GR, Fisher GW, Rogowska J, Taylor DL. Fluorescence ratio imaging microscopy. Methods Cell Biol. 1989;30:157-92.

151. Szanda G, Koncz P, Várnai P, Spät A. Mitochondrial Ca^{2+} uptake with and without the formation of high-Ca^{2+} microdomains. Cell Calcium. 2006;40(5-6):527-37.

152. Csordás G, Thomas AP, Hajnóczky G. Quasi-synaptic calcium signal transmission between endoplasmic reticulum and mitochondria. EMBO J. 1999;18(1):96-108.

153. Carlson HJ, Campbell RE. Genetically encoded FRET-based biosensors for multiparameter fluorescence imaging. Curr Opin Biotechnol. 2009;20(1):19-27.

154. Mizuno H, Sawano A, Eli P, Hama H, Miyawaki A. Red fluorescent protein from Discosoma as a fusion tag and a partner for fluorescence resonance energy transfer. Biochemistry. 2001;40(8):2502-10.

155. van der Krogt GNM, Ogink J, Ponsioen B, Jalink K. A comparison of donor-acceptor pairs for genetically encoded FRET sensors: application to the Epac cAMP sensor as an example. PloS one. 2008;3(4):e1916.

156. Piljic A, Schultz C. Simultaneous recording of multiple cellular events by FRET. ACS Chem Biol. 2008;3(3):156-60.

157. Ai HW, Hazelwood KL, Davidson MW, Campbell RE. Fluorescent protein FRET pairs for ratiometric imaging of dual biosensors. Nat Methods. 2008;5(5):401-3.

158. Filippin L, Abad MC, Gastaldello S, Magalhães PJ, Sandonà D, Pozzan T. Improved strategies for the delivery of GFP-based Ca^{2+} sensors into the mitochondrial matrix. Cell Calcium. 2005;37(2):129-36.

159. Giacomello M, Drago I, Bortolozzi M, Scorzeto M, Gianelle A, Pizzo P et al. Ca2+ hot spots on the mitochondrial surface are generated by Ca^{2+} mobilization from stores, but not by activation of store-operated Ca^{2+} channels. Mol Cell. 2010;38(2):280-90.

160. Carafoli E, Brini M. Calcium pumps: structural basis for and mechanism of calcium transmembrane transport. Curr Opin Chem Biol. 2000;4(2):152-61.

161. Brini M, Bano D, Manni S, Rizzuto R, Carafoli E. Effects of PMCA and SERCA pump overexpression on the kinetics of cell Ca^{2+} signalling. EMBO J. 2000;19(18):4926-35.

162. Camello C, Lomax R, Petersen OH, Tepikin AV. Calcium leak from intracellular stores--the enigma of calcium signalling. Cell Calcium. 2002;32(5-6):355-61.

163. Später A, Szanda G, Csordás G, Hajnóczky G. High- and low-calcium-dependent mechanisms of mitochondrial calcium signalling. Cell Calcium. 2008;44(1):51-63.

164. Später A, Fülöp L, Koncz P, Szanda G. When is high-Ca^{2+} microdomain required for mitochondrial Ca^{2+} uptake? Acta Physiol (Oxf). 2009;195(1):139-47.

165. Csordás G, Várnai P, Golenár T, Roy S, Purkins G, Schneider TG et al. Imaging interorganelle contacts and local calcium dynamics at the ER-mitochondrial interface. Mol Cell. 2010;39(1):121-32.

166. Santo-Domingo J, Demaurex N. Calcium uptake mechanisms of mitochondria. Biochim Biophys Acta. 2010;1797(6-7):907-12.

167. Malli R, Graier WF. Mitochondrial Ca^{2+} channels: Great unknowns with important functions. FEBS Lett. 2010;584(10):1942-7.

168. Trenker M, Fertschai I, Malli R, Graier W. UCP2/3 - likely to be fundamental for mitochondrial Ca^{2+} uniport. Nat Cell Biol. 2008;10(11):1237-40.

169. Bondarenko AI, Jean-Quartier C, Parichatikanond W, Alam MR, Waldeck-Weiermair M, Malli R et al. Mitochondrial Ca^{2+}uniporter (MCU)-dependent and MCU-independent Ca^{2+} channels coexist in the inner mitochondrial membrane. Pflugers Arch. 2013;

170. Rizzuto R, Pinton P, Brini M, Chiesa A, Filippin L, Pozzan T. Mitochondria as biosensors of calcium microdomains. Cell Calcium. 1999;26:193-9.

171. Collins TJ, Lipp P, Berridge MJ, Bootman MD. Mitochondrial Ca^{2+} uptake depends on the spatial and temporal profile of cytosolic Ca^{2+} signals. J Biol Chem. 2001;276(28):26411-20.

172. Arnaudeau S, Kelley WL, Walsh JV, Demaurex N. Mitochondria recycle Ca^{2+} to the endoplasmic reticulum and prevent the depletion of neighboring endoplasmic reticulum regions. J Biol Chem. 2001;276(31):29430-9.

173. Rudolf R, Magalhães PJ, Pozzan T. Direct in vivo monitoring of sarcoplasmic reticulum Ca^{2+} and cytosolic cAMP dynamics in mouse skeletal muscle. J Cell Biol. 2006;173(2):187-93.

174. Stathopulos PB, Li GY, Plevin MJ, Ames JB, Ikura M. Stored Ca^{2+} depletion-induced oligomerization of stromal interaction molecule 1 (STIM1) via the EF-SAM region: An initiation mechanism for capacitive Ca^{2+} entry. J Biol Chem. 2006;281(47):35855-62.

175. Arsenijevic D, Onuma H, Pecqueur C, Raimbault S, Manning BS, Miroux B et al. Disruption of the uncoupling protein-2 gene in mice reveals a role in immunity and reactive oxygen species production. Nat Genet. 2000;26(4):435-9.

176. Frischauf I, Schindl R, Derler I, Bergsmann J, Fahrner M, Romanin C. The STIM/Orai coupling machinery. Channels (Austin, Tex.). 2008;2(4):261-8.

177. Montalvo GB, Artalejo AR, Gilabert JA. ATP from subplasmalemmal mitochondria controls Ca^{2+}-dependent inactivation of CRAC channels. J Biol Chem. 2006;281(47):35616-23.

178. Shinde AV, Motiani RK, Zhang X, Abdullaev IF, Adam AP, González-Cobos JC et al. STIM1 controls endothelial barrier function independently of Orai1 and Ca^{2+} entry. Science signaling. 2013;6(267):ra18.

179. Ritchie MF, Samakai E, Soboloff J. STIM1 is required for attenuation of PMCA-mediated Ca^{2+} clearance during T-cell activation. EMBO J. 2012;31(5):1123-33.

PUBLICATIONS

The following original studies have been published in international SCI-listed journals. Current dissertation is based on the results of the publications No. 1, 2 & 5.

1. **Deak, A.T.**, Blass, S., Khan, M.J., Groschner, L.N., Waldeck-Weiermair, M., Hallström, S., Graier, W.F. & Malli, R. IP_3-mediated STIM1 oligomerization requires intact mitochondrial Ca^{2+} uptake. J. Cell. Sci. 127: 2944-2955, 2014

2. Waldeck-Weiermair, M*., **Deak, A.T.***, Groschner, L.N., Alam, M.R., Jean-Quartier, C.,Malli, R. & Graier, W.F. Molecularly distinct routes of mitochondrial Ca^{2+} uptake are activated depending on the activity of the sarco/endoplasmic reticulum Ca^{2+} ATPase (SERCA). J. Biol. Chem. 288: 15367-15379, 2013 (* authors equally contributed)

3. Bondarenko, A.I., Drachuk, K., Panasiuk, O., Sagach, V., **Deak, A. T.**, Malli, R. & Graier, W.F. N-arachidonoyl glycine suppresses Na^{+}/Ca^{2+} exchanger-mediated Ca^{2+} entry into endothelial cells and activates BKCa channels independently of G-protein coupled receptors. Br. J. Pharmacol. 169: 933-948, 2013

4. **Deak, A.T.**, Groschner, L.N., Alam, M.R., Seles, E., Bondarenko, A.I., Graier, W.F. & Malli, R. The endocannabinoid N-arachidonoylglycine (NAGly) inhibits store-operated Ca^{2+} entry by preventing STIM1/Orai1 interaction. J. Cell. Sci.126: 879-888, 2013

5. Waldeck-Weiermair, M., Alam, M.R., Khan, M.J., **Deak, A.T.**, Vishnu, N., Karsten, F., Imamura, H., Graier, W.F. & Malli, R. Spatiotemporal correlations between cytosolic and mitochondrial Ca^{2+} signals using a novel red-shifted mitochondrial targeted cameleon. PLOSone 7(9): e45917, 2012